

IDEA League

MASTER OF SCIENCE IN APPLIED GEOPHYSICS
RESEARCH THESIS

Seismic forward modelling of rock and fluid properties in carbonates

Reducing uncertainty in data-poor environments

Rowan van der Waal

August 12, 2016

Seismic forward modelling of rock and fluid properties in carbonates

Reducing uncertainty in data-poor environments

MASTER OF SCIENCE THESIS

for the degree of Master of Science in Applied Geophysics at
RWTH Aachen University

by

Rowan van der Waal

August 12, 2016

IDEA LEAGUE
JOINT MASTER'S IN APPLIED GEOPHYSICS

Delft University of Technology, The Netherlands
ETH Zürich, Switzerland
RWTH Aachen, Germany

Dated: *August 12, 2016*

Supervisor(s):

Prof. Florian Wellmann, PhD - RWTH Aachen University

Dr. Ir. Guy G. Drijkoningen - Delft University of Technology

Committee Members:

Prof. Florian Wellmann, PhD - RWTH Aachen University

Dr. Ir. Guy G. Drijkoningen - Delft University of Technology

John Solum, PhD - Shell Global Solutions International BV

Eidesstattliche Versicherung

van der Waal, Rowan

Name, Vorname

352223

Matrikelnummer (freiwillige Angabe)

Ich versichere hiermit an Eides Statt, dass ich die vorliegende ~~Arbeit/Bachelorarbeit/~~
Masterarbeit* mit dem Titel

Seismic forward modelling of rock and fluid properties in carbonates

Reducing uncertainty in data-poor environments

selbständig und ohne unzulässige fremde Hilfe erbracht habe. Ich habe keine anderen als die angegebenen Quellen und Hilfsmittel benutzt. Für den Fall, dass die Arbeit zusätzlich auf einem Datenträger eingereicht wird, erkläre ich, dass die schriftliche und die elektronische Form vollständig übereinstimmen. Die Arbeit hat in gleicher oder ähnlicher Form noch keiner Prüfungsbehörde vorgelegen.

Delft, August 12, 2016

Ort, Datum

Unterschrift

*Nichtzutreffendes bitte streichen

Belehrung:

§ 156 StGB: Falsche Versicherung an Eides Statt

Wer vor einer zur Abnahme einer Versicherung an Eides Statt zuständigen Behörde eine solche Versicherung falsch abgibt oder unter Berufung auf eine solche Versicherung falsch aussagt, wird mit Freiheitsstrafe bis zu drei Jahren oder mit Geldstrafe bestraft.

§ 161 StGB: Fahrlässiger Falscheid; fahrlässige falsche Versicherung an Eides Statt

(1) Wenn eine der in den §§ 154 bis 156 bezeichneten Handlungen aus Fahrlässigkeit begangen worden ist, so tritt Freiheitsstrafe bis zu einem Jahr oder Geldstrafe ein.

(2) Strafflosigkeit tritt ein, wenn der Täter die falsche Angabe rechtzeitig berichtigt. Die Vorschriften des § 158 Abs. 2 und 3 gelten entsprechend.

Die vorstehende Belehrung habe ich zur Kenntnis genommen:

Delft, August 12, 2016

Ort, Datum

Unterschrift

Abstract

The main challenge in frontier and near-field exploration is the limited availability of data to interpret the subsurface. In the absence (or prior to drilling) of an appraisal well, possibly only seismic data and prior geology knowledge are at hand.

In such data-poor environments, techniques are required that are able to quickly test large amounts of geology scenarios in a high dimensional (many unknown parameters) model space. Markov Chain Monte Carlo optimization techniques have previously shown to be capable of realizing reasonable solutions for large modelling problems, but are less efficient when the problem has very limited prior knowledge available.

Optimization techniques as Particle Swarm Optimization and Cuckoo Search may however be able to de-risk the seismic amplitudes with the use of limited prior knowledge, since they may evaluate large sets of potential rock and fluid property scenarios in parallel.

To validate the applicability of these techniques, they are tested on their capability of solving mineralogy and porosity in a case-study on the Shuaiba Formation, with only limited prior data available.

Cuckoo Search in particular has proven to be suitable to achieve reasonable mineralogy and porosity scenarios fitting a seismic section of the Shuaiba Formation. Particle Swarm Optimization has proven to be a robust technique as well, but due to its slightly less exploratory behavior, it has a greater risk of not finding the optimal solution. On the contrary however, if time is limited and efficiency is more important than detail, Particle Swarm Optimization may be the preferred tool to use.

Both techniques have provided an indication towards a carbonate mineralogy and porosity values only vary in the order of a few percent with respect to prior research. In overall, the model created has shown to be easily applicable by geologists and geophysicists as it requires only limited prior knowledge of the subsurface. The tool may therefore be of great value to the oil and gas business, since it may help decide whether it is worth drilling an appraisal well based on the probabilities of different scenarios, potentially yielding a great economic advantage.

Acknowledgements

First of all I want to thank all the people who have participated in this project.

RWTH Aachen University
Delft University of Technology
Shell Global Solutions International BV

Prof. Florian Wellmann, PhD
Dr. Ir. Guy G. Drijkoningen
John Solum, PhD
Elena Manzo, PhD
Conxita Taberner, PhD
Stephane Gesbert, PhD
Luuk Kleipool, PhD
Bastiaan Huisman, PhD
Nino Cilona, PhD
Wenche Asyee, PhD

Contents

Abstract	vii
Acknowledgements	ix
Nomenclature	xix
Acronyms	xix
1 Introduction	1
1-1 Motivation and aim	1
1-2 Forward model	1
1-3 Optimization	2
1-4 Case-study setup	2
I Materials and Methods	3
2 Forward model	5
2-1 Seismic section input	5
2-2 Geometry input	6
2-2-1 Layer picking	6
2-2-2 Body picking	6
2-3 Input properties	6
2-3-1 Environmental parameters	7
2-3-2 Mineralogy	7
2-3-3 Porosity	8
2-3-4 Fluid content	8
2-4 Acoustic impedance	9

2-4-1	Bulk density	9
2-4-2	Velocity	9
2-5	Synthetic seismic	11
2-5-1	Reflection coefficients	11
2-5-2	Wavelet	11
2-5-3	Synthetics	13
2-6	Area of interest	13
2-7	Objective function	14
3	Optimization in data-poor environments	15
3-1	Particle Swarm Optimization	16
3-1-1	Conceptual ideas	16
3-1-2	PSO algorithm	17
3-2	One Rank Cuckoo Search	18
3-2-1	Conceptual ideas	19
3-2-2	Cuckoo Search algorithm	19
3-2-3	One Rank Cuckoo Search	20
II	Case study and results	23
4	Case study setup	25
4-1	Regional geology	25
4-2	Geology of the Shuaiba Formation	26
4-3	Mineralogy and porosity of the Shuaiba Formation	26
4-4	Model input data	27
4-4-1	Mineralogy input data	27
4-4-2	Porosity input data	28
4-4-3	Pore fluid content	28
4-4-4	Sun's models specific input data	28
4-4-5	Theoretical porosity to velocity relations	29
4-4-6	Frequency and scaling model parameters	31
4-5	Assumptions	31
4-5-1	Assumptions on reservoir setting	31
4-5-2	Fluid property settings	31
4-5-3	Environmental settings	33
4-5-4	Synthetic section	33
4-5-5	Layer geometry and area of interest (AOI)	33
4-6	Objective function	34
4-7	Optimization updates	36
4-7-1	Particle swarm optimization modifications	36
4-7-2	One Rank Cuckoo Search parameter modifications	37

5	Simulation results and interpretation	39
5-1	ORCS simulation results	42
5-1-1	Mineralogy	42
5-1-2	Porosity	42
5-1-3	Overburden dependency and uncertainty	46
5-2	CP-PSO simulation results	50
5-2-1	Mineralogy	50
5-2-2	Porosity	50
5-2-3	Overburden dependency and uncertainty	50
5-3	Seismic parameters	56
III	Discussion, recommendations and conclusion	57
6	Discussion	59
6-1	Optimization comparison	59
6-2	Interpretation outcomes	65
7	Recommendations and conclusion	67
7-1	Recommendations	67
7-2	Conclusion	69
IV	Appendices	75
A	ORCS-simulation outcomes	77
A-1	ORCS-simulation with $P_a = 0.45$ and one rank update ratio = 0.10	79
A-2	ORCS-simulation with $P_a = 0.75$ and one rank update ratio = 0.10	83
A-3	ORCS-simulation with $P_a = 0.25$ and one rank update ratio = 0.03	87
B	PSO-simulation outcomes	91
B-1	PSO-simulation with cooling timestep 1.15	93
C	Sun model simulation outcomes	97
C-1	ORCS-simulation including the Sun-model ($P_a = 0.25$ and one rank update ratio = 0.10)	97

List of Figures

2-1	Zero-phase Ricker wavelet	12
3-1	Stability regions for PSO parameters	19
4-1	Shuaiba reservoir architecture	26
4-2	Shuaiba Formation porosity distribution for different entities	27
4-3	Theoretical porosity-velocity correlations for carbonates	29
4-4	Theoretical porosity-velocity correlations for clastics	30
4-5	Theoretical porosity-velocity correlations for carbonates	30
4-6	Shuaiba Formation case study seismic section	32
4-7	Shuaiba Formation interpreted horizons	35
5-1	Probable mineralogy scenarios for Shuaiba Formation using One Rank Cuckoo Search	43
5-2	Probable porosity scenarios for Shuaiba Formation using One Rank Cuckoo Search	44
5-3	Residuals of porosity scenarios for Shuaiba Formation when comparing synthetic to seismic using ORCS	45
5-4	Correlation points for overburden and reservoir porosity matching	47
5-5	Correlation between overburden and reservoir porosity at three points using ORCS	48
5-6	Standard deviation for carbonate models using ORCS	48
5-7	Entropy for carbonate models using ORCS	49
5-8	Probable mineralogy scenarios for the Shuaiba Formation using Particle Swarm Optimization	51
5-9	Probable porosity scenarios for the Shuaiba Formation using Particle Swarm Optimization	52
5-10	Residuals of porosity scenarios for the Shuaiba Formation when comparing synthetic to seismic using PSO	53
5-11	Correlation between overburden and reservoir porosity at three points using PSO	54
5-12	Standard deviation for carbonate models using PSO	55

5-13	Entropy for carbonate models using PSO	55
5-14	Scaled synthetic section of the Shuaiba Formation in comparison with seismic section	56
6-1	Smallest misfit found per iteration using ORCS.	60
6-2	Smallest misfit found per iteration using PSO.	61
6-3	Smallest misfit found per iteration using ORCS (sorted).	63
6-4	Smallest misfit found per iteration using PSO (sorted).	64
A-1	Probable mineralogy scenarios for the Shuaiba Formation using One Rank Cuckoo Search with $P_a = 0.45$ and $t_{or} = 0.10$	79
A-2	Probable porosity scenarios for the Shuaiba Formation using One Rank Cuckoo Search with $P_a = 0.45$ and $t_{or} = 0.10$	80
A-3	Residuals of porosity scenarios for the Shuaiba Formation when comparing synthetic to seismic using ORCS with $P_a = 0.45$ and $t_{or} = 0.10$	81
A-4	Probable mineralogy scenarios for the Shuaiba Formation using One Rank Cuckoo Search with $P_a = 0.75$ and $t_{or} = 0.10$	83
A-5	Probable porosity scenarios for the Shuaiba Formation using One Rank Cuckoo Search with $P_a = 0.75$ and $t_{or} = 0.10$	84
A-6	Residuals of porosity scenarios for the Shuaiba Formation when comparing synthetic to seismic using ORCS with $P_a = 0.75$ and $t_{or} = 0.10$	85
A-7	Probable mineralogy scenarios for the Shuaiba Formation using One Rank Cuckoo Search with $P_a = 0.25$ and $t_{or} = 0.03$	87
A-8	Probable porosity scenarios for the Shuaiba Formation using One Rank Cuckoo Search with $P_a = 0.25$ and $t_{or} = 0.03$	88
A-9	Residuals of porosity scenarios for the Shuaiba Formation when comparing synthetic to seismic using ORCS with $P_a = 0.25$ and $t_{or} = 0.03$	89
B-1	Probable mineralogy scenarios for the Shuaiba Formation using Particle Swarm Optimization with $\Delta t = 1.15$	93
B-2	Probable porosity scenarios for the Shuaiba Formation using Particle Swarm Optimization with $\Delta t = 1.15$	94
B-3	Residuals of porosity scenarios for the Shuaiba Formation when comparing synthetic to seismic using PSO with $\Delta t = 1.15$	95
C-1	Probable mineralogy scenarios according to the Sun-relation for the Shuaiba Formation using One Rank Cuckoo Search with $P_a = 0.25$ and $t_{or} = 0.10$	98
C-2	Probable porosity scenarios according to the Sun-relation for the Shuaiba Formation using One Rank Cuckoo Search with $P_a = 0.25$ and $t_{or} = 0.10$	99

List of Tables

4-1	Shuaiba Formation case study: mineralogy input data	28
5-1	Tested optimization parameters for Shuaiba Formation case-study.	39

Acronyms

ADCO Abu Dhabi Company for Onshore Petroleum Operations

AOI Area of interest

API American Petroleum Institute

CC-PSO Centered-centered particle swarm optimization

CP-PSO Centered-progressive particle swarm optimization

CS Cuckoo search

GGG Gardner - Gardner -Gregory

GPSO General particle swarm optimization

HH-RMSE Hanna and Heinold corrected root-mean- square error

MCMC Markov Chain Monte Carlo

NRMSE Normalized root-mean-square error

ORCS One Rank Cuckoo search

PSO Particle Swarm Optimization

RHG Raymer-Hunt-Gardner

RMSE Root-mean-square error

SEG Society of Exploration Geophysicists

SN Signal-to-Noise

TWT Two-way-traveltime

WGG Wyllie-Gregory-Gardner

Chapter 1

Introduction

1-1 Motivation and aim

Frontier geophysical exploration of potential hydrocarbon reservoirs is often done with the use of seismic data. Apart from regional geology or possibly a nearby well drilling, data and information about the section is usually limited. Although seismic surveys carried out in such environments contain a wealth of data, there is also much ambiguity in the interpretation due to poorly defined constraints.

In this research thesis, an attempt is made to de-risk realistic geologic scenarios by testing synthetic seismic of a range of realistic reservoir properties to an actual seismic section. The main aim will be to find a range of scenarios existing of mineralogy, porosity and fluid content, that fit the seismic section. These scenarios may then be interpreted by a geologist to find a geologic setting that matches prior knowledge about the area.

1-2 Forward model

To satisfy easy applicability, while still preserving a lot of freedom to the prospective user (geologist), the forward model (to generate the synthetic seismic) in this thesis was written from scratch, instead of using already existing alternatives. Another motivation to limit the use of external material comes from the potential commercial use of the model, since this thesis was written as a project for a company as well.

The forward model consists of user-defined input data and constraints. This data consists of geometry, rock and fluid properties as mineralogy, porosity and fluid density (fluid type), temperature and pressure distribution, reservoir depth and dimensions of the reservoir. It is up to the user to give a realistic range of these parameters, in order to achieve reasonable scenarios from the model. The input data will be translated to synthetic seismic using the bulk density, a zero-phase wavelet and four different velocity models (Raymer, Hunt, & Gardner, 1980; Dvorkin & Nur, 1998; Wyllie, Gregory, & Gardner, 1956; Sun, 2000).

1-3 Optimization

To increase the fit between the synthetic seismic and the real seismic, global optimization methods are used to test a wide range of parameters sets in a quick and efficient fashion. Although Markov Chain Monte Carlo techniques have proven to be very useful in optimizing solutions (Sambridge & Mosegaard, 2002), their usability has been questioned in the domain of large, poorly-constraint modelling problems (Prasad & Souradeep, 2012), due to their sampling technique being computationally inefficient in high dimensional problems (many unknown parameters).

In the domain of heuristic optimization tools however, efficiency is better captured when exploring large model spaces (many parameters to optimize), because they sample different areas of the model space at the same time.

In this research two particular heuristic optimization methods, particle swarm optimization (PSO) and one rank cuckoo search (ORCS) will be applied to a case-study on the Shuaiba Formation, in order to test their capability of resolving the mineralogy and porosity distribution interpreted by Alsharhan (1987) and Alsharhan (1993). The general algorithms for both techniques were available, but required modification to make them suitable for the case-study in this research.

1-4 Case-study setup

In exploration geology, two main types of reservoir rock types are often distinguished: clastics and carbonates. Another setting that may show characteristics of a reservoir in seismic data, are igneous rocks. Whereas carbonates and clastics have proven to be suitable oil and gas reservoirs, hydrocarbon accumulations in igneous rocks are much less likely to be found (but do exist). In a seismic section however, igneous rocks may show very similar amplitudes as carbonates. One could think of a subsurface volcano for example, which may show a shape that looks like a buried carbonate platform.

On the other hand, when comparing clastics to carbonates, both rock types could contain hydrocarbon accumulations. However, since their mineralogy is quite different, porosity and hence the potential volumes of present liquids may also differ significantly. Therefore, it is important to be able to distinguish these reservoir types, preferably before taking a risk in drilling an appraisal well or collecting more or higher quality seismic data.

The model in this research is especially designed to classify reservoir types based on input scenarios. The comparison of carbonates to clastics and igneous rocks is applied in this research, but another selection of rocks from a library or literature data can be created to generate different types of scenarios. The library is easily expandable if region specific rock (or fluid) data needs to be added. Other examples of scenarios may not be in the domain of mineralogy, but could for example be the distribution of fluids in a system or the variation in porosity of different entities. A combination of scenarios can also be applied, for instance the modelling of mineralogy and porosity ranges together, which is attempted in this research by using ORCS and PSO. The main hypothesis to test the optimizations on is stated as:

Assuming there would be a reservoir containing oil, will it be possible to give a good indication towards a carbonate, clastic or basaltic mineralogy setting with a reasonable porosity distribution, by only comparing synthetic sections to seismic sections.

Part I

Materials and Methods

Chapter 2

Forward model

In order to model a seismic section, a synthetic section should be generated. For this purpose, a model has been created that takes in an actual seismic section and rock and fluid properties as input. Furthermore, seismic parameters as sampling interval and wavelet frequency and environmental parameters as temperature and pressure distribution are passed to the model. On the output side, it provides a section of synthetic data that may be evaluated to the seismic section. The entire model is written in MATLAB R2015b.

2-1 Seismic section input

The first step in the creation of the model is to load a seismic section to compare the model parameters to. Typically, seismic data is read in through the SEG-Y (Society of Exploration Geophysicists) format, however others may be used as well. In this model, the input data has to be of 2-D format, as all the modelling is performed in a two-dimensional domain.

For the purpose of this model, a specific section of the seismic section can be extracted. The user can do so by setting the time range and horizontal extent of the section through four coordinates. The visualization is a variable density plot of the input section, which in fact is a two dimensional grid of nodes. The convention used for displaying the seismic section is red for a through reflection (increase of acoustic impedance) and black for a peak reflection (decrease of acoustic impedance).

At this phase, the seismic section is simply read, meaning it is not corrected for any scaling applied to the actual data behind the image. This means the range of values may be to any extend, depending on what processing has been done on the section (scaling, corrections, removal of traces) and the (not entirely unambiguous) format that was chosen when creating the section.

2-2 Geometry input

The input of the geometry is entirely user specified. Geometry creation occurs through picking of expected horizons in the seismic section. The picking method has two options to define different entities: layers and bodies.

2-2-1 Layer picking

First, the user picks layer horizons only. The amount and order of picking the horizons is unimportant, since the model implicitly reorganizes all horizons based on the first point (of each layer) picked. This allows complete freedom of the extend of detail to which entities can be defined. The model also automatically interpolates the picks to either the model boundaries (left-right) or the nearest intersecting horizon. Hence, it matters where the first pick is made in the vertical sense. The user can cause layers to disappear and reappear, by deliberately crossing another horizon once or twice, introducing variable thickness (or thinning out) of layers or small entities filling up a basin shape for example.

2-2-2 Body picking

After these horizons have been picked, further referred to as the background geometry, the user has the option to define geometries called 'bodies' here. These bodies can be of any shape, as they are drawn using a polygon. This option allows volcanic intrusions, salt domes or carbonate platforms to be drawn. Within these body geometries, a new set of layers can be defined, which allows realistic geologic features to be created within a larger setting. In terms of implementing, these bodies can be seen as a layer that is overlying the background geometry (initially drawn layers), replacing the data with a new set of parameters, thereby cutting off the background layers. Equally to the feature in the background layers, the layers defined in the body can also have a variable thickness and disappear and reappear by crossing the other horizons within the specific body.

For both the background layers and the bodies and body layers, there is virtually no maximum of entities that can be created, in order of achieve maximum freedom in the picking for the user.

2-3 Input properties

Once the seismic has been loaded and the geometry has been created, the different entities should be populated with geologic and environmental parameters. The assignment of these parameters occurs per node, to allow lateral and vertical variations to be implemented. The input (population) parameters are:

- Environmental parameters
 - Depth
 - Temperature distribution

– Pressure distribution

- Mineralogy
- Porosity
- Fluid content

2-3-1 Environmental parameters

The user should specify the environment of the geologic setting by determining the depth first. Since a seismic section is usually shown in the time domain, this leaves some assumptions to be made. Since the two-way-traveltime (TWT) for the section is known from the seismic section, the only unknown variable to acquire the depth is the velocity of the wave. To obtain a velocity, a rock type should be selected as overburden. By default, this will be shale, but it can be modified by the user to any mineral from the library, described in section 2-3-2. Using the p-wave velocity (V_p) of the mineral, in this case 3400m/s (Mavko, Mukerji, & Dvorkin, 2009), the depth (d) is calculated using:

$$d = \frac{V_p * TWT}{2} \quad (2-1)$$

With the depth of the section estimated, a temperature and pressure distribution should be defined. Whereas mineral properties are assumed to be inelastic for this model, fluid properties will vary with depth (described in paragraph 2-3-4). Therefore, the user could specify a surface temperature and pressure, which by default are 20 degrees Celsius and 0.101325 MPa (1 Atmosphere). Also, the gradient for temperature and pressure can be defined, but by default these are set to 25 C/km and 22.6 MPa/km, respectively.

2-3-2 Mineralogy

The actual layers picked by the user will be populated with mineral compositions. From Mavko et al. (2009), a set of mineral densities, p-wave velocities and s-wave velocities for sandstones, shales, carbonates and volcanic rocks have been selected. This library is easily expandable or adjustable to the needs of each modelling problem, since the user can simply add new mineral density and velocity values to a list.

From the library, the user can select any type of these minerals for each entity. Also, a selection of multiple minerals can be selected and fractions of each mineral can be specified, to create a mineral composition for each layer. The density and bulk and shear moduli for these compositions are calculated through the weighted average (arithmetic mean) of each mineral type within the rock.

In a seismic section however, averaging a compositions density (and bulk moduli) neglects the internal contrast differences in an alternating rock stratigraphy. To be able to account for alternating stratigraphy layers, the user can subdivide an entity in *sublayers*. By doing so, the time thickness of the sublayers should be defined as well as a the amount of sublayers within the entity and the mineral type (uniform) of the sublayers. The model then distributes the sublayers through the entity with equal spacing. If the total thickness of the sublayers

exceeds the thickness of the entity, the sublayers get pressed against each other, creating a uniform layer of the sublayers causing the original layer mineral composition to no longer be present (this is unfavorable, so implementing sublayers should be done with caution).

The same methodology applies to the layers of the body entities. Within each body entity, sublayers can be generated. The option to create sublayers in this manner saves a lot of time in picking on the seismic section if the user expects or knows that a large part of the section exists of an alternating sequence of (equally spaced) strata.

2-3-3 Porosity

After mineralogy has been specified in each entity, porosity should be defined. There is a difference in porosity definition for background geometry layers and body layers. Whereas in body layer porosity can only be stated as a single value for each body layer (and sublayer), the background geometry layers can also have a lateral variation in porosity. The user is able to mark three points of porosity; the left boundary of layer, the center point of the layer and the right boundary of the layer. On top of that, the center point of the layer may be shifted to the left and right by a user-defined percentage, steepening the porosity curve on one side and flattening it on the other side of the center point (assuming the user specified three different porosity values).

To complete the lateral porosity function, the user can finally set a plateau area of the porosity around the center point (in a percentage of the total layer width), in order to control when the increase or decrease of porosity to one of the boundaries occurs.

Together, by specifying a three constraint points, the steepness of the porosity function and a possible plateau, the porosity becomes an easily adjustable function which creates a lot of freedom to the user.

2-3-4 Fluid content

The final geologic property is fluid content. Five different types of fluid content can be selected for each entity. Please note that it is assumed that fluid content in sublayers is the same as in the entity they belong too. The different fluid types are:

- Fresh water
- Brine
- Oil
- Gas
- Air

By default, only brine, oil and gas are tested as potential pore fluids. As mentioned in section 2-3-1, the fluid properties are dependent on the depth they are modelled. To calculate the density and velocity of each fluid at each depth, the equations of Batzle and Wang (1992) are used. Using these equations, fresh water properties can be calculated using temperature and pressure at each depth. To obtain the brine properties, the user could specify the salinity,

which by default is set to 80000 ppm (0.08). To calculate the oil and gas density and velocity, values for API gravity and hence specific gravity are required. By default, API gravity is set to 39 degrees, which results in a specific gravity of 0.876. Finally, the GOR (gas to oil ratio) should be known, which by default is set to 0.

Since the seismic input section is in time, again the entire section has to be translated to depth, in order to find the density and velocity to depth relations for these fluids. This requires a rock to be chosen for the p-wave velocity, which is the same as the overburden rock, by default shale. This results in density and velocity distributions of each fluid with depth. Lastly, air is assumed to be incompressible, therefore using a density of 0.012 g/cm^3 and a bulk modulus of $1.2e^{-5} \text{ GPa}$.

Again, background geometry layers and body layers may differ in fluid content as fluid can be specified per layer in all entities.

2-4 Acoustic impedance

The previous sections describe how the geologic model is created. In this section, the properties will be translated to acoustic impedance, using the bulk density and velocity.

2-4-1 Bulk density

The bulk density is simply calculated using the arithmetic mean (depending on porosity) of the matrix density and fluid density at each of the nodes in the grid:

$$\rho_b = \rho_m(1 - \phi) + \rho_f\phi \quad (2-2)$$

Where ρ_b is the bulk density, ρ_m the matrix density, ϕ the porosity and ρ_f the fluid density at the corresponding depth.

2-4-2 Velocity

For the velocity, four different relations are tested (all units are m/s):

1. Raymer-Hunt-Gardner relation (RHG) (Raymer et al., 1980)
2. Gardner-Gardner-Gardner relation (GGG) (Dvorkin & Nur, 1998)
3. Wylie-Gardner-Gardner relation (WGG) (Wyllie et al., 1956)
4. Sun-relation (Sun) (Sun, 2000)

The Raymer-Hunt-Gardner relation, after (Raymer et al., 1980) relates porosity, matrix velocity and fluid velocity:

$$V_p = (1 - \phi)^2 V_{mat} + \phi V_f \quad (2-3)$$

Where V_{mat} is the matrix velocity of the mineral composition calculated through the sum of the fractions of the bulk and shear moduli of all minerals using the equation:

$$V_p = \sqrt{\frac{K + \frac{4}{3}\mu}{\rho}} \quad (2-4)$$

The Gardner-Gardner-Gardner relation (Dvorkin & Nur, 1998) is only based on the bulk density (which has porosity incorporated):

$$0.3048 \left(\frac{\rho_b}{0.23} \right)^4 \quad (2-5)$$

Please note that the last two parameters (0.23 and 4 here) are generalized numbers and may vary if the relation is correlated to a specific rock type. However, for the scope of this research, the generalized form is kept to limit complexity. The factor 0.3048 is a conversion factor to calculate velocity measured in feet per second to meter per second.

The Wylie-Gardner-Gardner-relation (Wyllie, Gregory, & Gardner, 1958) also relates porosity with matrix and fluid velocity, but in a different way than the RHG-relation does:

$$\frac{1}{V_p} = \frac{(1 - \phi)}{V_{mat}} + \frac{\phi}{V_f} \quad (2-6)$$

Lastly, a more recent approach from (Sun, 2000) calculates the bulk p-wave velocity as in equation 2-4. However, the bulk and shear moduli are calculated differently. The bulk modulus, K , is calculated using:

$$K = (1 - \phi_k)K_{mat} + \phi_k K_f \quad (2-7)$$

Where K_{mat} is the matrix bulk modulus, K_f the fluid bulk modulus and ϕ_k is the effective porosity:

$$\phi_k = F_k \phi \quad (2-8)$$

The formation factor F_k arises from the bulk moduli of the fluid and matrix, the porosity and the effective bulk formation factor f_k :

$$F_k = \frac{1 - (1 - \phi) f_k}{(1 - (1 - \phi) f_k) \frac{K_f}{K_{mat}} + \left(1 - \frac{K_f}{K_{mat}}\right) \phi} \quad (2-9)$$

The effective bulk formation factor is defined as:

$$f_k = (1 - \phi)^{\gamma_k - 1} \quad (2-10)$$

Where γ_k is a frame flexibility factor, determined through:

$$\gamma_k = \frac{\left(1 - \left(\frac{K_f}{K_{mat}}\right)\right) \left(1 - \frac{4}{3} \frac{\mu_{mat}}{K_{mat}} - \frac{2}{3} \left(1 - \frac{5}{3} \frac{\mu_{mat}}{K_{mat}}\right) aG_c\right)}{2 \frac{\mu_{mat}}{K_{mat}} \left(1 + \left(\frac{\mu_{mat}}{K_{mat}}\right)\right) aG_c + \left(\frac{1 - \frac{K_f}{K_{mat}}}{1 + \frac{4}{3} \frac{\mu_{mat}}{K_{mat}}}\right) \phi - \frac{K_f}{K_{mat}}} \left(1 - \frac{4}{3} \frac{\mu_{mat}}{K_{mat}} - \frac{2}{3} \left(1 - \left(\frac{5}{3} \frac{\mu_{mat}}{K_{mat}}\right) aG_c\right)\right) \quad (2-11)$$

Where μ_{mat} is the bulk modulus of the matrix, a is the pore aspect ratio and G_c is the geometrical coupling factor.

Going back to equation 2-4, only the bulk shear modulus should now be obtained. This is done using:

$$\mu = \mu_{mat}(1 - \phi)f_\mu \quad (2-12)$$

Where f_μ can be assumed, to the first order approximation, to be equal to f_k .

Each of the four velocity relations is calibrated for brine saturated rocks. In the model however, different fluid types may be used. In order to recalculate the velocity for a different fluid saturation, Gassmann's substitution is used (Gassmann et al., 1951; Nolen-Hoeksma, 2000; Berryman, 1992). The approximations for the shear-wave velocity (required input for Gassmann's substitution) are obtained from the relations of Greenberg and Castagna (1992) and may vary per scenario model. In chapter 4, the relations for the case-study of this research are mentioned.

These four different velocity relations, multiplied with the bulk density distribution, each yield a representation of the acoustic impedance:

$$Z = \rho_b V_p \quad (2-13)$$

2-5 Synthetic seismic

2-5-1 Reflection coefficients

Each of the acoustic impedance realizations is used to calculate reflection coefficients between each two nodes (vertically) using:

$$R = \frac{Z_2 - Z_1}{Z_1 + Z_2} \quad (2-14)$$

Where Z_1 is the acoustic impedance of the upper node and Z_2 is the acoustic impedance of the lower node.

2-5-2 Wavelet

The wavelet used for convolution is a zero-phase (Ricker) wavelet with user defined frequency. An example of a 35Hz peak-frequency zero-phase Ricker wavelet is shown in figure 2-1. The sampling interval is equal to the sampling interval in the seismic section. The synthetic seismic section is resampled at the sampling interval before it is convolved with the wavelet.

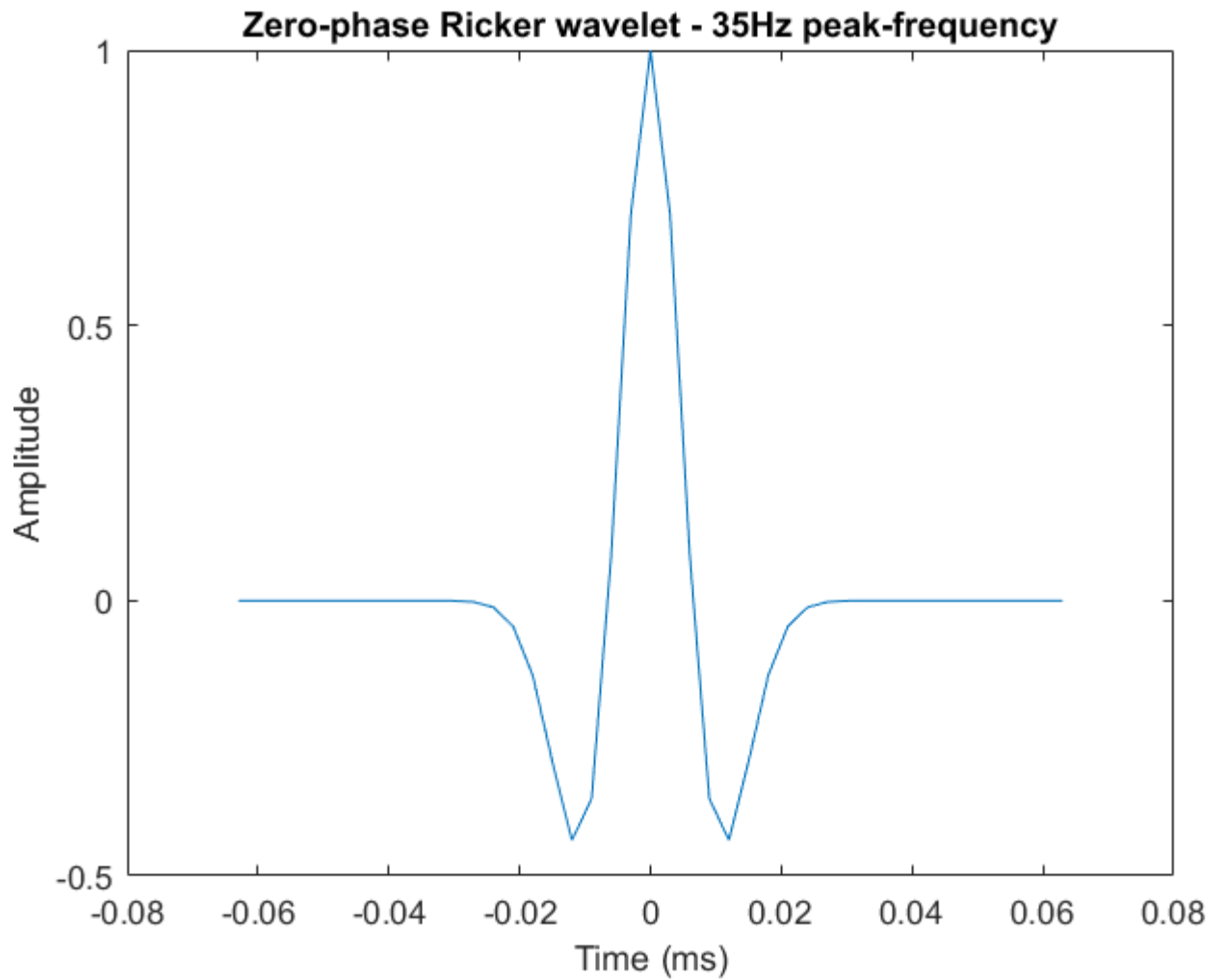


Figure 2-1: Zero-phase Ricker wavelet with 35Hz peak-frequency and a sampling time of 3 milliseconds.

2-5-3 Synthetics

The reflection coefficients and the zero-phase wavelet are convolved to synthetic seismic. This occurs trace-wise, so the actual synthetic seismic is 1D. Since the wavelet is not scaled, the values range within the synthetic section lies between -1 and 1, unlike the actual seismic section. The deviation in scaling prohibits meaningful quantitative interpretation at this time, unless the scaling factor is known.

Another way to obtain data sets of equal value range is to normalize the seismic section. However, the major assumption would then be that the maximum value found in the seismic section corresponds to 1, which is very unlikely in terms of reflections. One could opt to correct for this, by assuming the maximum value in the synthetics should correspond to the maximum value in the seismic section (assuming the range of values is equal). Still this would only be meaningful if the synthetic section originates from reasonable geology models, which is exactly what the model is trying to resolve. Therefore the scaling factor will be a modelled parameter, as described in chapter 3.

Since the model convolves the section in a 1D fashion, assumptions on the wavelet and synthetic section are implicitly made. By applying a 1D-convolution, treatment of effects from seismic processing, acquisition geometry, angle of incidence and migration are assumed to all be captured in a single wavelet (Hoek & Salomons, 2006). This also inquires that the model will only try to resolve the vertical dimension. As a result, it will only 'match' the actual seismic section if the data is processed 'correctly' and in terms of lateral resolution, it should be taken in consideration that event terminations may show up sharper on the 1D synthetic model than the actual seismic section (Hoek & Salomons, 2006).

This assumption may hold for this particular research, since it is mostly after resolving rock properties rather than geometry, but still it should be taken into account when evaluating the synthetic seismic section. The research of Hoek and Salomons (2006) confirmed that assuming lateral amplitude variations are not the prior concern, the overall 1-D synthetic section and 3-D synthetic section do not vary significantly. Therefore, the computation time advantage of a 1-D convolution outweigh the resolution increase of a higher-dimension convolution for this model.

2-6 Area of interest

To narrow down the amount of modelling required, it makes sense to specify an area of interest (AOI). The model allows multiple options to do so. First, the AOI can simply be the entire 2D section, hence the grid size of the input section. Secondly, one can pick an AOI manually by creating a polygon. As this polygon drawing may be inconvenient (time wise), one can also choose to let the model automatically create an area of interest. If the user opts for the automatic AOI creation, the AOI by default ranges from the upper horizon picked to the bottom horizon picked with an extension of 0.5 percent of the cell above and below the horizons, to ensure the reflection is captured entirely.

The model treats the section outside the AOI as unimportant and replaces it by the actual seismic and just uses the synthetic data within the AOI.

2-7 Objective function

Matching of two matrices of data is not as straight forward as it is for comparing lines. As continuity in the image is required to make it geologically feasible, one objective function should apply to the entire section. Multiple objective function options are incorporated in the model to find the smallest misfit between the seismic section and the created synthetics (only within the AOI):

1. Absolute error (L1 norm)
2. Squared error (L2 norm)
3. Root-mean-square error (RMSE)
4. Normalized RMSE (NRMSE)
5. Peak signal to noise ratio (PSNR)
6. Correlation coefficient
7. Hanna and Heinold corrected RMSE (HH) (Mentaschi, Besio, Cassola, & Mazzino, 2013)

Whereas objective functions 1-6 are well known, the HH-RMSE is less known, but is an adapted way of normalizing the RMSE. Normalized RMSE is calculated through:

$$NRMSE = \frac{\sqrt{\frac{1}{N} \sum_{i=1}^N (S_i - O_i)^2}}{O_i^{max} - O_i^{min}} \quad (2-15)$$

Where N is the amount of points measured, S_i is the modelled data at point i and O_i is the observed data at point i .

The corrected version, as explained in Mentaschi et al. (2013), does not divide by the range in the data and also takes out the $\frac{1}{N}$ under the square root, leaving only the L2-norm in the numerator. To compensate, the denominator is the sum of the product of the model and observed data, which in fact is the normalization factor for the L2-norm (numerator):

$$HH = \frac{\sqrt{\sum_{i=1}^N (S_i - O_i)^2}}{\sum_{i=1}^N (S_i O_i)} \quad (2-16)$$

The advantage in using this objective function is that the size of the normalization factor is dependent on the range of the values in the model and observed data, rather than a static value, which may be influenced by a single large or small event.

Optimization in data-poor environments

The main challenge when modelling in data-poor environments is the limit of constraints on the input parameters and the potentially wide range of possible geologic solutions. In terms of limited constraints in frontier exploration, one might think of unknowns in possible mineralogy, porosity and fluids in the subsurface. Therefore, wide ranges on density (mineralogy and fluids), velocity (mineralogy and fluids) and porosity are used, to capture as many possible outcomes. As a result however, the amount of possible scenarios as input to test the model on quickly run into the order of billions. Such orders of magnitude are beyond the solving capability of brute force. Also, due to these wide constraints, there may not be a single best solution, even if all sets of input data would (theoretically) be tested. This may be referred to as a multi-modal model. Since the preferred output is an overview of these likely scenarios rather than one (assumed best) solution, optimization is used to detect areas where potentially well fitting models are found.

In general, Markov Chain Monte Carlo (MCMC) techniques have shown to be very good at solving optimization problems (Sambridge & Mosegaard, 2002). However, it has also been argued that MCMC is not the best optimization to use if the target function contains multiple local minima (or maxima) and is highly dimensional (has a very large amount of unknowns). This may be due to the sampling technique, which takes a sample and updates its parameters in the direction of a better solution.

However, when in a large dimensional space with many local minima (or maxima), updating the sample may occur very regional and exploring all of these local (minima) regions and searching for the most likely solution within each region (exploit), may be computationally exhaustive and hence unfavored (Prasad & Souradeep, 2012). Using some constraints (in seismic forward modelling these may come from well-log data) on the model, the amount of dimensions (and local minima) may be reduced significantly, making MCMC extremely useful at sampling such seismic forward modelling problems.

In the absence of sufficient prior data (as in frontier exploration), which is the case in the scope of this research, alternatives are sought to quickly test multiple samples at the same

time (within one iteration). These alternatives come from the domain of heuristics, where optimality, completeness, accuracy and precision may be traded for speed. This sounds unfavored, but since the aim of the model in this research is finding overall distributions of rock and fluids properties rather than high resolution in specific seismic amplitudes, the increase in speed in exploring the model space may outweigh the loss in resolution. In this research, two particular heuristic techniques are applied:

- Particle Swarm Optimization 3-1-2
- One Rank Cuckoo Search 3-2-3

Both of these techniques evaluate the model space to search for likely outcomes, but their search algorithm differs them from each other.

3-1 Particle Swarm Optimization

Particle swarm optimization is a nature-inspired, stochastic optimization technique developed in 1995 (Eberhart & Kennedy, 1995). The algorithm tests the model space by generating random solutions and updates these to search for optima.

3-1-1 Conceptual ideas

The concept of particle swarm optimization (PSO) comes from the behavior of a group of animals moving together (e.g. a flock of birds, a school of fish or a swarm of insects). Such behavior describes synchronous movement, but also sudden direction change and scattering and regrouping of the flock.

If one would apply the concepts of particle swarm optimization to such a flock, analysis should proceed on the level of individual birds. The best solution or possible best solutions will be represented as food, which each individual bird tries to reach. However, neither of the birds knows exactly what the food is or where in the search space it may be found.

All the knowledge that the birds may gain comes from their own behavior and that of the other members in their flock. This knowledge gets updated at each time the flock communicates. The birds information update comprises the following:

- How far the bird itself is from the food.
- How far each other bird is from the food.
- The dimensions of the area where the birds fly in.
- The fact that the food is present within this flight area (assumption that there is at least one sample of food to be found).

Based on the information the birds fly in the direction of the prospected food at a certain velocity for a predefined amount of time or when the food is found. The location of the food might change however, if a bird finds a 'more likely' food in another neighborhood than the one initially chased after. If a more likely food is found, the direction and velocity of all birds is changed to the direction of the new food and so new areas of the flight area get explored.

3-1-2 PSO algorithm

If this bird behavior is translated to model parameters, the birds may be represented as 'particles' (samples). Each of these particles is thus a set of input parameters. The flock of birds then becomes a swarm of particles. The swarm thus exists of an x -amount of sample sets of input parameters which are measured at the same time (one iteration). The food is a minimum of the objective function and presumably also the global minimum. Using this translation, the methodology of the algorithm becomes (Gonzalo & Martínez, 2009; Martínez & Gonzalo, 2009; Martínez, Gonzalo, & Naudet, 2010; Martínez, Gonzalo, Muñiz, & Mukerji, 2012; Panigrahi, Shi, & Lim, 2011):

1. Initialize (random) particles of the swarm (within constraints).
2. Evaluate objective function for each particle individually.
3. If the current result of each particle is better than its personal best result so far, set the current value as new personal best.
4. Choose the particle with the best objective function and set this as global best solution.
5. Update the velocity of the particles.
6. Update the positions of the particles according to the new velocity of each particle and its previous location.
7. Return to step (2) and iterate until a maximum of iterations is achieved or another tolerance condition is satisfied.

Within the PSO methodology, the most important steps are (5) and (6), since these actually determine how the model space is searched. Now within the PSO algorithm, different family members exist, each having their own way of updating the velocity. In general, the update of the velocity is governed by six parameters:

- inertia (w)
- timestep (Δt)
- local acceleration (a_{local})
- global acceleration (a_{global})
- random number for local acceleration updates (r_1)
- random number for global acceleration updates (r_2)

These parameters define the rate of convergence towards the (assumed) global minimum. Inertia defines how fast the system cools, hence large inertia causes fast cooling, causing areas to be locally explored (exploitation) and small inertia results in slow cooling, causing the sampling to occur at high velocity, but with less 'detail' (exploration). The acceleration and time step factors determine the size of the steps each iteration takes to the next update.

The random numbers are applied to the accelerations of each particle to obtain vectors of accelerations at each time step: ϕ_{local} and ϕ_{global} . These random numbers used as acceleration updates, together with the random sample drawing (step 1), make the PSO a stochastic process.

Since the problem of seismic forward modelling has broad constraints and a large amount of unknowns, it is important to get a wide exploration of the model space before exploiting local areas, in order to avoid getting trapped in local minima. Within the PSO-family, the member best complying to this condition is called centered-progressive PSO (CP-PSO) (Martínez et al., 2012). This type of PSO updates the velocity and position at the same time, in contrast two other family members as the general PSO (GPSO) and centered-centered PSO (CC-PSO), which update in series or independently of each other. The equation to update velocity in the CP-PSO method is:

$$v(t+\Delta t) = \frac{1 - (\phi_{local} + \phi_{global})\Delta t^2}{1 + (1 - w)\Delta t}v(t) + \frac{\Delta t\phi_{local}}{1 + (1 - w)\Delta t}(g(t) - x(t)) + \frac{\Delta t\phi_{global}}{1 + (1 - w)\Delta t}(l(t) - x(t)) \quad (3-1)$$

Where $g(t)$ is the global best solution (lowest misfit particle) and $l(t)$ is the historic best position of each particle; $x(t)$ is the current position of the particle.

Using this velocity, each particles position for the next iteration can be updated directly using:

$$x(t + \Delta t) = x(t) + v(t)\Delta t \quad (3-2)$$

For the initial parameters set for the inertia and accelerations, research of Martínez et al. (2012) has given some reference for exploratory PSO. The convergence is related to the stability of their first (mean trajectories) and second order moments (variance and temporal covariance) (Martínez et al., 2012). Figure 3-1 shows the areas where combinations of inertia and acceleration parameter choices ensure stability.

The blue areas in figure 3-1 represent strong convergence (less exploration), whereas the red areas cause the model to become unbounded (no convergence). Since the aim is to let the PSO algorithm explore as much of the model space as possible, Martínez et al. (2012) suggested inertia and acceleration parameters near inside the first order stability regions and close to the upper border of their respective second order stability region should be chosen. These choices cause very weak attractions of the particles (high exploratory behavior), but still result in convergence. In case of the CP-PSO member, these values are 5/7 for the inertia and 12/7 as average of the accelerations (Martínez et al., 2012; Prasad & Souradeep, 2012). In addition, the Δt should also be chosen carefully, in order to ensure the model is explored enough before convergence to a (correct) local area occurs.

3-2 One Rank Cuckoo Search

Cuckoo search is, with respect to particle swarm optimization, a more recent, nature-inspired metaheuristic algorithm, developed by Yang and Deb (2009). The technique finds its origin in the brood parasitism of some cuckoo bird species, combined with the application of Lévy flights random walks (Lévy, 1954; Mandelbrot, 1982).

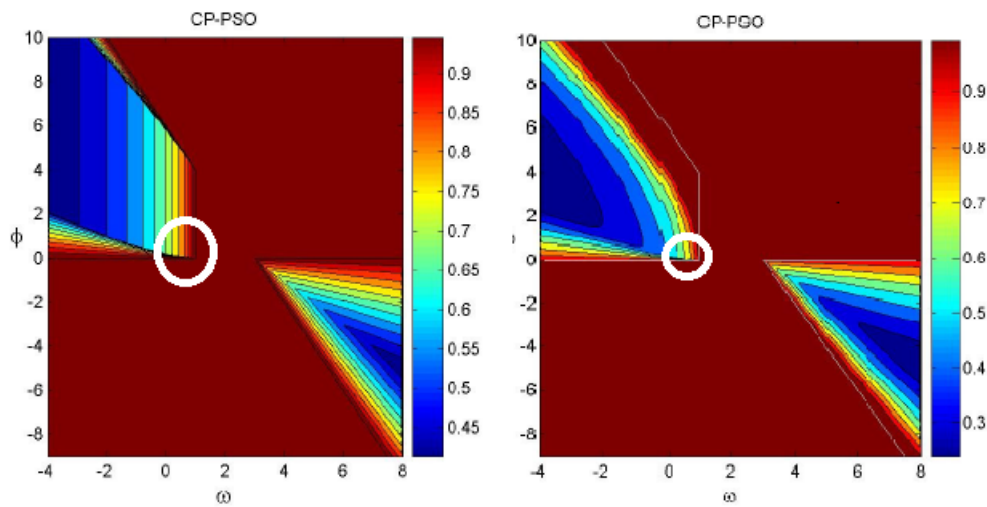


Figure 3-1: First (left) and second (right) order stability regions for PSO parameters (w , ϕ), found by Martínez, Gonzalo, Muñiz, and Mukerji (2012). Circles indicate parameter ranges for exploratory (yet still converging) behavior.

3-2-1 Conceptual ideas

The cuckoo types that are of specific interest to this algorithm are those who lay their eggs in communal nests of other host birds. In addition, they may remove the other eggs to increase the chance of their own being hatched. The algorithm adopts a similar behavior, which can be summarized as (Yang & Deb, 2009):

1. Each cuckoo lays one egg at each time step, which is placed in a random nest.
2. The highest quality eggs will survive to the next generation.
3. The amount of available nests is fixed and the cuckoo's egg being discovered by the host bird has a probability between 0 and 1 (p_a).
4. If the host bird finds the egg, it can either throw it out, or abandon the nest and build a new nest.

The exploitation close to the nests, in order to improve the local solutions, is governed by the Lévy flight random walks. However, to prevent the solutions to jump out of the search space, the step size should be carefully chosen.

3-2-2 Cuckoo Search algorithm

Combining the behavior of the cuckoo's and the ideas of the Lévy flights in one algorithm, the pseudo code becomes (Yang & Deb, 2009; Tawfik, Badr, & Abdel-Rahman, 2013):

1. **Exploration** Initialize the first population of N nests (randomly within the search space).

2. Update each nest by a Lévy flight in each dimension.
3. Evaluate the nests by the objective function.
4. If the updated nest is better than the original nest, replace the original nest by the updated version.
5. **Exploitation:** now to replace a fraction of the nests: get two random permutation arrays (rp_x and rp_y for each sample (N length)).
 - Generate a random number (0-1)
 - if a random number (r_n) $< p_a$, set the new nest as:

$$Nest_{new}(n, d) = r_n (nest(rp_x(n), d) - nest(rp_y(n), d))$$
6. Evaluate the new nests by the objective function.
7. Rank the new nests by their misfit to the objection function.
8. Get the current best nest and return to step (2) for a pre-defined amount of iterations or until another stop criterium is satisfied.

3-2-3 One Rank Cuckoo Search

From the scheme in the previous paragraph, one could point out that the nests get evaluated twice by the objective functions; once after the exploration phase and once after the exploitation phase. As this is computationally unfavorable, Tawfik et al. (2013) proposed a slightly alternative algorithm, referred to as the 'One Rank Cuckoo Search' (ORCS). Instead of evaluating the nests twice, it attempts to combine the exploration and exploitation phase, so applying the Lévy flights and replacing a fraction of the models before evaluating them with the objective function. This reduces the amount of evaluations per iterations from $2N$ to N .

The amount of exploration and exploitation is governed by the one rank ratio r_{or} . This ratio determines the likelihood of the fraction of nests (p_a) to be replaced. It starts of at 1, to allow the algorithm to combine all explorations and exploitation. This may proceed until it does not find any better nests for t_{or} iterations, after which it starts to gradually decrease. The decrease is dependent on the amount of dimensions D (unknown parameters) in the model:

$$r_{or}^{t+1} = r_{or}^t (1 - 0.5/D) \quad (3-3)$$

Furthermore, to ensure the updated solutions remain within the search space when the Lévy flights update the samples, the algorithm introduces a 'bound-by-best ratio' (r_{bbb}). This ratio is described by:

$$r_{bbb} = 1 - 1/\sqrt{D} \quad (3-4)$$

This ratio only affects the algorithm if one of more dimensions of a sample are outside of the constraints when updated through the Lévy flights. For those samples' dimensions, a random

number is drawn. If the random number is smaller than the r_{bbb} , the dimensions are replaced by the values of the best solutions to create a new solution (sample). If the random number is larger than the r_{bbb} , the new solution is drawn randomly from the entire model space.

When applying the one rank ratio and bound-by-best ratio to the algorithm, it can be updated to:

1. **Exploration** Initialize the first population of N nests (randomly within the search space).
2. Update each nest by a Lévy flight in each dimension.
3. **Exploitation**: draw a random number (0-1) and compare it with the r_{or} ratio.
 - if the random number is smaller than r_{or} : replace a fraction of the nests:
 - Get two random permutation arrays (rp_x and rp_y for each sample (N length)).
 - * Generate another random number (0-1) for each dimension of each sample
 - * if the random number $< p_a$ the new nest as:

$$Nest_{new}(n, d) = r_n (nest(rp_x(n), d) - nest(rp_y(n), d))$$
 - Apply the concept of 'bound-by-best', ensuring the samples are all within the model space.
 - Evaluate the new nests.
 - Rank and keep the current best nests.
 - if the random number is larger than r_{or} , directly apply the concept of bound-by-best.
 - Evaluate the new nests by the objective function.
 - Rank the new nests by their misfit to the objection function and keep the current best nests.
4. Get the current best nest.
5. If there are no better nests since t_{or} iterations, decrease r_{or} using equation 3-3.
6. Return to step 2 until the maximum pre-defined amount of iterations is reached or another stop criterium is satisfied.

The ORCS algorithm has been tested on benchmark functions and in the financial world, where it has shown to almost always outperform the original Cuckoo search algorithm (Tawfik et al., 2013).

Furthermore, many comparisons have been made on the general Cuckoo search and particle swarm optimization (Civicioglu & Besdok, 2011; Adnan & Razzaque, 2013; Singh & Singh, 2014), showing both methods may achieve small misfit values, but Cuckoo search travels through a larger amount of space before arriving at these values. This may sound unfavorable, but it should be considered that searching a larger space also decreases the risk of being trapped in a local minimum. A case-study (chapter 4) is used in this research to verify the convergence capability of ORCS in poorly constraint seismic forward modelling problems and compare this capability with the PSO performance.

Part II

Case study and results

Chapter 4

Case study setup

To evaluate the performance of the forward model and verify the optimization tools, a case study on the Shuaiba Formation, which contains a giant onshore oil field (stretching over 40 kilometers) and is found in the United Arab Emirates, is carried out.

Extensive research carried out by Exxon Mobil (Yose et al., 2006), ADCO (Lawrence et al., 2010; Yin et al., 2010; Melville, Al Jeelani, & Grötsch, 2004) and Alsharhan (Alsharhan, 1987, 1993) have provided a good interpretation of the Shuaiba Formation.

The interpretation shows the fields mineralogy (carbonate) and porosity distribution for the different entities. In this research, it is assumed that the interpretations of Alsharhan (1987, 1993) on porosity may tell something about the seismic figures and interpretations as shown in the Exxon Mobil and ADCO research. However, there is no evidence that the fields researched by Exxon Mobil and ADCO are in the same area as those from Alsharhan. The interpretations, as shown in the ADCO research, are based on multiple sources of seismic data, well log data and production and performance data.

The field can be divided in a northern and southern survey area. For the northern area, the seismic is very high quality for a carbonate field, covering an area of nearly 2000 km^2 . It's obtained with a 3D-seismic survey, where the data is 300-fold with 25 meter trace spacing and wavelet peak frequency around 35 Hz at reservoir depth (2440-2775 meter) (Yose et al., 2006). The seismic survey in the southern area provided seismic data that are 150-fold and also provide high quality imaging of the reservoir (Yose et al., 2006). In addition, well log samples of more than one hundred cored wells and prior information of the environment are available to constraint the interpretation throughout the field. Furthermore, the field is in production for more than fifty years and has a wealth of production and performance data available to validate geologic interpretations as this research is trying to simulate (Yose et al., 2006).

4-1 Regional geology

The Shuaiba Formation is part of the second-order supersequence that spans the Valanginian to Aptian stages and is found across the Arabian platform. The Shuaiba Formation is found

in the Aptian sequence set, which is the upper of three sequence sets of the Lower Cretaceous supersequence.

The reservoir itself is the highstand portion of a long-term sequence depositional sequence and has a thickness of about 50-120 meter (Grammer & Harris, 2005). The reservoir is a platform that has two well developed margins. The one on the northern side, which has long been recognized, shows progradation into the Bab Basin, whilst the southern margin is mainly aggradational (Yose et al., 2006).

On top of the reservoir, a new supersequence is found, which consists of Nahr Umr shale. On the bottom side lies the Kharaib Formation, which is the transgressive portion of the sequence which the Shuaiba Formation belongs to (Yose et al., 2006).

4-2 Geology of the Shuaiba Formation

On the reservoir level, four major phases can be distinguished, which correspond to phases of long-term sea level cycles. Furthermore, six depositional sequences can be classified, which correspond to intermediate-scale sea level changes (Yose et al., 2006). In the lower area of the Shuaiba platform, two sequences representing transgression can be found. On top of those, a sequence showing transgression and later highstand can be seen, which also form the top of the reservoir. Further on the northern side, two sequences representing late highstand are visible. These sequences show a clinoformal shape, which suggest the progradation in the northern direction. Further to the north and into more recent depositions, the Bab member and Nahr Umr shale are recognizable, which are the lowstand to transgressive sequences of the next overlying supersequence (Lawrence et al., 2010).

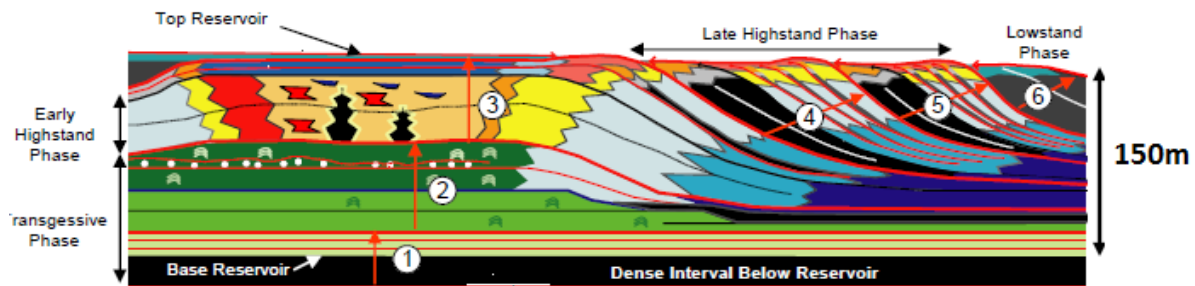


Figure 4-1: Shuaiba reservoir architecture as found by Yose et al. (2006)

4-3 Mineralogy and porosity of the Shuaiba Formation

Porosity distribution throughout the reservoir has been investigated by Alsharhan (1987). In terms of mineralogy and porosity entities, the Shuaiba Formation has been subdivided in facies A to H (Alsharhan, 1993). The distribution is shown in figure 4-2.

From figure 4-2 it may be observed that the highest porosity values are found in the top facies (H: 24.5%), the lower layers (A & B: 20.5% and 23%) and the southern layer (C: 26%). Overlying the H layer in the southern extent of the reservoir, the I layer shows a significantly

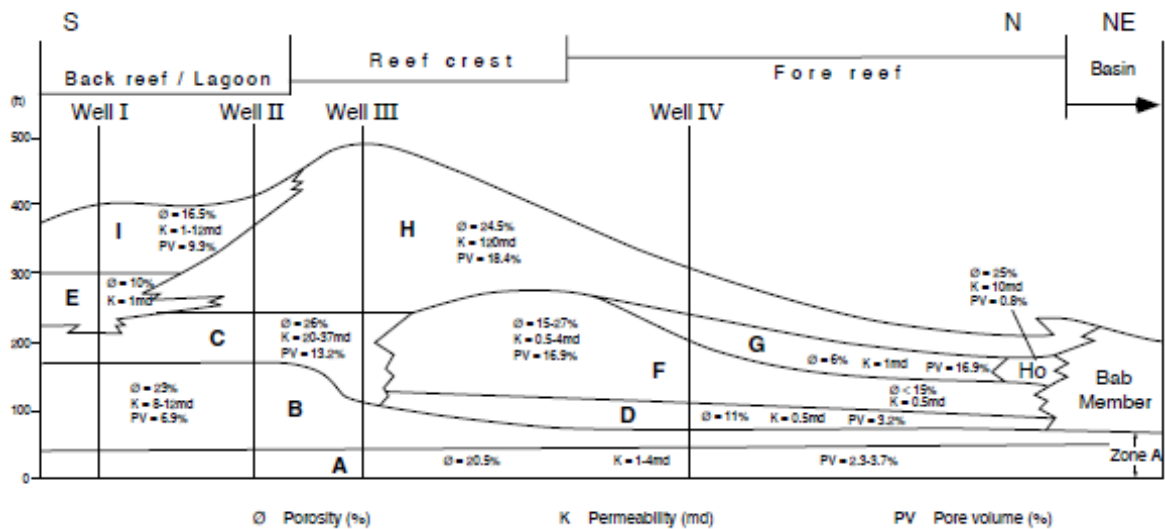


Figure 4-2: Shuaiba Formation porosity (and also permeability and pore volume) as found by Alsharhan (1987).

lower porosity (16.5%). Right below the I layer, the low porous E entity (10%) is found. On the northern side of the reservoir, the clinofolds are found, existing of layers G and F. Porosity in these layers is lower than the crest of the reservoir (H), but may still be around 15% for the F layer, while only around 6% in the G-layer.

Furthermore, prior research concluded that the large majority of the reservoir exists of calcite carbonate rocks. Some dolomite may be present in the H and G layers and also in the lower part of the A and B layers), but the main mineral composition throughout is calcite (Alsharhan, 1987, 1993).

4-4 Model input data

The aim of the model will be to simulate similar porosity distributions as described in paragraph 4-3. Its procedure will main exist of testing different scenarios without putting too many constraints on the input data, since those might not be available during its prospective application (frontier and near-field exploration).

4-4-1 Mineralogy input data

In this case study, three different mineralogy scenarios will be tested as if it is not known that the reservoir is a carbonate. The first scenario will be the actual carbonates, the second will be a clastic (sandstone) environment and the third will be a basaltic environment. The ranges for the input data are show in tabel 4-1; these are literature values from Mavko et al. (2009).

Scenario	Carbonate	Clastic	Basalt
Mineral density range (g/cm^3)	2.65-2.71	2.62-2.65	3.285-3.32
P-wave velocity range (m/s)	5800-6406	4680-6050	7500-8495
S-wave velocity range (m/s)	3000-3346	4112-4295	4295-4975

Table 4-1: Shuaiba Formation case study: mineralogy input data

For the overburden, Nahr Umr shale is used, with a mineral density of $2.625 g/cm^3$, a P-wave velocity of $3400 m/s$ and a S-wave velocity of $1771 m/s$ (Yu, Yan, & Nie, 2013). The underburden varies per scenario. For the carbonate scenario, a dolomite-anhydrite layer is used (ρ : $2.87-2.97 g/cm^3$, P-wave velocity: $5640-7107 m/s$ and S-wave velocity: $3130-4117 m/s$). In the clastic and basaltic scenario, the underburden exists of sandstone or basalt, respectively. The parameter ranges used are described in tabel 4-1.

4-4-2 Porosity input data

On top of the mineralogy scenarios, porosity is another parameter to be modelled for each entity. However, some constraint on porosity will be made to keep it within reasonable range. Three different porosity models will therefore be tested:

- 1% - 30%
- 1% - 40%
- 1% - 50%

The ranges may vary on each of the assign points as described in paragraph 2-3-3 and may vary for each entity defined. Exceptions are the underburden and overburden. From regional knowledge and characteristic reservoir settings, it is assumed to have a low porous overburden (Nahr Umr shale, 0% - 15% porosity) and a high porous underburden (25%-33%), which is set equal for each scenario.

4-4-3 Pore fluid content

Since the hypothesis in this case study is mainly set to verify mineralogy and porosity rather than fluid content, the fluid content in the pores within the crest of the reservoir (top layer) is assumed to be oil, while it is brine in the over- and underburden and the other reservoir layers. This of course is an assumption, fluid content could be used as an unknown variable as well in a different case-study.

4-4-4 Sun's models specific input data

In addition to the acoustic properties to calculate velocity, Sun's velocity model requires an extra parameter, known as the frame flexibility factor. This variable is dependent on pore

aspect ratio and the geometrical coupling factor (see section 2-4-2). Since the Sun relation is typically only used for carbonates, frame flexibility factors between 0.2 and 0.38 have been used (Sun, 2000). Since the relation is not valid for the clastic and basaltic scenario, it is omitted from simulation for these scenarios, to save computation time and prevent errant interpretations as output.

4-4-5 Theoretical porosity to velocity relations

Using the mineralogy and porosity input data as described in sections 4-4-1 and 4-4-2, theoretical relations can be created for porosity and p-wave velocity. To do so, the pore volume is assumed to be completely filled with brine ($\rho = 1.05$, $K = 3.04$ and $Vp = 1774$). The frame flexibility factor for the carbonate relation is set to 0.29. For a porosity range of 1%-50%, the relations for each rock type are shown in figure 4-3 to 4-5.

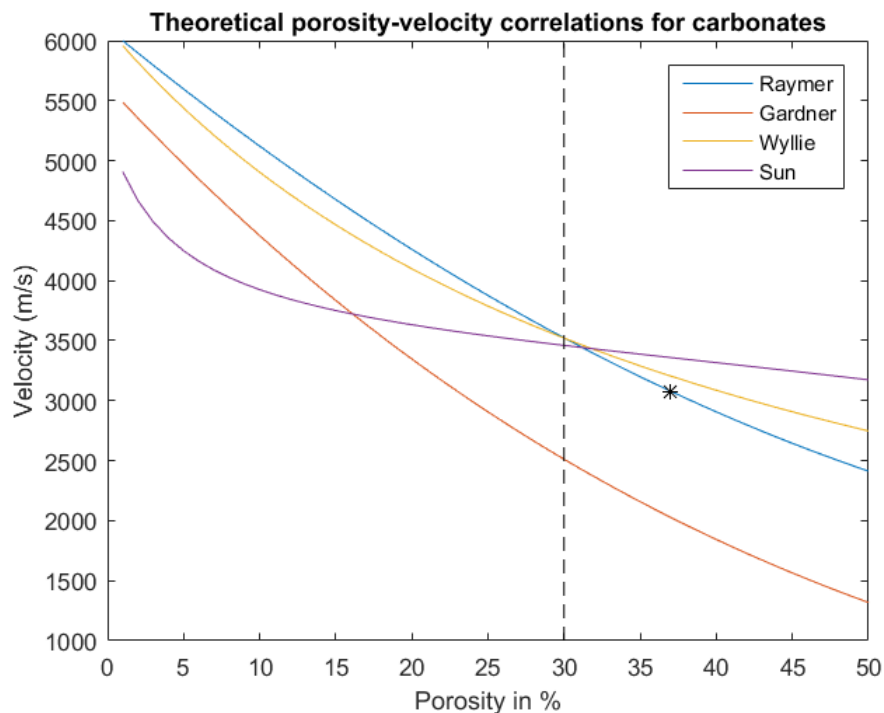


Figure 4-3: Theoretical porosity-velocity correlations for carbonates with a brine-saturated pore volume of 1%-50%. For the Sun relation, the frame flexibility factor is set at 0.29. The dashed line (30%) indicates the maximum porosity for calibration of most velocity models (except Sun, which is calibrated up to 45%). The star on the Raymer-relation indicates the equation is no longer valid for porosity values above 37%.

Figures 4-3 to 4-5 show that the relations may result in very different results for velocity in rocks with higher porosity. It should be noted therefore, that the porosity correlations have been calibrated on data sets with porosity up to 30% (Wyllie et al., 1956; Wyllie et al., 1958; Raymer et al., 1980; Dvorkin & Nur, 1998), with the exception of the Sun model, which also has some sets up to 45% (Sun, 2000). Above the 30% porosity range (denoted by the dashed line in figures 4-3 to 4-5), extrapolation has been applied. One should be careful

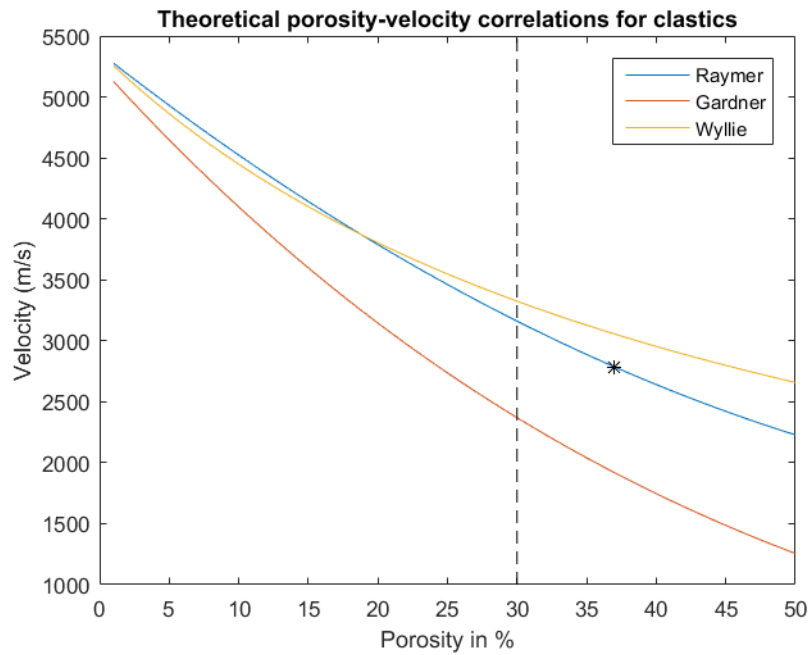


Figure 4-4: Theoretical porosity-velocity correlations for clastics with a brine-saturated pore volume of 1%-50%. The dashed line (30%) indicates the maximum porosity for calibration of most velocity models. The star on the Raymer-relation indicates the equation is no longer valid for porosity values above 37%.

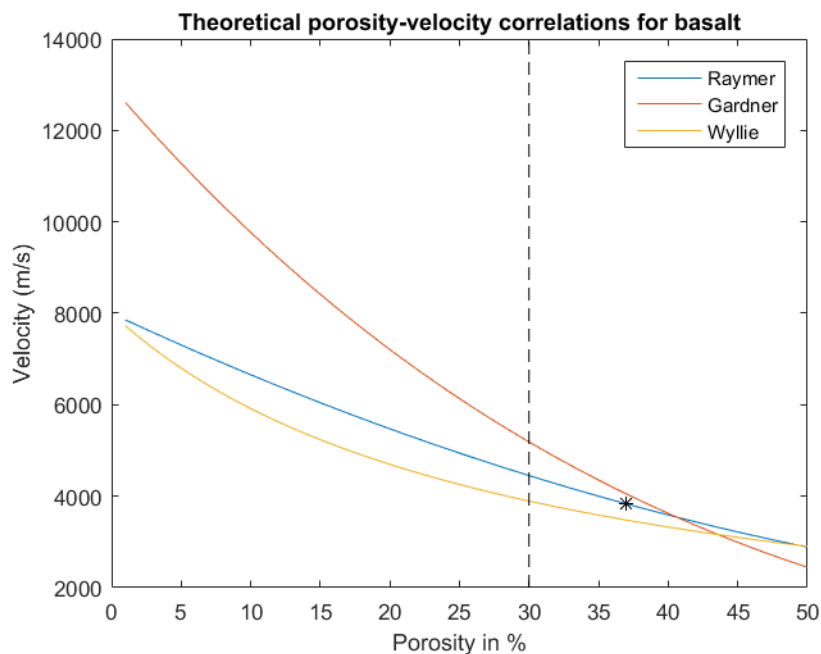


Figure 4-5: Theoretical porosity-velocity correlations for basalts with a brine-saturated pore volume of 1%-50%. The dashed line (30%) indicates the maximum porosity for calibration of most velocity models. The star on the Raymer-relation indicates the equation is no longer valid for porosity values above 37%.

however, to use these relations for such high porosity, as some may give unreasonable values. Furthermore, the equation used for the Raymer-Hunt-Gardner equation is only valid up to around 37% (Raymer et al., 1980), as denoted by a star in figures 4-3 to 4-5. Therefore, the Raymer-Hunt-Gardner relation is not used in scenario modelling above 40%.

4-4-6 Frequency and scaling model parameters

Apart from the geologic model parameters, there are also seismic unknown parameters to the section. As described in paragraph 2-5-2, the peak-frequency of the Ricker wavelet will be used as an unknown model parameter. For the Shuaiba Formation, earlier interpretations by Lawrence et al. (2010) have shown the best frequency to match the seismic for a Ricker wavelet to be 35Hz. As input range, a wider seismic frequency range of 25-60 Hz will be used however, to check if the model will resolve the right frequency for the section. The sampling interval in the seismic is 3 ms.

In addition to the wavelet frequency, scaling of amplitudes in the seismic with respect to generated synthetics is a further unknown variable. To control the extend of this variable slightly, the range is defined by the range of values found in the seismic. The actual scale limit may vary such that the absolute maximum reflection (coefficient) found in the seismic ranges between 0.2 and 0.4. In case of the Shuaiba Formation case-study, the seismic values in the order of $0 - 3e^4$. As a result, the scaling factor for the synthetic data ranges from $7.5e^4 - 1.5e^5$.

4-5 Assumptions

In addition to the constraints to the model input data, certain assumptions are required to perform the computations of the model.

4-5-1 Assumptions on reservoir setting

The seismic input section where the Shuaiba reservoir is found is shown in figure 4-6. The section originates from the survey from ADCO (post-stack migrated). For this research, the image has been used to generate a seismic section by the color intensity. The value range used is found in figure 4-7 ($-3.2767e^4$ to $3.2767e^4$). An assumption made here is that the reflections in the survey from the ADCO (Lawrence et al., 2010) research are in the same order as the ones in the Exxon Mobil research (Yose et al., 2006). Also, it is assumed that the section shown in the research of Yose et al. (2006) is part of the section of Lawrence et al. (2010), based on equal geometrical features observed. However, the only evidence for this assumption comes from the reference to the Shuaiba Formation, which is used both Lawrence et al. (2010) and Yose et al. (2006). The section created from color analysis is further referred to as the seismic (section).

4-5-2 Fluid property settings

To apply the equations of Batzle and Wang (1992) for the calculation of fluid properties with depth, the time depth needs to be converted to depth. An assumption is made here, that the

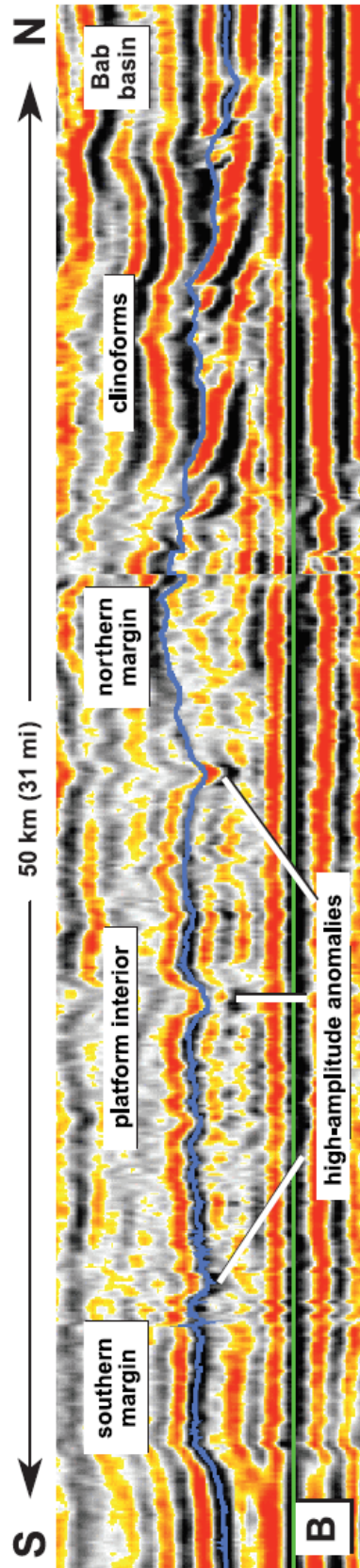


Figure 4-6: Shuaiba Formation case study seismic section, from Yose et al. (2006). (European polarity convention: red is an increase in A1, black is a decrease in A1)

overburden is existent of shale ($V_p = 3400$ m/s), after which the actual depth can be calculated using the equation as described in paragraph 2-3-1. In addition to the reservoir settings, the characteristics of the fluids are also required for the calculations of Batzle and Wang (1992). Since the modelled fluids are brine and oil, the gas/oil ratio is set to 0 and an API of 39 is used for the oil (light crude oil). For the brine in the over and underburden, a salinity of 0.08 (8%) is used. To apply oil saturation, Gassmann's substitution is used (Gassmann et al., 1951; Nolen-Hoeksma, 2000; Berryman, 1992). The shear velocity approximations from Greenberg and Castagna (1992) for different rock types are:

$$V_{s_{limestone}} = -0.05508V_p^2 + 1.01677V_p - 1.0349 \quad (4-1)$$

$$V_{s_{dolomite}} = 0V_p^2 + 0.58321V_p - 0.07775 \quad (4-2)$$

$$V_{s_{sandstone}} = 0V_p^2 + 0.80416V_p - 0.85588 \quad (4-3)$$

$$V_{s_{shale}} = 0V_p^2 + 0.76969V_p - 0.86735 \quad (4-4)$$

The V_s and V_p velocity are measured in km/s here. With respect to the proposed scenarios, one may observe that there is no relation for basalt. This is done on purpose, since for this case-study, no likely hydrocarbon filled basalt reservoir is assumed. Therefore, all scenarios with a basaltic reservoir are modelled with brine inside them. For the clastic and carbonate scenarios, the central crest structure (as shown in figure 4-7), known as the 'H' entity, is modelled with oil, while the other layers in the reservoir are assumed to be brine.

4-5-3 Environmental settings

Since the Shuaba Formation is found onshore, temperature and pressure distribution used are not influenced by a water layer and hence have not to be corrected to the water-bottom depth (ocean floor). The surface temperature is assumed to be 20 °C, with a gradient of 25 °C per kilometer. The pressure is 1 atmosphere at the surface, with a gradient of 1 psi/ft (22.6206 MPa/km).

4-5-4 Synthetic section

The synthetic section to be created with the same sampling rate as the seismic section (3 ms). The wavelet to convolve the acoustic impedance with is assumed to be zero-phase, with modelled frequency (one frequency per iteration). The seismic section as described in paragraph 4-5-1 will be transformed to a grid (matrix).

4-5-5 Layer geometry and area of interest (AOI)

The final, yet most important, assumption is the geometry of the layers. Although these are manually picked by the user, it is essential to pick the 'correct' horizons on the model, in order to get an 'expected' result. In seismic, the polarity of the amplitude of the reflections contains the information of the acoustic impedance contrast (convolved with the wavelet information). For the Shuaiba Formation case, where the overburden is (low porous) Nahr Umr Shale,

the first reflection of interest is on the boundary to the carbonate reservoir. Depending on whether this is a positive or negative pick, defines whether to model will try to resolve to carbonate layer as highly porous (negative pick) or less porous (positive pick). It therefore has to be emphasized that the results of the model may only be interpreted correct, if the user is confident that the geometry picked is correctly or at least likely.

Apart from the geometry, it is important to select the area of interest correctly. Since the model is trying to match all data within the area of interest to the area outside the AOI, a wrong selection of the AOI may result in faulty outcomes. The user therefore needs to pick all horizons in the section carefully, or select a smaller region (AOI) within the section. In the case of the Shuaiba Formation case study, the AOI has been set to be between the (picked) top and bottom horizon plus 0.5% on either side (to capture the entire amplitude of the upper and lower horizon).

The geometry picked for the Shuaiba Formation case study is similar to the interpreted horizons from previous studies (Lawrence et al., 2010; Yin et al., 2010; Yose et al., 2006). The horizons picked are shown in figure 4-7.

4-6 Objective function

The created synthetics (not visualized at each iteration) should be evaluated for their misfit with the seismic section using an objective function. After evaluation, optimization is used to draw new sets of model parameters to attempt to enhance the result (decrease the misfit).

The synthetic seismic section of the Shuaiba Formation is evaluated for its fit with respect to the actual seismic section using the HH-RMSE objective function as described in section 2-7. The motivation to use the HH-RMSE is the strong variation of reflections through the reservoir. The HH-RMSE is an absolute measure of the misfit between the observed and modelled data. If there is a polarity mismatch between the two, the error is double punished (both in the denominator and numerator). Still, large errors in the model also get punished harder than smaller errors, so strong reflections should be modelled better than noise, with the assumption the processing of the post-stack seismic section has been performed correctly. This will result in the largest amplitudes to be most prominently modelled throughout the section, but the normalization of the product of the two sets of data (observed and modelled) controls the impact of overemphasizing the largest reflections. On the other hand, noise gets slightly blown up, therefore it is important to have a good signal-to-noise data set using this objective function. Further advantages on the HH-RMSE error have been shown in Mentaschi et al. (2013).

For each simulation iteration, the objective function gets evaluated using each velocity model as described in paragraph 2-4-2. For the Shuaiba Formation case study, Sun's velocity model is excluded for clastic and basaltic scenarios (since Sun's velocity model is especially derived for carbonates). In case of a full carbonate simulation however, it may be used throughout.

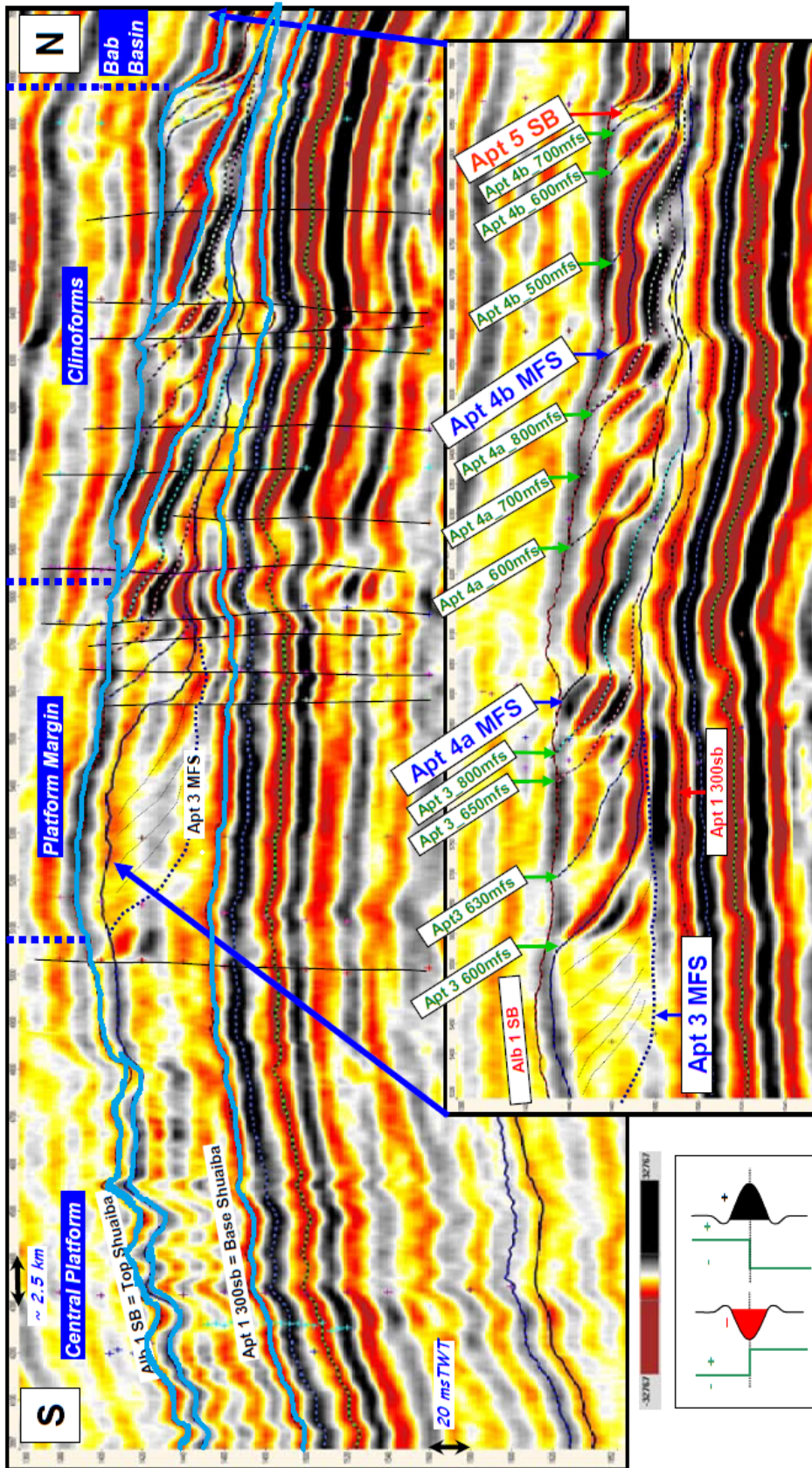


Figure 4-7: Shuaiba Formation horizons picked as in combined interpretations of Lawrence et al. (2010), Yin et al. (2010), Yose et al. (2006). The area of interest stretches from 0.5% of the nodes above the top horizon down to 0.5% below the bottom horizon.

4-7 Optimization updates

Either of the optimization tools explained in chapter 3 can be used for the purpose of seismic forward modelling, but different parameters should be defined. In this case-study, both of the optimization methods are used, in order to compare them to each other.

4-7-1 Particle swarm optimization modifications

The particle swarm optimization algorithm, as provided by Martínez et al. (2012), should be set such that it performs enough exploration to minimize the risk of focussing on a single local minimum. In paragraph 3-1-2, it has already been shown that CP-PSO allows most exploration, before exploiting local areas. To further enhance the exploration capabilities of the algorithm, Martínez et al. (2012) showed a variety of adjustments to PSO, in order to get a proxy of the posterior:

1. Set the PSO parameters (w , a_{local} , a_{global}) in the area of weak attraction or in the upper region of the second order stability (or even above).
2. Increase time step Δt to values greater than one if the swarm is stagnating (becoming too local oriented).
3. Introduction of repulsive forces when the mean distance of the swarm and the global best is less than a percentage of the initial dispersion. This is done by switching to negative acceleration constants.

These modifications are translated to the algorithm; the first modification is setting the initial inertia and acceleration parameters to the values of the upper region of the second order stability, as described in paragraph 3-1-2 and in Martínez et al. (2012), Prasad and Souradeep (2012). Furthermore, if the best fit has not increased by 1.5% for more than three iterations, the Δt becomes larger than one according to:

$$\Delta t_{i+1} = 1 + (1 - \Delta t_i) \quad (4-5)$$

After the Δt has been reset, it starts to slowly cool again starting with its original cooling gradient.

In addition to these two changes, repulsive acceleration forces become active if the mean distance of the swarm to the global best falls within 3%. The repulsion occurs at $-7.5 * a_{local}$ and $-7.5 * a_{global}$ and the Δt is reset to the original value (cooling of the swarm has been reset). After one iteration, the acceleration constants are set to the initial values, to prevent the particles to evolve into an infinitely diverging swarm. Different initial values for Δt may be applied for evaluation on the exploration capability of the PSO-algorithm.

4-7-2 One Rank Cuckoo Search parameter modifications

Within the ORCS algorithm, as provided by Tawfik et al. (2013), the stepsize should be suitable for the problem to resolve. Since the Shuaiba Formation case-study has wide constraints, the default step size of 0.01 (Tawfik et al., 2013) is unlikely to explore the search space fast enough. Therefore, the step size is increased to 0.3 for this case-study. This is still within reasonable, preventing too many particles to go out of the model space, which would be unfavorable as it would make the model more random at each iteration (potential divergence).

The other ORCS parameters (r_{bbb} , R_{or}) will initially be set to values either described in paragraph 3-2-3 or will be used as testing parameter for the ORCS performance. The latter of these are the probability of abandon ratio (p_a) and the one rank ratio update trigger (t_{or}), since these are likely to change the performance of the ORCS simulation, depending on the choice of value, as stated by Tawfik et al. (2013).

Simulation results and interpretation

The results in this chapter have been obtained through various simulations using either of the two optimization tools. Multiple simulations have been performed with different optimization specific parameters as described in paragraph 4-7. The parameters used are summarized in table 5-1.

Analyzing the simulations, it was quickly found that the Sun model consistently overestimates the porosity. Referring back to figure 4-3, this may be due to the very slight decrease of velocity with porosity: when increasing porosity from 10% to 50%, p-wave velocity only decreases from $\approx 4100m/s$ to $\approx 3500m/s$. Although correlations between data sets and this type of relation have been found (Sun, 2000), it may be unsuitable for modelling carbonates in general with. Therefore, the results in this section have been computed from the RHG-, GGG- and WGG-relations only. Computations using only the Sun-relation may however be found in appendix C.

Optimization	CP-PSO	ORCS
Swarm size (samples)	25	25
Iterations (per scenario)	125	125
Total tested models	28125	28125
Stepsize (Δt)	0.95 - 1.15 (cooling)	0.3 (update step)
P_a	not used	0.25 - 0.45 - 0.75
t_{or}	not used	0.03 - 0.10

Table 5-1: Tested optimization parameters for Shuaiba Formation case-study.

The results shown in this chapter use ORCS parameters $P_a = 0.25$ and $t_{or} = 0.10$ and PSO parameter $\Delta t = 0.95$ (since these have been suggested by the authors and yield the best results). All other simulations may be found in appendix A and B.

The results have been classified in mineralogy probability and porosity probability scenarios (as explained in paragraph 4-4-1 and 4-4-2). The distribution of probable mineralogy scenarios for ORCS and PSO is shown in figures 5-1 and 5-8, respectively. For the mineralogy, the model gives an output to the condition: given a mineralogy scenario with porosity values within predefined limits, how often does the result show up within the 10% best misfit values (as measured by the objective function) after one entire simulation (swarm size and iterations as shown in table 5-1).

The scenarios shown are those within 10% of the best misfit found for all (9) simulations. The y-axis shows the amount of occurrences for each of the (3) scenarios of carbonate, clastic and basalt that are found within this criterium. They are classified by simulation of upper porosity bound (as described in paragraph 4-4-2). The legend percentages represent the total output per mineralogy scenario, regardless of the upper porosity bound. These numbers thus indicate the probability (P) of finding a certain type of mineralogy (S_m) after a predefined amount of tested sample evaluations: $P(S_m)$.

After achieving probability values for different types of mineralogy, a same approach on porosity is performed. However, before being able to find probability values for porosity, they should be distinguished in porosity scenarios (just as the mineralogy scenarios). The categorization of porosity scenarios occurs per mineralogy, to be able to see the difference in porosity with respect to the mineralogy. Within all the samples that have satisfied the condition of being within the 10% of the best objective function value, the porosity distributions are separated with respect to their mineralogy. The conditions for distinguishing porosity scenarios from each other in this particular case-study then proceeds as:

1. Take the first two porosity distributions (within one mineralogy setting).
2. For every node in the AOI, verify if the porosity varies more than 3% between those porosity distributions.
3. If the node varies more than 3%, assign node as not being the same. If the node varies less than 3%, assign the node as the same.
4. If more than 10% of all nodes in the AOI are assigned as 'not the same', save the scenario distribution as a new scenario. If less than 10% are assigned as 'not the same', save the porosity distribution as being the same.
5. Proceed to the next sample (porosity distribution) and repeat steps 2-4. Continue this process until all porosity distribution samples have been evaluated (i.e. until all samples have been compared to all scenarios).
6. Proceed to the next mineralogy and repeat steps 1-5 until all mineralogy settings have been evaluated.

Having distinguished all scenarios, probability is calculated for each of the scenarios. This is done by counting the amount of samples that are classified as the 'same' within each scenario and dividing it by the total scenario samples within the mineralogy. By pre-division of the porosity scenarios to their respective mineralogy scenario however, the probability measured implicitly becomes a conditional probability instead of the probability of an independent

event. The conditional probability of achieving the specific porosity scenario (S_ϕ), given the mineralogy would be 'known', may then be defined as:

$$P(S_\phi|S_m) = \frac{P(S_\phi \cap S_m)}{P(S_m)} \quad (5-1)$$

Note that the upper constraints of porosity are taken together here in calculating the probability. This done because the aim is to find the probability of a certain porosity distribution and not the probability of finding a good solution depending on the upper boundary (this, indirectly, is already visualized in the mineralogy probability distributions (figures 5-1 and 5-8)).

Since these probabilities are measured within their respective mineralogy setting, one additional step is made to achieve the definition of the probability of finding an actual porosity distribution together with a certain mineralogy. This probability is obtained by rearranging equation 5-1:

$$P(S_\phi \cap S_m) = P(S_\phi|S_m)P(S_m) \quad (5-2)$$

The probability value found using equation 5-2 is shown in the headers of each scenario in figures 5-2 and 5-9. This thus indicates how likely each of the porosity distributions shown is, if it also belongs to the mineralogy distribution meant in the corresponding header.

The technique on evaluating porosity and mineralogy as described above is found suitable for this particular research, since it gives an overview of probability values of a certain mineralogy combined with a certain porosity distribution. One could also think of other evaluation and selection criteria however (techniques as Bayesian inference), to calculate and interpret likelihood for all scenarios for example. These and other quantitative interpretation techniques may be applied and validated in future research.

5-1 ORCS simulation results

5-1-1 Mineralogy

Figure 5-1 shows the distribution of well-fitting mineralogy models (HH-value 1.05-1.155). The model clearly favors carbonate scenarios (80.04%) over clastic (13.16%) and basaltic (6.80%) scenarios. As expected, the 50% upper bound porosity simulations result in larger amounts of fitting results, as the model has more freedom than with the lower bounds.

5-1-2 Porosity

In figure 5-2 the three most probable porosity scenarios for each mineralogy are shown. There may be more (but less) probable porosity scenarios per mineralogy, but these are not shown for visualization purposes.

Figure 5-2 shows the most probable scenario for porosity is found in a carbonate, where porosity ranges from 15%-26%, with the exception of the first clinofom, which has porosity values ranging between 5%-15%. The velocity relation most used for this porosity mode is the GGG-relation (eq. 2-5). The other two (less) probable porosity scenarios are found using the WGG-relation (eq. 2-6). There is a significant difference between porosity mode 1 and porosity mode 2 and 3 for the carbonate mineralogy. Whereas the GGG-relation finds lower porosity in general, the WGG-relation finds porosity ranging from 15%-35% (with exception of the low-porous first clinofom (5%-15%).

In overall, it may be observed that the porosity in basalt is much higher than the other two mineralogy scenarios (ranging from 20% to 40+%). When looking at the residuals (figure 5-2)- which are calculated using the best synthetic match of each of the nine scenarios and are then compared to the actual seismic section - the basalt scenarios match worse than the carbonates, suggesting basalt scenarios are less probable.

Figure 5-3 shows the residuals of the three carbonate scenarios do not vary significantly. When combining the concept of figure 5-2 and figure 4-3, this may be caused by the different relation used for carbonate porosity mode 1 to carbonate porosity scenarios 2 and 3. Whereas the GGG-relation generally finds lower velocity at lower porosity than the WGG-relation does. Therefore, the WGG-relation applies higher porosity to find the same velocity (and hence the same acoustic impedance).

When comparing the residuals of the carbonate porosity scenarios to the clastic ones, one may observe that the overall trend is similar. All probable clastic scenarios use the WGG-relation, therefore having similar velocity ranges as the carbonate porosity scenarios 2 and 3. The porosity in clastic scenario 1 is much higher than any of the carbonate scenarios, whereas the other two are slightly lower overall. Based on the residuals, the clastic scenarios may not be much worse than the carbonate scenarios, but many more carbonate scenarios have made it within the 10% error margin. The basaltic scenarios generally show a larger mismatch with the seismic section, especially on the left side of the section and in the clinofoms.

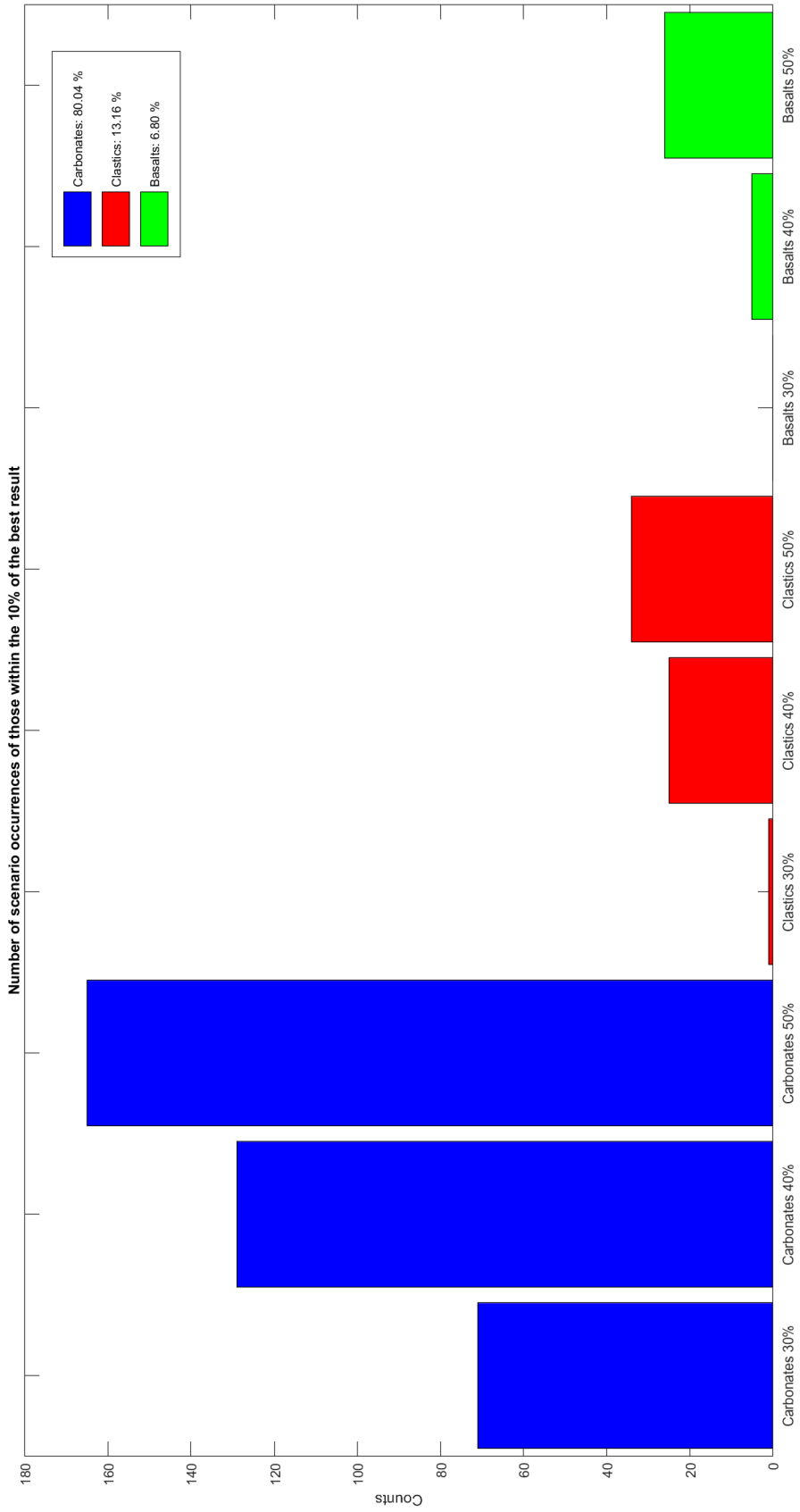


Figure 5-1: Probable mineralogy scenarios for Shuaiba Formation using One Rank Cuckoo Search. Parameters for ORCS: $P_a = 0.25$, $t_{or} = 0.10$. Scenarios are obtained after counting outcomes within 10% of the best results after the entire simulation has finished (HH-value range: 1.05-1.16).

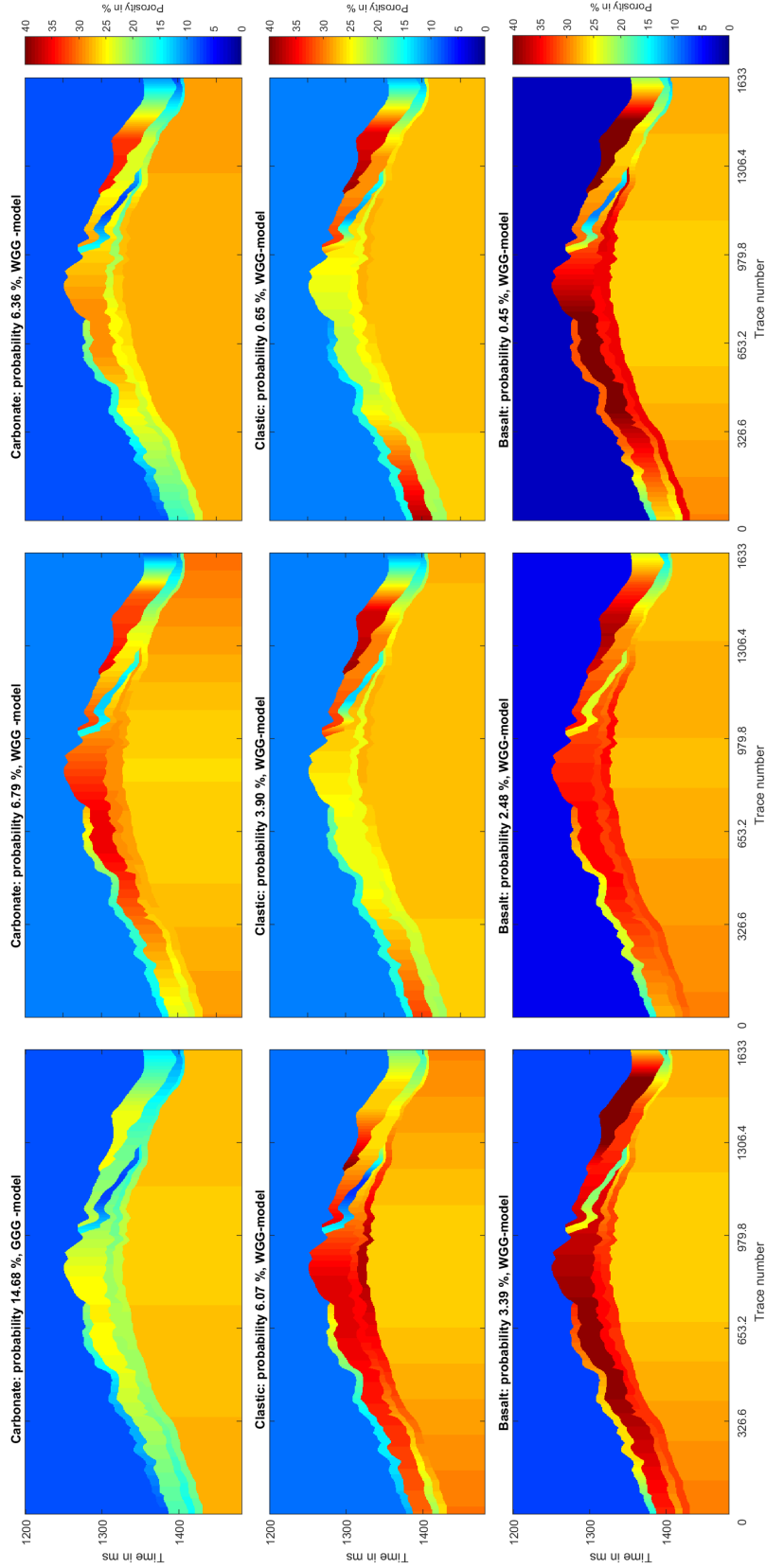


Figure 5-2: Probable porosity scenarios for Shuaiba Formation using One Rank Cuckoo Search. Parameters for ORCS: $P_a = 0.25$, $t_{or} = 0.10$. The scenarios show probability (based on their occurrences) and the most used velocity model to create the scenario.

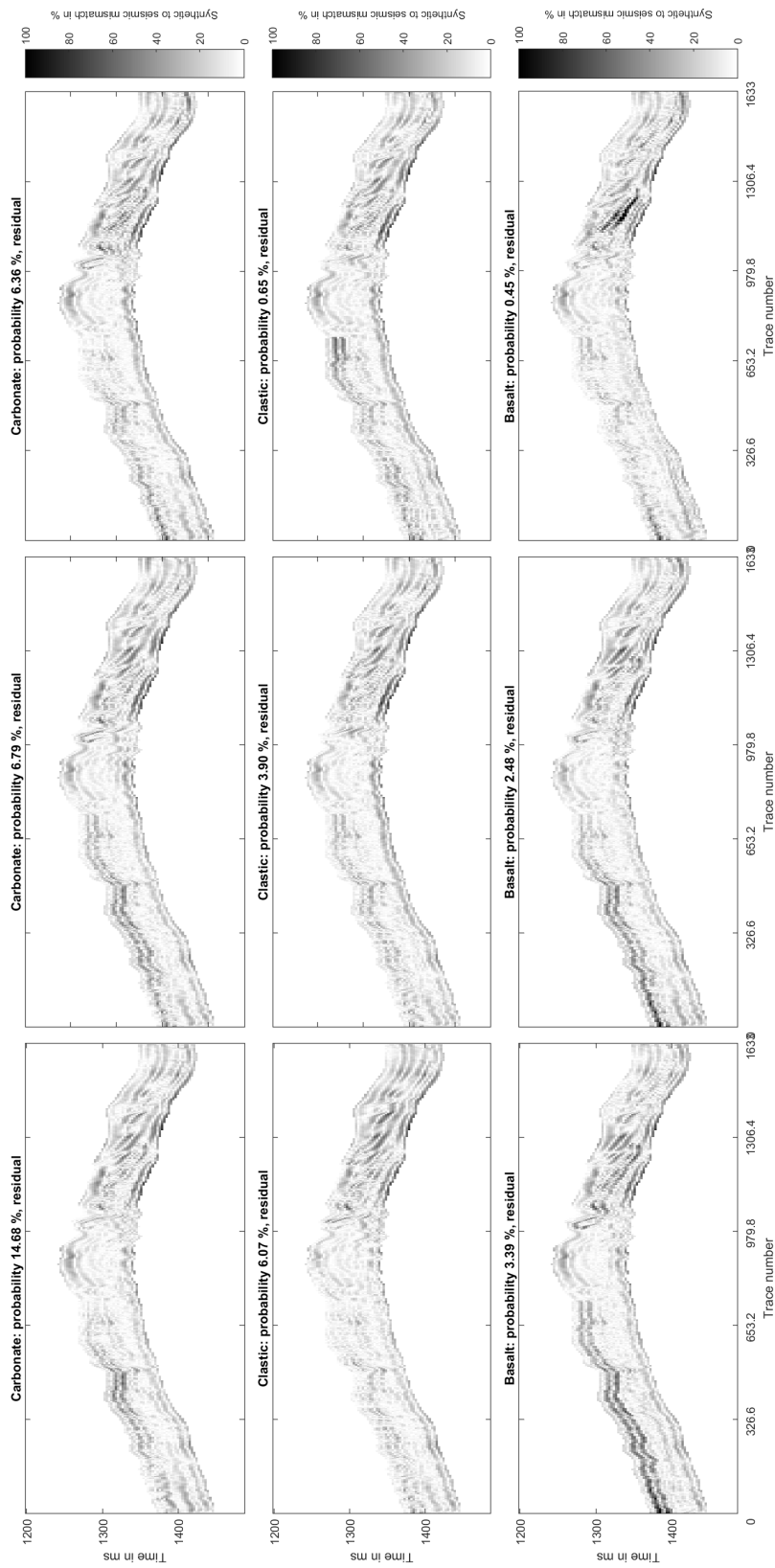


Figure 5-3: Residuals of porosity scenarios for Shuaiba Formation when comparing synthetic to seismic using ORCS. Mismatch is the absolute deviation between the seismic section and the synthetics and is shown relative to the strongest amplitude in the seismic.

5-1-3 Overburden dependency and uncertainty

Apart from the dependency on the velocity relation used, the overburden is of great importance, since it determines the effect on the initial reflection (top of the reservoir). The porosity in the overburden has a degree of freedom ranging from 0% to 15%. Since the mineral density of the Nahr Umr shale is assumed to be constant, the effect of porosity of the overburden with respect to the porosity in the top layer can be correlated. To do so, three points of reference have been selected (in three different entities) to see if there is a correlation on either side of the vertical layer boundary. The points selected are shown in figure 5-4.

Figure 5-5 shows the dependency of the three entities on the porosity in the overburden by measuring the correlation.

For neither of the three points, a significant correlation coefficient is found. The porosity in the top reservoir layers is only explained by the overburden porosity by 26%-33%. The overburden thus has a limited impact on the reservoir porosity, if a reasonable assumption is made. The effect may grow larger if the amount of freedom in the overburden is larger. It is therefore important to apply some prior knowledge of the overburden, in order to achieve reasonable results.

Additionally, the statistics of the entire model may be evaluated. Standard deviation and entropy measurements are used to validate the existence of different scenarios. Standard deviation however, is only valid if the values it is measured over show a Gaussian distribution. As shown in figure 5-6, the standard deviation of the carbonate scenarios is too small (averaging at 5%-6%) to explain all different scenarios, which have a spread of more than 10% in many places. This may be caused due to multi-modality of the porosity scenarios and suggest the spread is not Gaussian.

To validate this hypothesis, entropy is used to measure the modality in the results. To measure entropy, the porosity range is classified in eight different 'discrete' intervals of 5% (range of 0%-40% in the carbonate models). The entropy equation is applied on each node. At each node, the entire assembly of probable porosity scenarios is evaluated and classified in the 5% intervals. Using the amount of occurrences of each porosity interval at each node, the probability of each 5% interval at each node is found (Wellmann & Regenauer-Lieb, 2011). These probabilities may then be used to calculate entropy (Wellmann & Regenauer-Lieb, 2011):

$$H(i, j) = - \sum_{n=1}^N p_n(i, j) \log(p_n(i, j)) \quad (5-3)$$

Where N is the amount of possible intervals (8) and i and j are the coordinates of the node within the model. The logarithm has a base of 2, determining the porosity found in each sample either fits the interval or not. The amount of bins present is 8, so the maximum entropy found is $\log_2(8) = 3$. An entropy of 3 means the node has a maximum uncertainty and may fit equally well in each 5% porosity interval. An entropy of 0 means it only matches one interval (Wellmann & Regenauer-Lieb, 2011). Figure 5-7 shows the entropy in the reservoir is around 2, suggesting there are $2^2 = 4$ possible outcomes. This confirms the standard deviation cannot be interpreted correctly, since the model is indeed multi-modal.

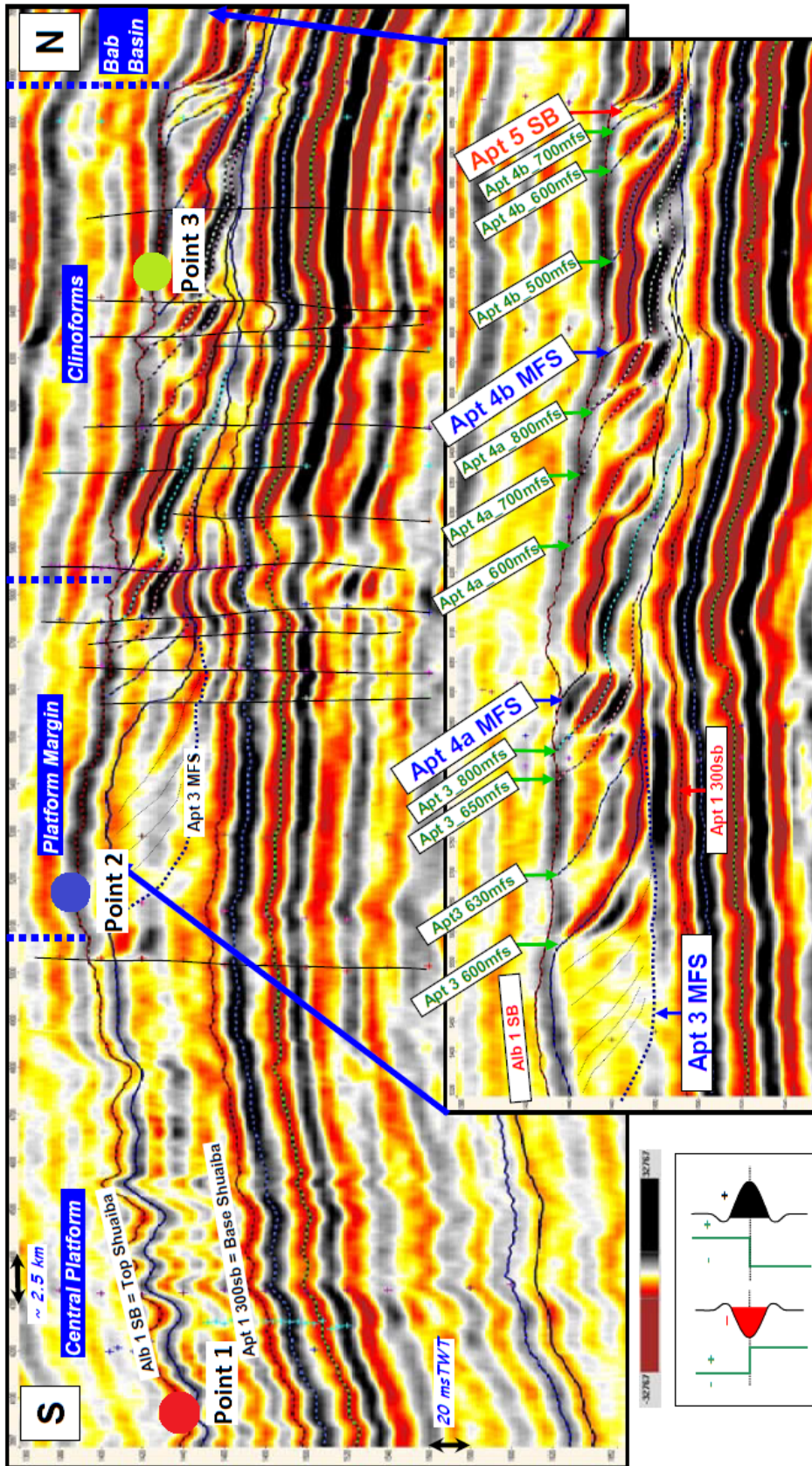


Figure 5-4: Three correlation points on the Shuaiba section to verify if the reservoir porosity is dependent on the overburden porosity.

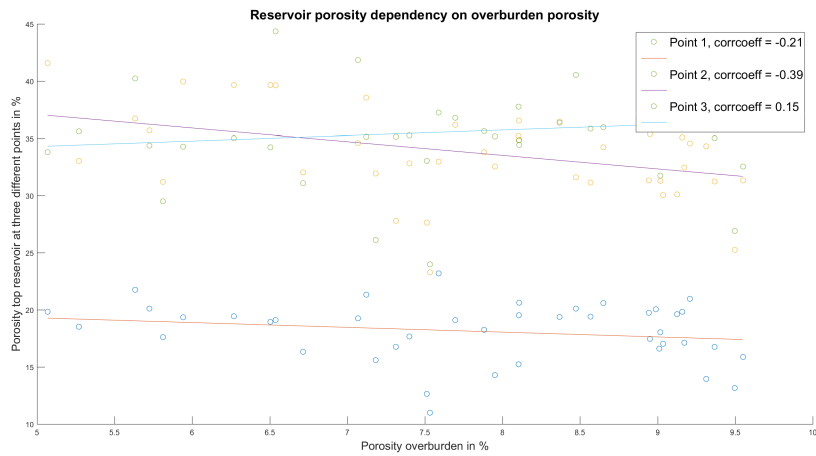


Figure 5-5: Correlation between overburden and reservoir porosity at three points (location of points is shown in figure 5-4 for the ORCS-optimizer).

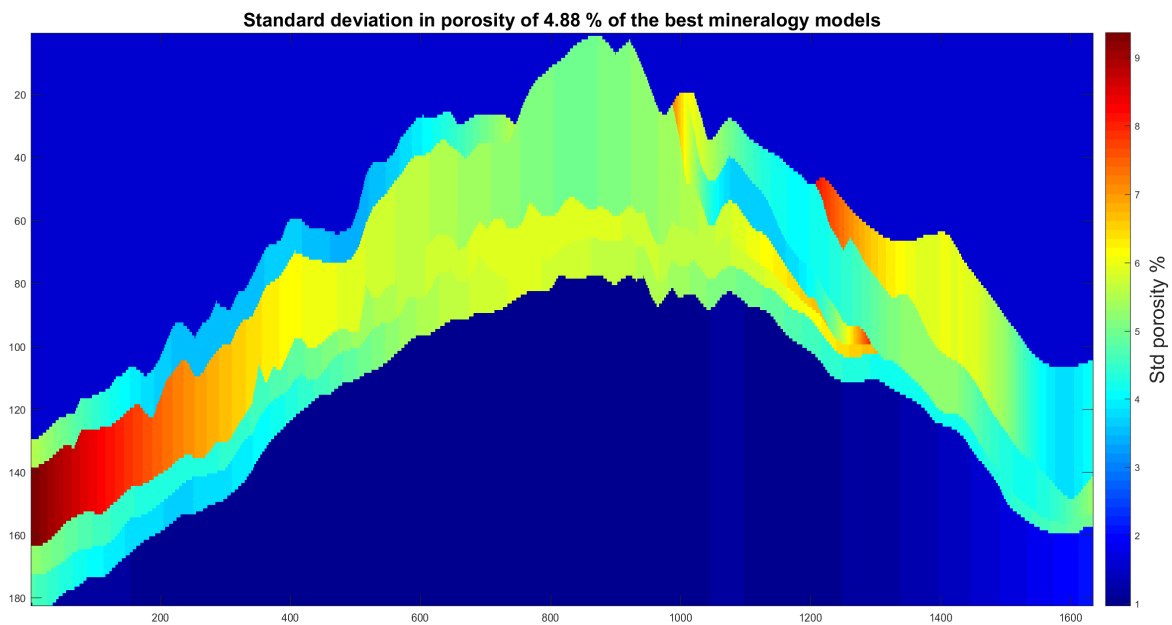


Figure 5-6: Standard deviation for carbonate models using ORCS. The standard deviation is much smaller (averaging at 5%-6%) than the spread between the two probable scenarios (> 10% in most of the layers). This may be explained due to the presence of multi-modality.

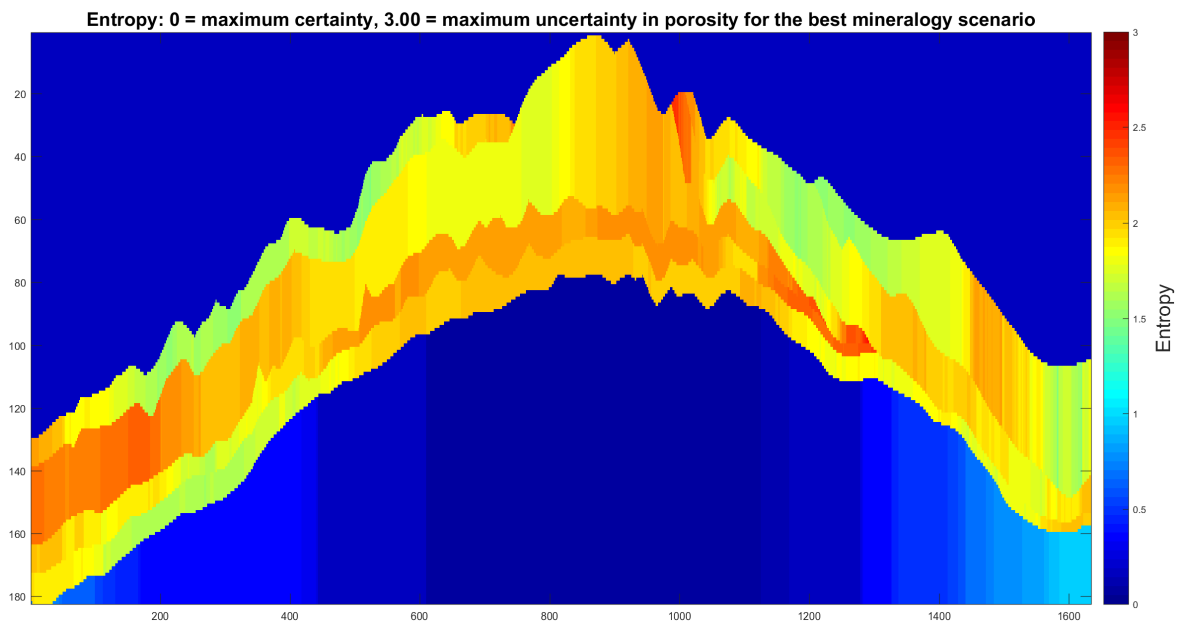


Figure 5-7: Entropy for carbonate models using ORCS. The entropy averages around 2, suggesting there are 4 probable outcomes for porosity throughout the assembly of possible porosity scenarios. This confirms the presence of multi-modality and suggests the standard deviation is not Gaussian.

5-2 CP-PSO simulation results

5-2-1 Mineralogy

The CP-PSO method results, as shown in figure 5-8, shows a more divided mineralogy spread (HH-value range:1.05-1.15). PSO still favors carbonates (46.34%), but basaltic scenarios also show abundant probable scenarios (42.68%). Clastic scenarios are almost equally probable as in the ORCS simulation (10.98%). What is interesting, is the basaltic scenario with a porosity freedom of 1%-40%, since it occurs more often than the basaltic scenario with a freedom of 1%-50%.

5-2-2 Porosity

When looking at the probable porosity scenarios (figure 5-9), the most occurring scenarios within the entire assembly are a carbonate model (8.23%) with porosity ranging from 8% > 40% and a basaltic scenario (9.10% with porosity ranging between 12% and 40%. This is different from the outcome of the ORCS simulation. The difference in probability with the next carbonate and basalt scenarios is fairly small however (< 1%). Therefore, it seems that PSO is less definitive about the outcomes. When observing the residuals, it is clear that the first carbonate porosity model has smaller residuals in general than the second one. Both fit the 10% error margin, but potentially the best few are found in the second porosity output. This emphasizes why it is important to validate the residuals as well as the probability of occurrence.

The clastic scenarios show a generally small occurrence in the total output, but still should not entirely be discarded when looking at the residuals. These fit quite well, with the exception of the the left top reflections, which show a large misfit.

Within the basalt scenarios, the first and second perform the best when combining the residual plot with the probability plot. The residuals fit roughly equally well as the carbonate (second scenario) one. In overall, carbonate scenario 1 and basalt scenario 1 seem the most probable when combining figures 5-9 and 5-10.

One should however be cautious in interpreting the basalt scenarios when observing figure 4-5. The high porosity occurring in the scenarios come from the extrapolated area of the WGG-relation (eq. 2-6). The carbonate output is found using the RHG-relation however (eq. 2-3). The porosity found in this plot are mostly in the range below the extrapolated region (with exception of the upper right reservoir layer) and could therefore be interpreted with more certainty.

5-2-3 Overburden dependency and uncertainty

Equally to the ORCS simulation, overburden porosity dependency in the top reservoir level is evaluated at the three points shown in figure 5-4. The correlation between the porosity in the overburden top layers of the reservoir at these three points (in carbonate mineralogy) are shown in figure 5-11.

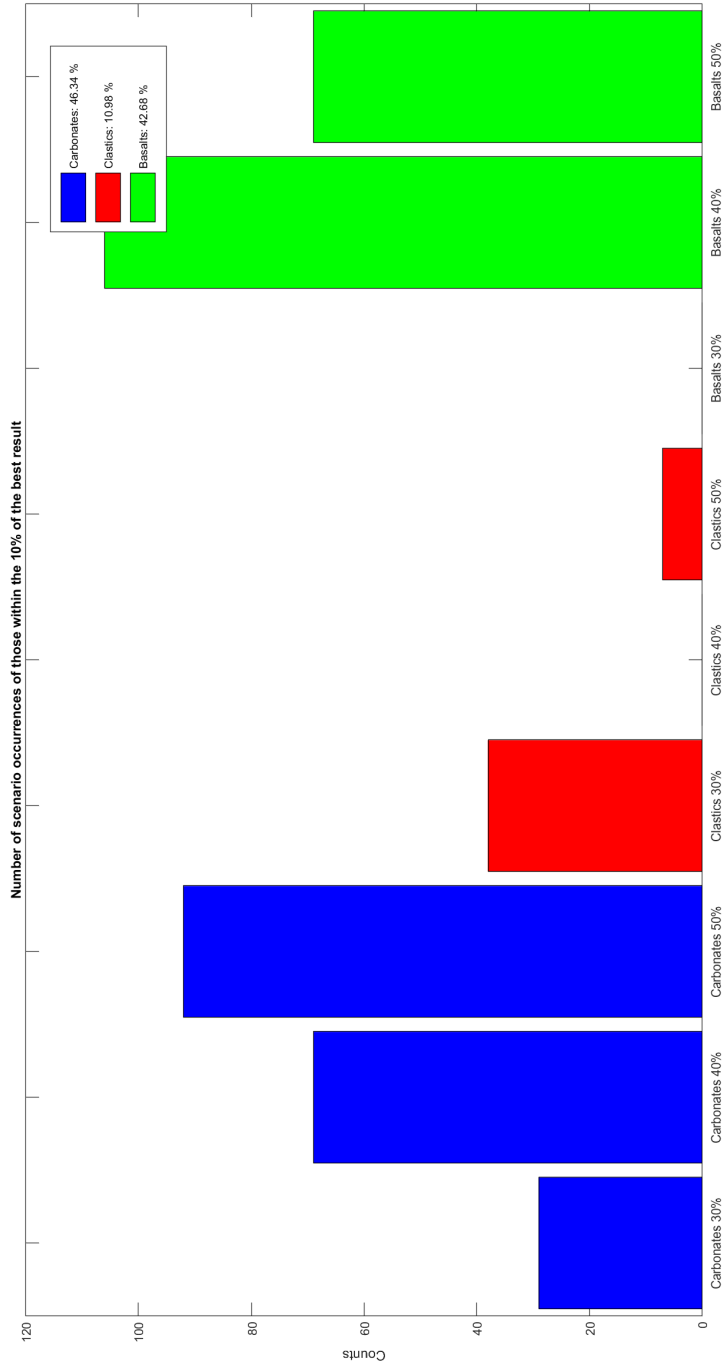


Figure 5-8: Probable mineralogy scenarios for the Shuaiba Formation using Centered-Progressive Particle Swarm Optimization. Parameters for PSO: $\Delta t = 0.95$. Scenarios are obtained after counting outcomes within 10% of the best results after the entire simulation has finished (HH-value range: 1.05–1.16).

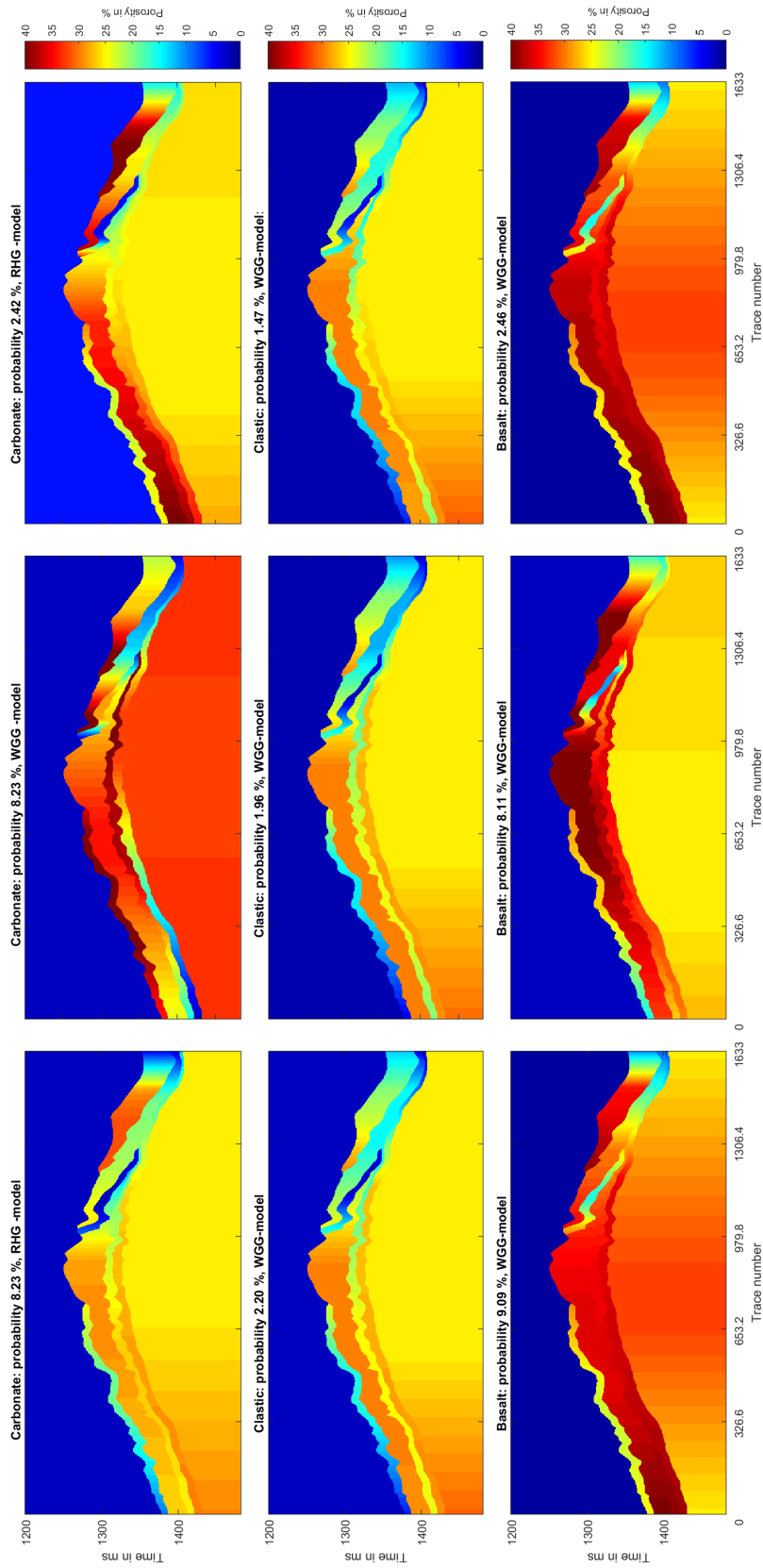


Figure 5-9: Probable porosity scenarios for the Shuaiba Formation using Centered-Progressive Particle Swarm Optimization. Parameters for PSO: $\Delta t = 0.95$. The scenarios show probability (based on their occurrences) and the most used velocity model to create the scenario.

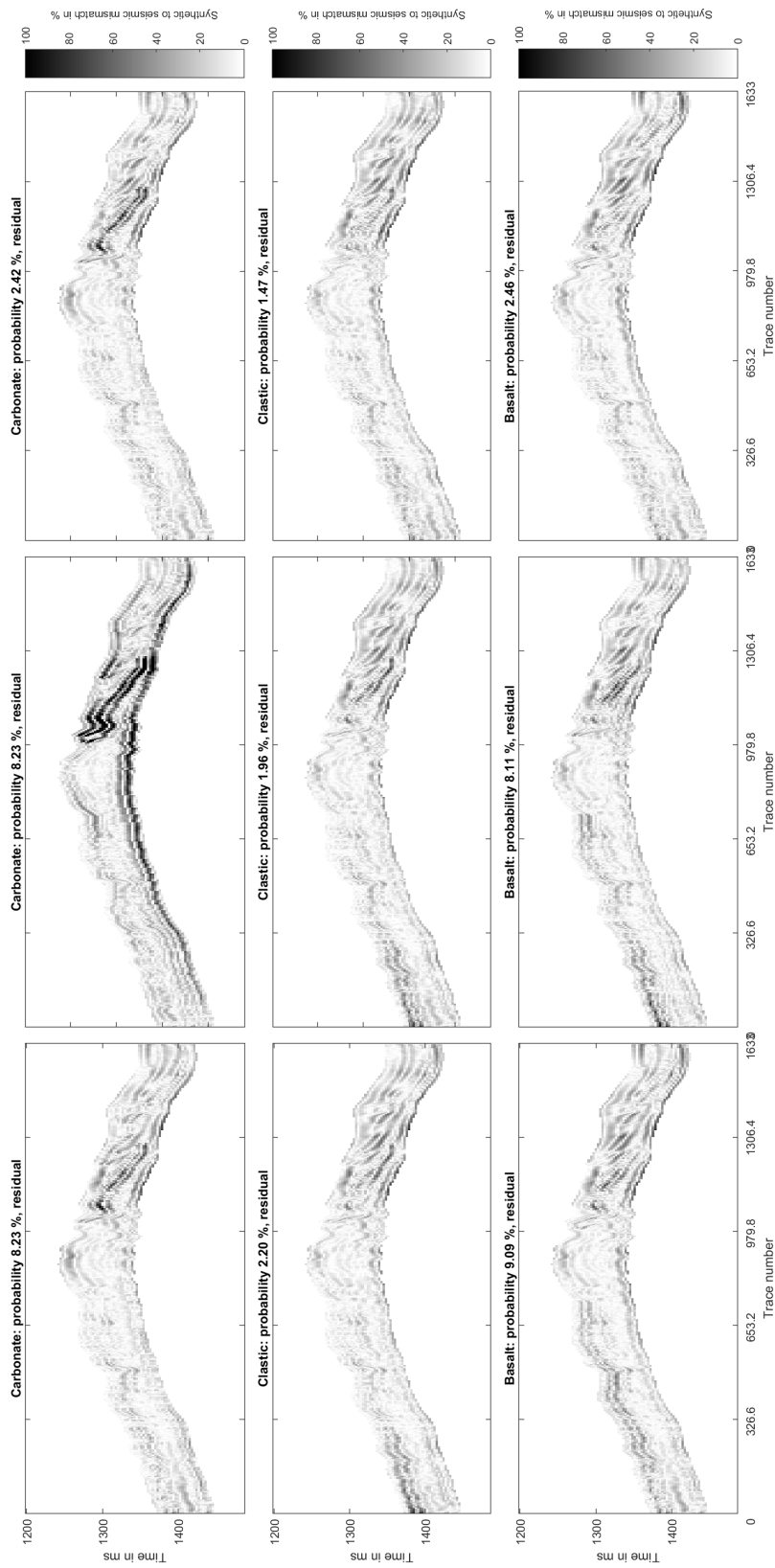


Figure 5-10: Residuals of porosity scenarios for the Shuaiba Formation when comparing synthetic to seismic using PSO. Mismatch is the absolute deviation between the seismic section and the synthetics and is shown relative to the strongest amplitude in the seismic.

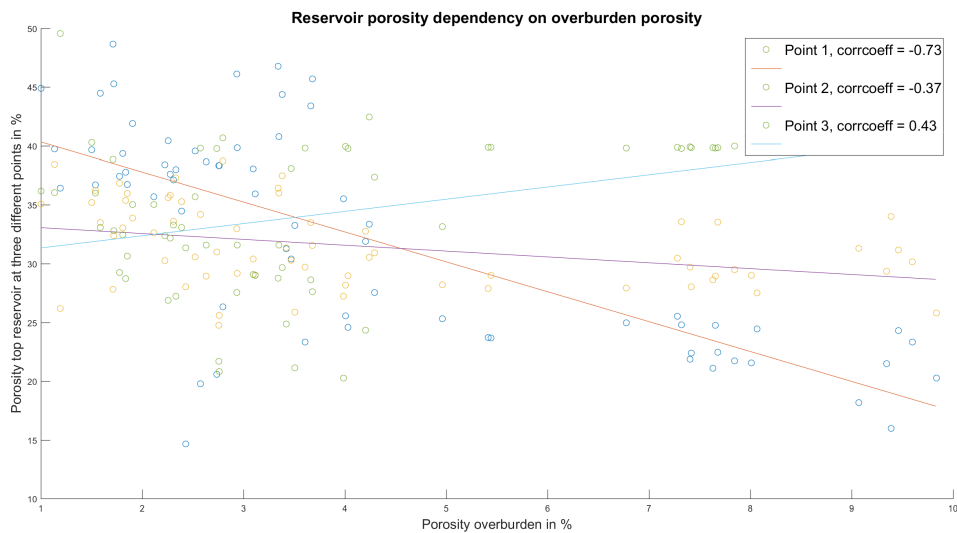


Figure 5-11: Correlation between overburden and reservoir porosity at three points (location of points is shown in figure 5-4 for the PSO-optimizer).

Like the ORCS simulation, the PSO simulation does not find a strong trend on the overburden porosity with respect to the top reservoir layer porosity for points 2 and 3 (37%-43% dependency). Point 1 however shows a stronger dependency (73%), which should be considered when interpreting the scenarios.

Similar to the ORCS simulation, one would expect a multi-modality in the porosity outcomes, as can be seen in figure 5-9. This would imply again that the standard deviation is non-Gaussian and should underestimate the error found between the different probable scenarios, which is confirmed when observing figure 5-12.

When applying entropy on the model assembly again (Wellmann & Regenauer-Lieb, 2011), the multi-modality may be further confirmed. Figure 5-13, just as in the ORCS-simulation (figure 5-7), confirms the multi-modality of the model and a single definitive interpretation of one porosity outcome is unlikely without applying prior knowledge or further constraints.

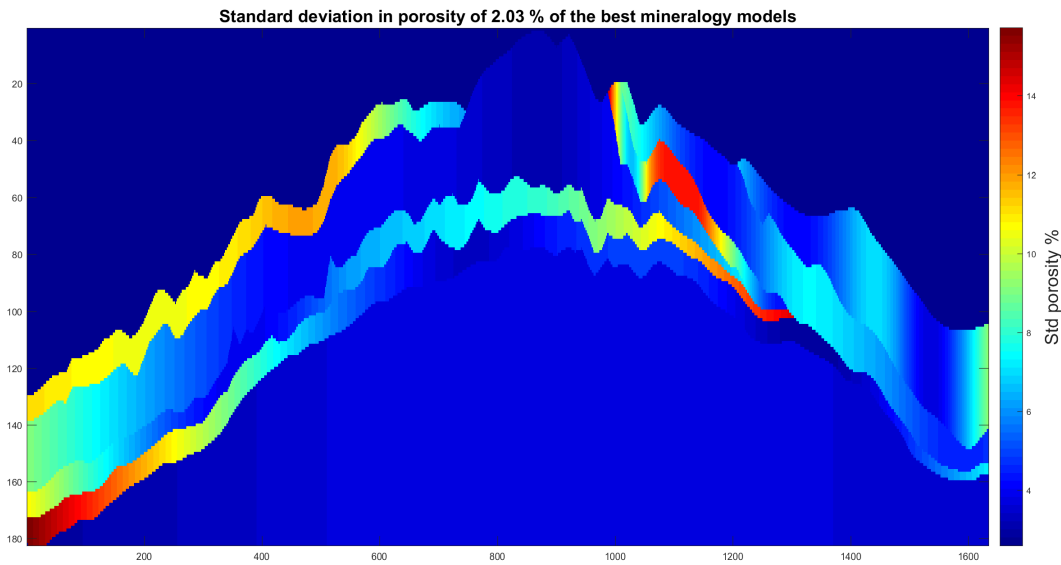


Figure 5-12: Standard deviation for carbonate models using PSO. The standard deviation is smaller (averaging at 6%-14%) than the spread between the two probable scenarios (10%-20% in most of the layers). This may be explained due to the presence of multi-modality. Interestingly, the standard deviation is smaller (5% - 6%) in the clinoforms, which can be traced back in the difference in the porosity scenarios (10% difference (with smaller areas still varying up to 20%)).

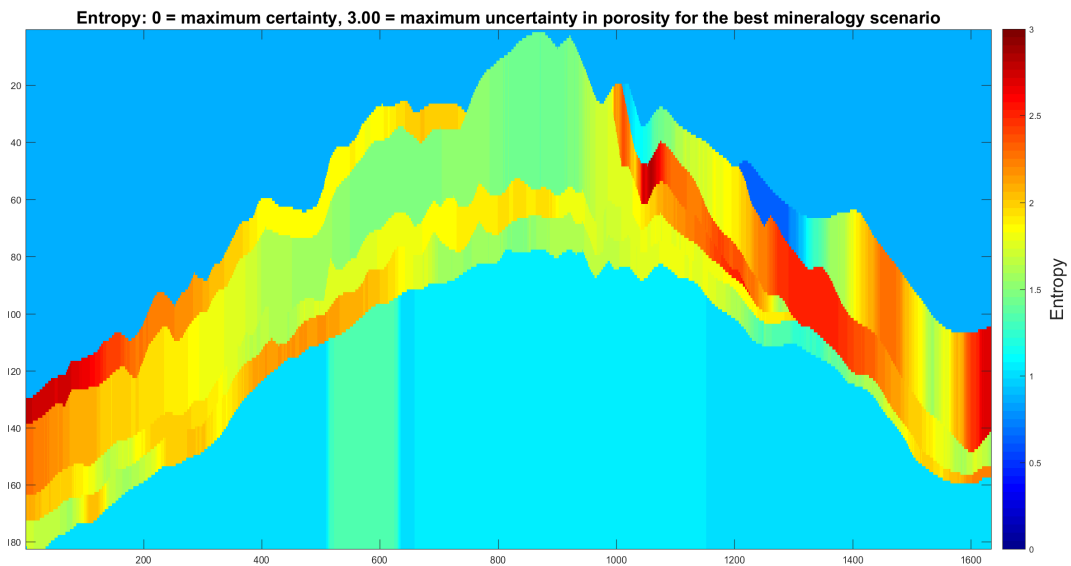


Figure 5-13: Entropy for carbonate models using PSO. The entropy averages around 2, suggesting there are 4 probable outcomes for porosity throughout the assembly of porosity scenarios. The entropy is found to only be around 1.5 in the clinoform areas however, suggesting there are nearly 3 equally probable outcomes for the clinoform porosity, which is in agreement with the smaller standard deviation and porosity spread shown in the probable scenarios (figures 5-12 and 5-9). The entropy confirms the presence of multi-modality and suggests the standard deviation is not Gaussian.

5-3 Seismic parameters

The wavelet frequency found by the model varies between 37 Hz and 42 Hz for both the ORCS simulation and the PSO simulation. The scaling of the amplitude between the synthetic and the seismic ranges from $8.45e^4$ to $9.2e^4$ for the ORCS-simulation and $8.25e^4$ to $9.5e^4$ in the PSO-simulation. The frequencies are slightly higher, but still in accordance with prior research by Yin et al. (2010), whereas the scaling factor is assumed to be correct by the visual comparison of synthetic sections to seismic sections. Figure 5-14 shows such a visualization, which may be compared to figure 4-6.

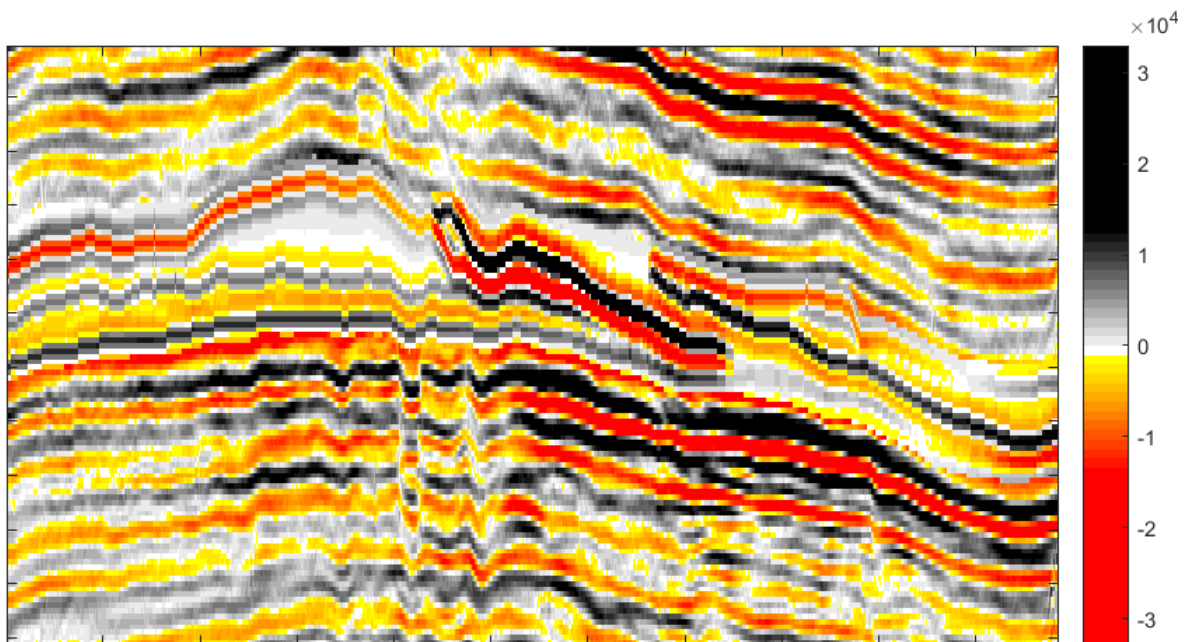


Figure 5-14: Scaled synthetic (sub)section of the Shuaiba Formation. Note the reservoir reflection strength is in the same order as the seismic section (between 0 and $3.3e^4$).

Part III

Discussion, recommendations and conclusion

Chapter 6

Discussion

6-1 Optimization comparison

With the results of the PSO and ORCS simulation created, the optimizers may be evaluated on their capability of solving mineralogy and porosity in seismic forward modelling. From chapter 5, the ORCS-optimizer shows a more definitive mineralogy solution (carbonates) than PSO (carbonates-basalts). Also, in terms of porosity models, the ORCS-optimizer is more certain about a single scenario than PSO (four probable scenarios). In general, the scenarios found by PSO show a slightly higher porosity and a larger contrast between the layers. When comparing the two, ORCS seems to take a broader range of possible values for each parameter into account. When looking at the objective function evolution (figures 6-1 and 6-2), the difference in nature of the algorithms is visible. Whereas ORCS always keeps its best result and updates it into a next generation by modifying the parameters (like MCMC), PSO may discard its best solution and find a complete new set of solutions, not necessarily better than the previous set at all. PSO requires to perform this 'bouncing' behavior through the model space by dispersion and conversion of the swarm, in order to achieve enough exploration. ORCS however, with its nature of keeping only the best samples and replacing the worst at the same time, incorporates the exploration while exploiting local areas for better results at the same time. Therefore, as shown in figures 6-1 and 6-2, the evolution of the objective function (misfit) with iterations is much less smooth for PSO than it is for ORCS.

From figures 6-1 and 6-2 it may be observed that the PSO converges faster initially than the ORCS. However, the PSO hits a plateau, whereas the ORCS continues to decline with a shallow slope. The initial slower convergence of the ORCS optimization may originate from its behaviour of maximum exploration and exploitation in the beginning of the simulation (as described in paragraph 3-2-3. This allows the algorithm to explore a wider range of samples initially, before it converges and explores more local areas. At the expense, the changes of finding samples with a small misfit is less likely in this phase. The PSO may, depending on the initial samples drawn, converge more rapidly and then tries to disperse the swarm again to find other possible minima. This is slightly more prone to being stuck in a local minimum however, if the dispersion rate is not large enough or the local minimum is very large. When

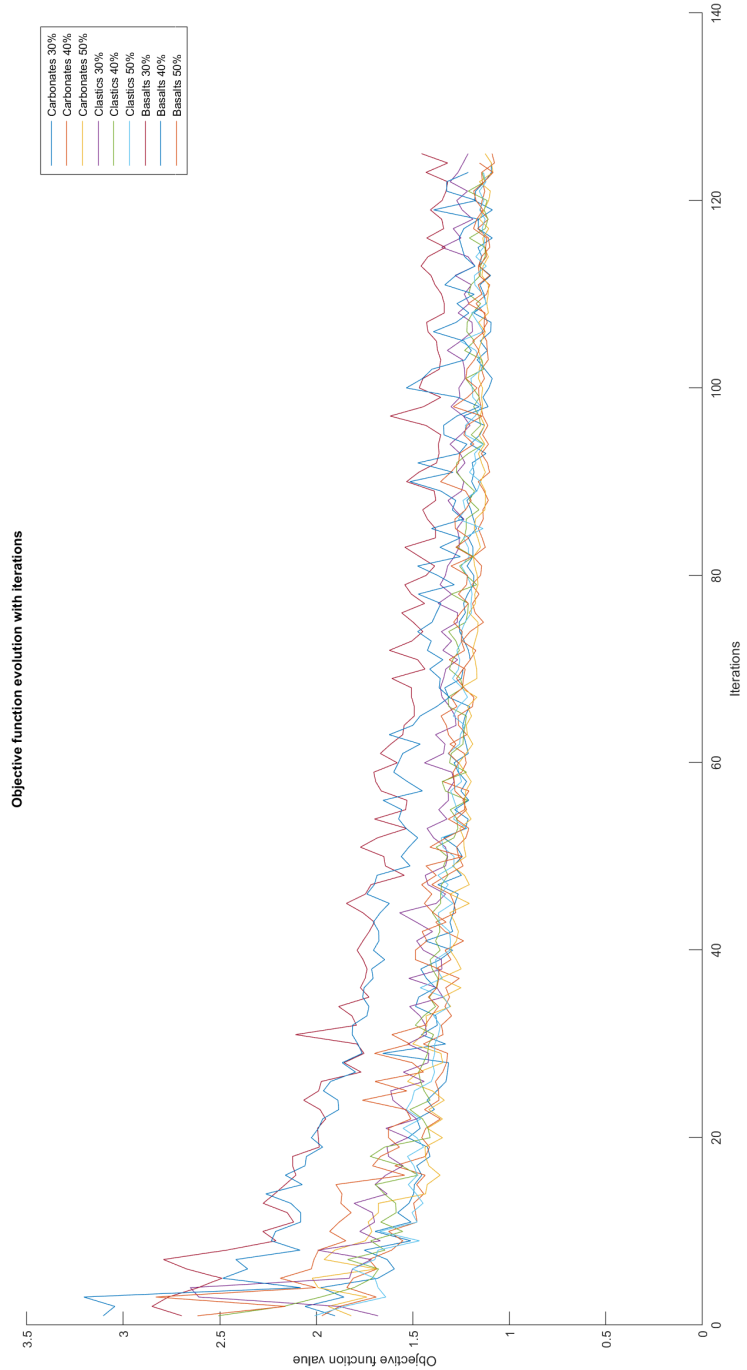


Figure 6-1: Smallest misfit found per iteration for the entire simulation using ORCS.

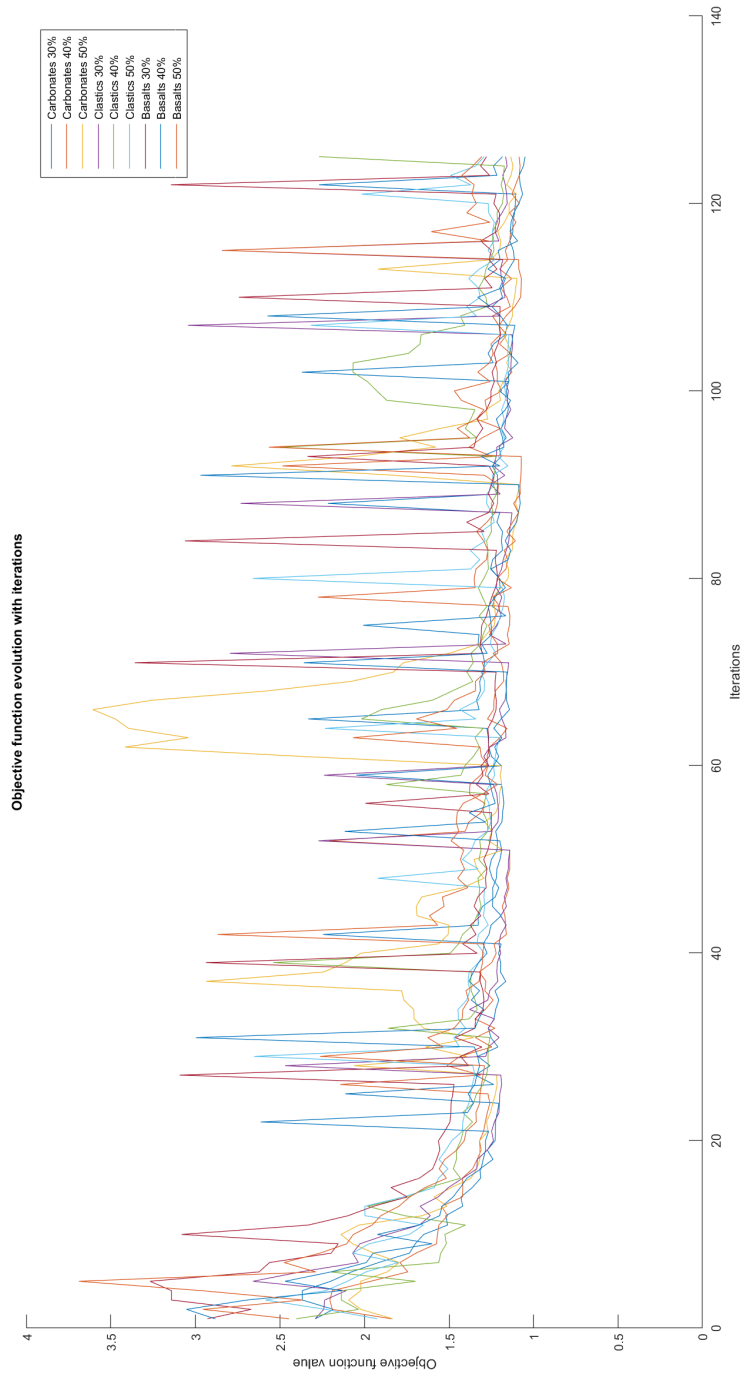


Figure 6-2: Smallest misfit found per iteration for the entire simulation using PSO.

sorting the objective function values per iteration of the two simulations, the behavior of the two optimizers is better visualized (figure 6-3 and 6-4).

The plateau reached by PSO is visible for more than 80 iterations (not necessarily the last 80), whereas the ORCS clearly shows a (though shallow) slope, suggesting the model is converging slower but more continuously. Although complete convergence is not reached in figure 6-3, one could see new iterations do not decrease the objective function value significantly anymore (therefore, the simulation may be cut at this point).

The final HH-RMSE values for the 10% best solutions for both simulations range from $\approx 1.05 - 1.155$. However, while arriving at this objective function value range, the ORCS has potentially evaluated more areas of the model space, therefore it is more likely to come up with reasonable results. This is in accordance with results from research performed in the financial world, where both methods (and others) have been tested and verified (Adnan & Razzaque, 2013; Civicioglu & Besdok, 2011; Singh & Singh, 2014). In forward seismic modelling, the effect of 'infinitely smaller' misfits is not necessarily required in all cases however and if one would purely observe convergence, PSO seems the more robust technology, as it achieves smaller misfits faster than ORCS.

When looking at large, poorly-constraint modelling problems however, where exploration is most important, ORCS proves to be the more trustworthy optimization tool of the two. In the end it finds slightly better results than PSO, which for this case-study (since computation time is not the first priority) is the preferred approach.

In general, the tools are a good addition to the current 'golden-standard': MCMC-techniques. Whereas MCMC has a strong capability of updating certain parameters by posterior sampling, it is more prone to get stuck in local minima for large poorly-constrained problems (Sambridge & Mosegaard, 2002; Prasad & Souradeep, 2012). The heuristic techniques as PSO and ORCS however, avoid this risk partly by using the application of a swarm, which draws multiple samples from the model space at each iteration, thereby continuously resampling a larger area of the model space while converging to potential minima eventually (or at the same time in the case of ORCS). However, one should consider the risk of slow or no convergence using these techniques, if not enough prior input data is used. Therefore, it would be interesting to combine the PSO and ORCS approach and try to possibly optimize likely scenarios using MCMC.

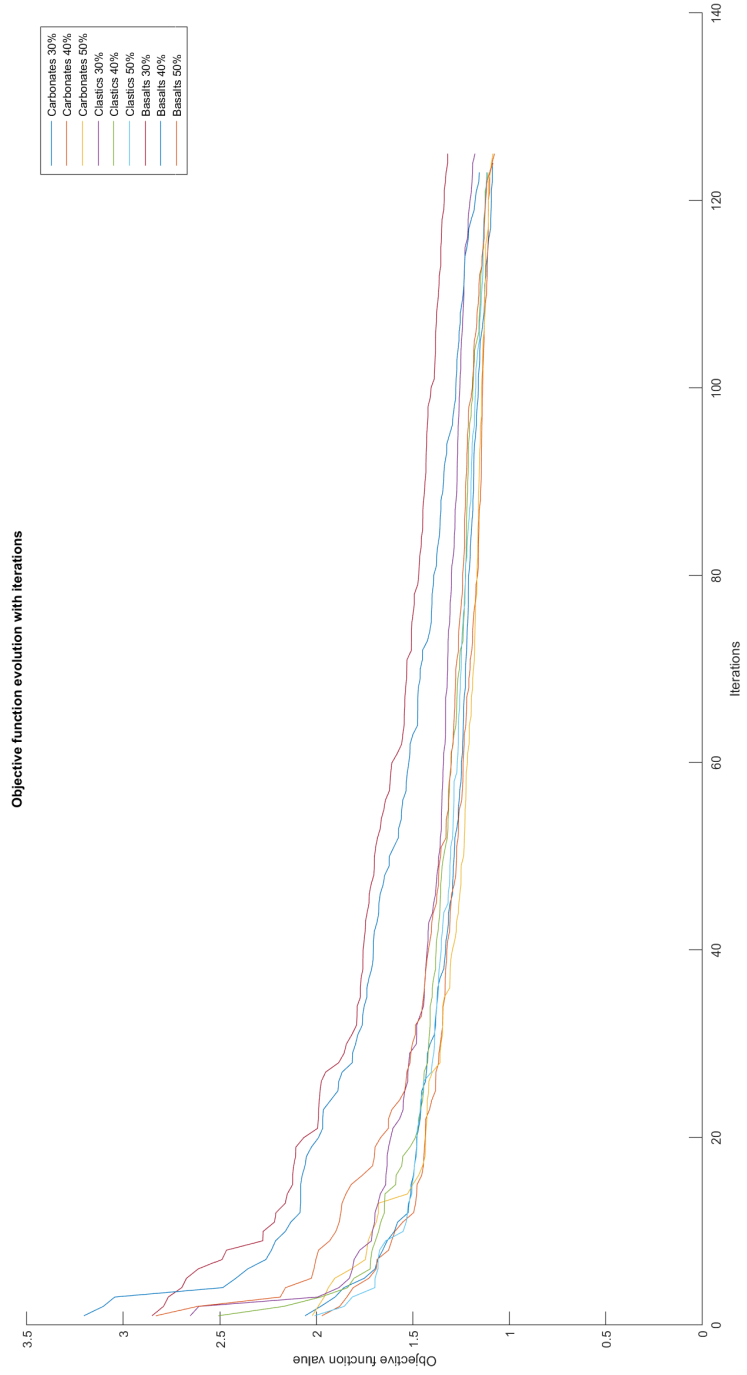


Figure 6-3: Smallest misfit found per iteration for the entire simulation using ORCS (sorted).

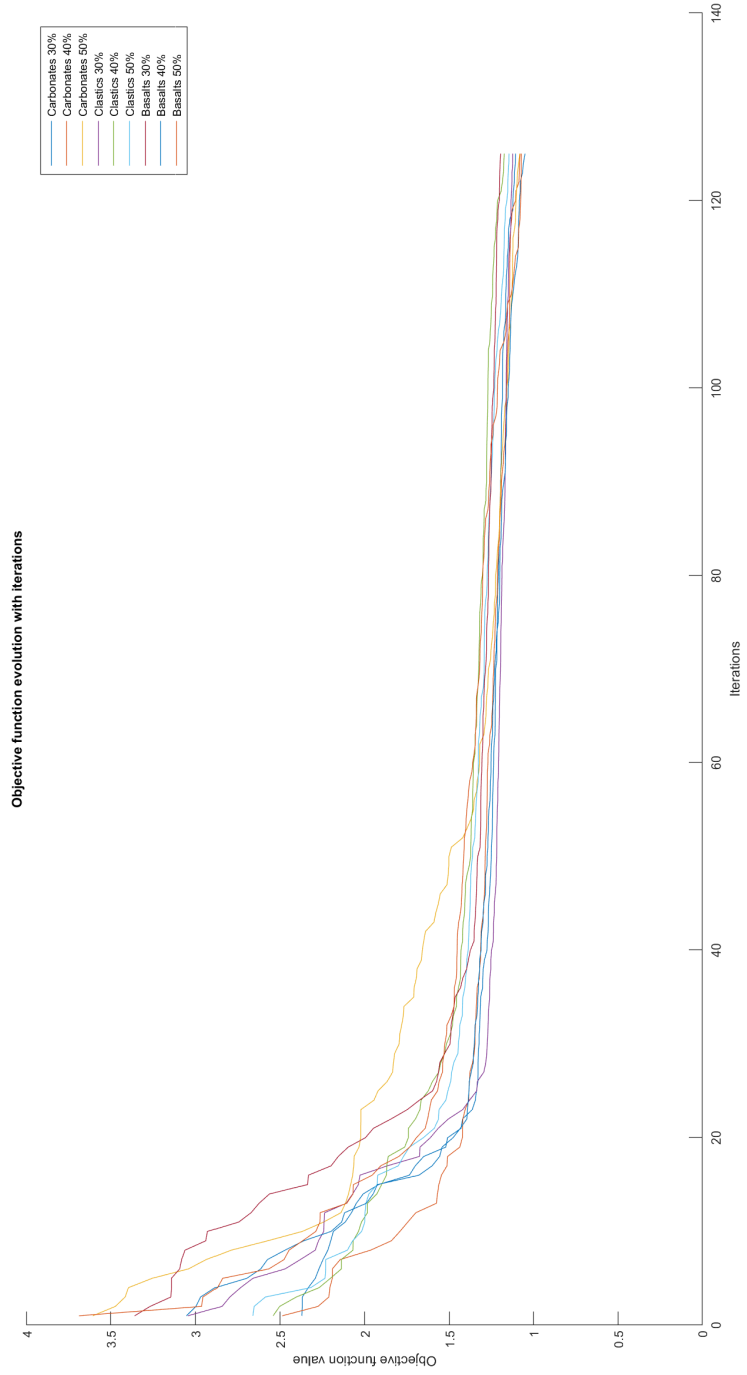


Figure 6-4: Smallest misfit found per iteration for the entire simulation using PSO (sorted).

6-2 Interpretation outcomes

If one would solely believe the outcomes of the optimization tools, respecting the residuals and velocity relations, the ORCS carbonates scenario 1 (figure 5-2) and PSO carbonate scenario 2 (figure 5-9) would be the most likely. The PSO basalt scenario 1 is discarded because of the high porosity values found in combination with the WGG-relation (eq. 2-6). Almost the entire porosity model (figure 5-9) of the most likely basalt scenario shows porosity values of 35% or higher. Since the velocity relations were calibrated up to around 30%, almost the entire model is found in the extrapolated region. Therefore, it is assumed to be a less trustworthy solution than the second carbonate porosity model.

The ORCS scenario shows a similar porosity distribution as the interpretation from Alsharhan, shown in figure 4-2 (Alsharhan, 1987). The reservoir top (H-layer) has porosity values of 23%-25% (24.5% in Alsharhan (1987)). The upper southern layer (layer I in figure 4-2), shows a porosity of 10%-18% (16.5% in Alsharhan (1987)). The lower two layers (A and B) show porosity values of 20%-22% and 18%-21%, respectively (20.5% and 23% in Alsharhan (1987)). The clinoform layers (F and G) show porosity values of 15%-19% and 5%-10%, respectively (15%-27% and 6% in Alsharhan (1987)). The Bab member, as it is called in figure 4-2, shows a porosity between 15%-25%. Unfortunately, no interpretation has been made on this particular layer in the Alsharhan (1987) interpretation. Research by Alsuwaidi (2007) has found that the Bab member has similar or even a little higher (pseudo) porosity values in comparison with the crest of the reservoir, which is found in this research as well. Note that the geometry of the layers as shown in figure 4-2 is not matched by the seismic section (in terms of horizons picked). The geometry of the seismic picking fits better to the geologic interpretation by Yose et al. (2006).

When comparing the PSO scenario to the Alsharhan interpretation, the crest (H-layer) shows a porosity of 25%-30% in the PSO-scenario (24.5% in Alsharhan (1987)). The I entity has a porosity of 12%-23% (16.5% in Alsharhan (1987)). The layers A and B show porosity values of 26%-28% and 20%-30%, respectively (20.5% and 23% in Alsharhan (1987)). The clinoform layers (F and G) show porosity values of 15%-26% and 1%-7%, respectively (15%-27% and 6% in Alsharhan (1987)). The Bab member, as it is called in figure 4-2, shows a porosity ranging from 15%-35% (in accordance with Alsuwaidi (2007)). In overall, the PSO simulation shows slightly higher porosity than interpreted by Alsharhan (1987). This may be due to the smaller exploration factor in the PSO-nature (with respect to ORCS).

In addition to the interpretation of Alsharhan (1987), research by Yose et al. (2006) on well log data and core samples shows porosity values that are slightly higher than those found by Alsharhan (1987). If these porosity values are assumed to be right, the crest of the reservoir has a porosity of nearly 29%, whereas the clinoforms range from 20% in the bottom to 29% at the top (F-layer in Alsharhan (1987)). The dense, low porous layer (G in Alsharhan), is found to be of 6% porosity still, alike what is found by the PSO simulation and Alsharhan (1987). The A and B entities in Alsharhan (1987) are still overestimated by the PSO simulation (20%-30%), as Yose et al. (2006) finds a porosity of 22% for in these layers.

Depending on the data sets used to validate the outcome of this research, either of the optimizers may achieve a reasonable result. However, ORCS in general is more conservative in applying porosity values close to the constraints, whereas PSO tends to use these values more in order to gain optimal contrast between the layers.

Recommendations and conclusion

7-1 Recommendations

Although the model has made a good effort and provides reasonable results in resolving the mineralogy and porosity of the Shuaiba Formation, several features strongly depend on assumptions or prior knowledge, making it prone to come up with wrong results. Therefore, future research may enhance the model further. Some recommendations on the assumptions, as described in sections 4-4 and 4-5, are:

- **Geometry modifications**

The most influencing assumptions are found in the user's input by the picking of geometry.

For the geometry, as it is static parameter in the current model, it would be useful to develop a degree of freedom such that the horizons could shift to nearby horizons or change angle slightly, if it favors the model. Also, a feature called snapping may enhance the maximum amplitude picking, to improve the results further.

- **Velocity relations**

Another strong assumption is found in the calculation of the velocity models. The four velocity relations used (RHG-, GGG-, WGG- and the Sun-relation) have shown strong trends for clastic and carbonate rocks, but show weaker correlations for basaltic scenarios (figure 4-5). These relations, or correlations, may be updated based on new data sets of specific rock types, to enhance the velocity model further and make the model more accurate.

- **Synthetic seismic**

If the model is used in problems where high resolution is required, 1D-convolution of a (zero-phase) wavelet may not suffice. Therefore, 2D (or even 3D) AVO synthetic seismic should be created, allowing more detail and geometry features as pinch outs to be captured in the synthetics. These could then be used to validate the actual seismic

section on tuning effects. Furthermore, the effect of noise in the seismic section could be investigated. Whereas the current model assumes the reflections in the post-stacked section have a good signal-to-noise ratio, other sections may not have such a SN-ratio and could potentially not be interpreted as well.

- **Objective function**

The objective function evaluation for this case-study was done with the HH-RMSE error measurement, but this may not be the optimal way of evaluating a 2D-seismic section still. Although good results were obtained using the HH-RMSE in this case-study, sections with a low SN-ratio will be prone to wrong misfit calculations. A general, strong performing objective function would therefore provide a more solid evaluation of the synthetic sections.

- **Overburden modelling**

For this case-study, the overburden was fairly well constraint (static value for mineral density and small degree of freedom for the porosity), but this may not be the case in frontier exploration. Therefore, a way to mitigate the effect of the overburden 'choice' on the results, or at least a good evaluation of the results with respect to the overburden is required to give proper results in even more unconstrained problems. Low-frequency models might help to constrain the overburden possibilities for example.

- **Optimization performance**

The performance of PSO and ORCS needs to be evaluated more. New, more complex concepts as multi-swarm particle swarm optimization (Niu, Zhu, He, & Wu, 2007) and other (heuristic) optimization tools may be used to validate convergence speed and effectiveness in unconstrained seismic forward modelling. The current optimization tools may also be evaluated further for an optimal combination of optimization parameters. In addition, the (best) results of the optimization methods found in this research may be further evaluated using posterior sampling techniques as MCMC, to see if, assuming the results found in this research are approximately right, can be updated to further detail.

- **Mineralogy library**

The current model uses most of its mineral data from literature. Whereas it currently takes carbonates, clastics and basalts, new rocks types may be added and mineral data may be refined, in order to obtain wider variability of scenario testing.

- **Improvement of the algorithm**

Currently, the algorithm is mostly written to be functional, rather than having the optimal optimization speed. Although some computation efficiency is taken into account, updates to the algorithm could make its performance better. Currently, testing a sample for all velocity models takes roughly 1.1 seconds. If this could be reduced slightly, the total computation time decreases significantly for larger simulations like the one in the case-study (28125 samples for both ORCS and PSO). A suggestion for general increase of performance would be a rewritten version of the model in another compiler such as C++, which is generally faster in large computations. Another compiler which may have an economic advantage of MATLAB R2015b is Python, which is free to use, whereas MATLAB R2015b requires a license to be operated (which is not

available for free). Furthermore, the algorithm may be adapted in terms of quantitative interpretation, like Bayesian inference and other methods, as mentioned in chapter 5.

7-2 Conclusion

Different optimization tools have been applied to a poorly-constraint seismic forward modelling case-study on the Shuaiba Formation. Some key insights gained from analysis on optimization and forward modelling in this research are summarized:

1. **Analysis on different optimization methods:** Centered-progressive particle swarm optimization and one rank cuckoo search both have proven to be robust in minimizing the misfit between a synthetic section created from rock and fluid property data and an actual seismic section.
2. **Resolving mineralogy and porosity of the Shuaiba Formation:** In overall, CP-PSO and ORCS retrieve the common Shuaiba Formation interpretation to the extent of a few percent porosity and both resolve the mineralogy to be a carbonate. ORCS performance is slightly better when observing the porosity and mineralogy probability, probably due to it being a more exploratory technique by its nature. CP-PSO however, being the most exploratory family member of PSO, converges toward minimum misfits slightly faster and may therefore explore a smaller search space (than ORCS). This goes at the cost of some detail in porosity, but saves time on the computation side.
3. **Creation of an easily applicable tool to de-risk seismic amplitudes:** The model itself has shown to give a good indication on the potential mineralogy of a prospective reservoir and to some extent it may also give an idea about the porosity of the rock section, based on a seismic section and prior knowledge only. These indications may be of great value to the oil and gas business, as the tool could de-risk seismic amplitudes prior to drilling an appraisal well. If the tool (after testing it on more case-studies) could predict mineralogy or exclude mineralogy scenarios and possibly even give an indication on probable porosity scenarios, it may have a strong economic advantage, since it may decrease the risk when drilling an appraisal well.
4. **Model has good potential of being further developed:** In general, the model shows it is capable of resolving mineralogy and porosity, but certain assumptions and prior knowledge are required. To further develop the functionality and applicability of this model, future research should be carried out on improving and constraining the assumptions made. This may result in more (lateral) resolution, geometry de-risking and resolving seismic tuning effect.
Furthermore, computation efficiency improvements could be achieved by revising the algorithm. In addition, attempts may be made to combine the results from this model and further update them with other optimization techniques as MCMC.

Bibliography

- Adnan, A. & Razzaque, M. A. (2013). A Comparative Study of Particle Swarm Optimization and Cuckoo Search Techniques Through Problem-Specific Distance Function. *International Conference of Information and Communication Technology*.
- Alsharhan, A. S. (1987). Geology and reservoir characteristics of carbonate buildup in giant Bu Hasa oil field, Abu Dhabi, United Arab Emirates. *AAPG Bulletin*, 71, 1304–1318.
- Alsharhan, A. S. (1993). Bu Hasa Field - United Arab Emirates, Rub Al Khali Basin, Abu Dhabi. *AAPG Treatise of Petroleum Geology, Atlas of Oil and Gas Fields*, 99–127.
- Alsuwaidi, M. E. (2007). Lower Bab Member (A0): A study of sequence stratigraphy, porosity characterization and tight reservoir development, Abu Dhabi, UAE. (Doctoral dissertation, Colorado School of Mines).
- Batzle, M. & Wang, Z. (1992). Seismic properties of pore fluids. *Geophysics*, 57, 1396–1408.
- Berryman, J. G. (1992). Origin of Gassmann's equations. *Geophysics*, 64, 1627–1629.
- Civicioglu, P. & Besdok, E. (2011). A conceptual comparison of the Cuckoo-search, particle swarm optimization, differential evolution and artificial bee colony algorithms. *Artif Intell Rev*. Springer Science and Business Media B.V.
- Dvorkin, J. & Nur, A. (1998). Time-average equation revisited. *Geophysics*, 63, 460–464.
- Eberhart, R. & Kennedy, J. (1995). Particle Swarm Optimization. *Conference on Neural Networks*. IEEE International.
- Gassmann, F. et al. (1951). Über die Elastizität poröser Medien. *Vierteljahrsschrift der Naturforschenden Gesellschaft in Zürich*, 96. Gebr. Pretz AG., Zürich.
- Gonzalo, E. G. & Martínez, J. L. F. (2009). Design of a simple and powerful Particle Swarm Optimizer. *Proceedings of the International Conference on Computational and Mathematical Methods in Science and Engineering*.
- Grammer, G. M. & Harris, P. M. (2005). *Integration of Outcrop and Modern Analogs in Reservoir modeling*. Memoir 80, 394p. AAPG.
- Greenberg, M. L. & Castagna, J. P. (1992). Shear-wave velocity estimation in porous rocks: theoretical formulation, preliminary verification and applications. *Geophysical Prospecting*, 40, 195–209. Blackwell Publishing Ltd.
- Hoek, T. v. & Salomons, B. (2006). Understanding the Seismic Expression of Complex Turbidite Reservoirs Through Synthetic Seismic Forward Modeling: 1D-Convolutional Ver-

- sus 3D-Modeling Approaches. *26th annual Gulf Coast section SEPM Foundation Bob F. Perkins research conference*, 345–372.
- Lawrence, D. A. et al. (2010). Sequence Stratigraphy of a Giant Middle East Oil Field - Integration of Core, Log and Seismic Data. *Abu Dhabi International Petroleum Exhibition and Conference*. Society of Petroleum Engineers.
- Lévy, P. (1954). *Théorie de l'addition des variables aléatoires*. Second edition. Gauthier-Villars.
- Mandelbrot, B. B. (1982). *The Fractal Geometry of Nature*. p.288-300. W.H. Freeman and Company.
- Martínez, J. L. F. & Gonzalo, E. G. (2009). The PSO family: deduction, stochastic analysis and comparison. *Swarm Intell*, 3, 245–273. Springer.
- Martínez, J. L. F., Gonzalo, E. G., Muñiz, Z. F., & Mukerji, T. (2012). How to design a powerful family of Particle Swarm Optimizers for inverse modeling. University of Oviedo.
- Martínez, J. L. F., Gonzalo, E. G., & Naudet, V. (2010). Particle swarm optimization applied to solving and appraising the streaming-potential inverse problem. *Geophysics*, 75. Society of Exploration Geophysicists.
- Mavko, G., Mukerji, T., & Dvorkin, J. (2009). *The Rock Physics Handbook - Tools for Seismic Analysis of Porous Media - 2nd edition*. 511p. Cambridge University Press.
- Melville, P., Al Jeelani, O., & Grötsch, J. (2004). Three-Dimensional Seismic Analysis in the Characterization of a Giant Carbonate Field, Onshore Abu Dhabi, United Arab Emirates. *Seismic imaging of carbonate reservoirs and systems: AAPG Memoir*. American Association of Petroleum Reservoirs.
- Mentaschi, L., Besio, G., Cassola, F., & Mazzino, A. (2013). Problems in RMSE-based wave model validations. *Elsevier*.
- Niu, B., Zhu, Y., He, X., & Wu, H. (2007). MCPSO: A multi-swarm cooperative particle swarm optimizer. *Applied Mathematics and Computation*, 185, 1050–1062.
- Nolen-Hoeksma, R. C. (2000). Modulus-porosity relations, Gassmann's equations, and the low-frequency elastic-wave response to fluids. *Geophysics*, 65, 1355–1363.
- Panigrahi, B. K., Shi, Y., & Lim, M. H. (2011). *Handbook of Swarm Intelligence - Concepts, Principles and Applications*. 556p. Springer.
- Prasad, J. & Souradeep, T. (2012). Cosmological parameter estimation using Particle Swarm Optimization (PSO). IUCAA.
- Raymer, L. L., Hunt, E. R., & Gardner, J. S. (1980). An improved sonic transit time-to-porosity transform. *SPWLA Twenty-first annual logging symposium*.
- Sambridge, M. & Mosegaard, K. (2002). Monte Carlo methods in geophysical inverse problems. *Reviews of Geophysics*, 40.
- Singh, G. P. & Singh, A. (2014). Comparative Study of Krill Herd, Firefly and Cuckoo Search Algorithms for Unimodal and Multimodal Optimization. *I.J. Intelligent Systems and Applications*. MECS.
- Sun, Y. F. (2000). Core-log-seismic integration in hemipelagic marine sediments on the eastern flank of the Juan de Fuca Ridge. *Proceedings of the Ocean Drilling Program, Scientific Results*, 168. Fisher, A., Davis, E.E., and Escutia, C. (Eds.)
- Tawfik, A. S., Badr, A., & Abdel-Rahman, I. F. (2013). One Rank Cuckoo Search Algorithm with Application to Algorithmic Trading Systems Optimization. *International Journal of Computer Applications*, 64.

- Wellmann, J. F. & Regenauer-Lieb, K. (2011). Uncertainties have a meaning: Information entropy as a quality measure for 3-D geological models. *Tectonophysics*, 526-529, 207–216. Elsevier.
- Wyllie, M. R. J., Gregory, A. R., & Gardner, G. H. F. (1958). An experimental investigation of factors affecting elastic wave velocities in porous media. *Geophysics*, 23, 459–493.
- Wyllie, M. R. J., Gregory, A. R., & Gardner, L. W. (1956). Elastic wave velocities in heterogeneous and porous media. *Geophysics*, 21, 41–70.
- Yang, X. S. & Deb, S. (2009). Cuckoo Search via Lévy Flights. IEEE.
- Yin, Y., Lawrence, D. A., Vahrenkamp, V., Kourbaj, A., Helmy, H., Gashut, M., & Al-Mehairy, Y. (2010). Seismic Characterization of Reservoir Architecture and Facies Distribution in a Carbonate Platform Setting: Dynamic Implications for Production in a Super-giant Middle East Field. *Abu Dhabi International Petroleum Exhibition and Conference*. Society of Petroleum Engineers.
- Yose, L. A., Schuelke, J. S., Ruf, A. S., Gombos, A., Strohmenger, C. J., Al-Hosani, I., ... Johnson, I. G. (2006). Three-dimensional Characterization of a Heterogeneous Carbonate Reservoir, Lower Cretaceous, Abu Dhabi (United Arab Emirates). *AAPG Memoir 88/SEPM Special Publication*, 173–212. The American Association of Petroleum Geologists.
- Yu, B., Yan, C., & Nie, Z. (2013). Chemical Effect on Wellbore Instability of Nahr Umr Shale. *The Scientific World Journal*, 2013, 1–7.

Part IV

Appendices

Appendix A

ORCS-simulation outcomes

A-1 ORCS-simulation with $P_a = 0.45$ and one rank update ratio = 0.10

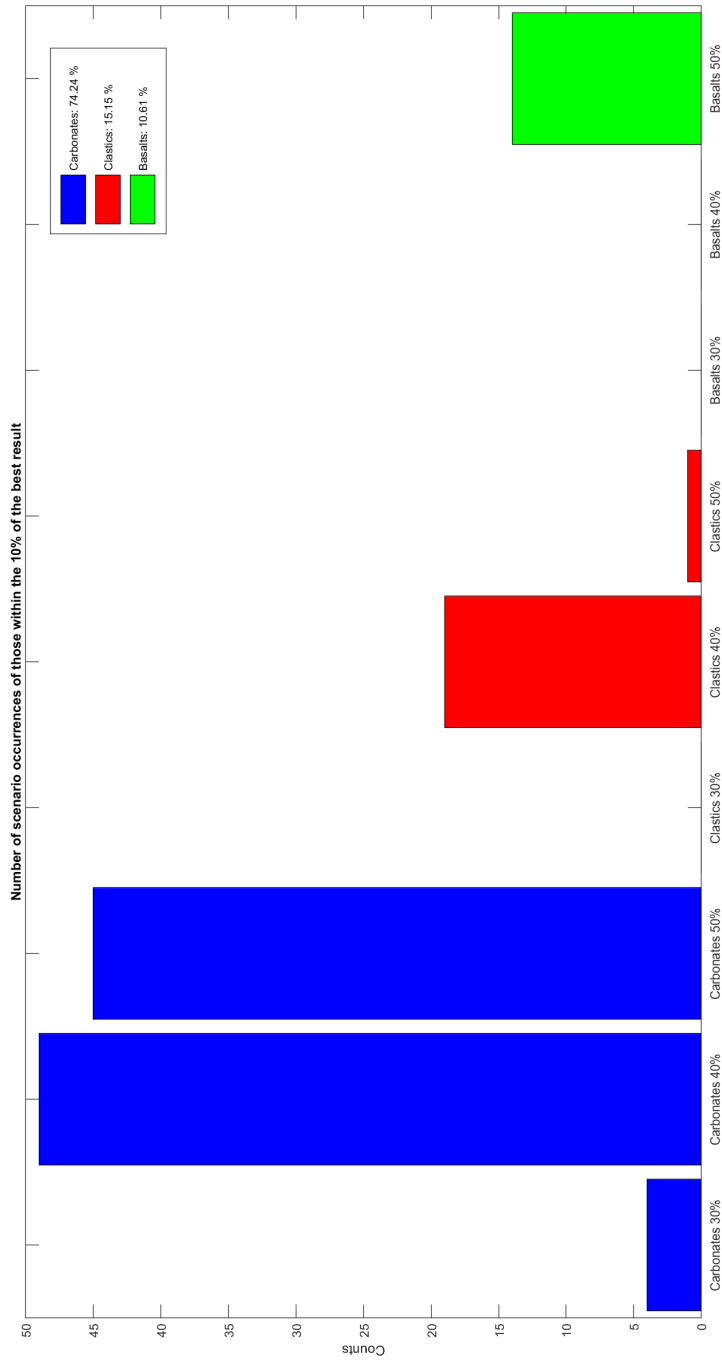


Figure A-1: Probable mineralogy scenarios for the Shuaiba Formation using One Rank Cuckoo Search. Parameters for ORCS: $P_a = 0.45$, $t_{or} = 0.10$. Scenarios are obtained after counting outcomes within 10% of the best results after the entire simulation has finished (HH-value range: 1.07-1.18).

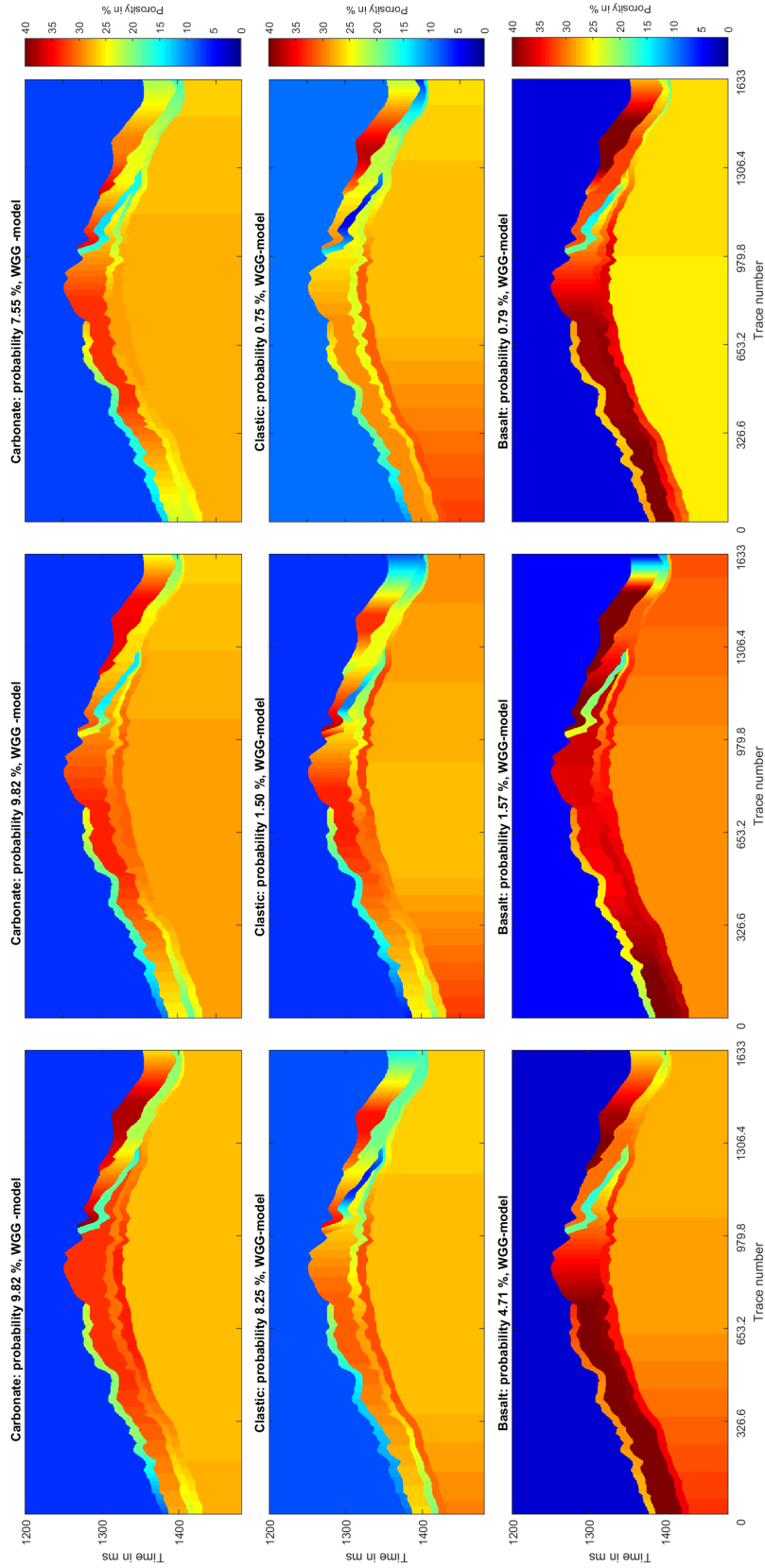


Figure A-2: Probable porosity scenarios for the Shuaiba Formation using One Rank Cuckoo Search. Parameters for ORCS: $P_a = 0.45$, $t_{or} = 0.10$. The scenarios show probability (based on their occurrences) and the most used velocity model to create the scenario.

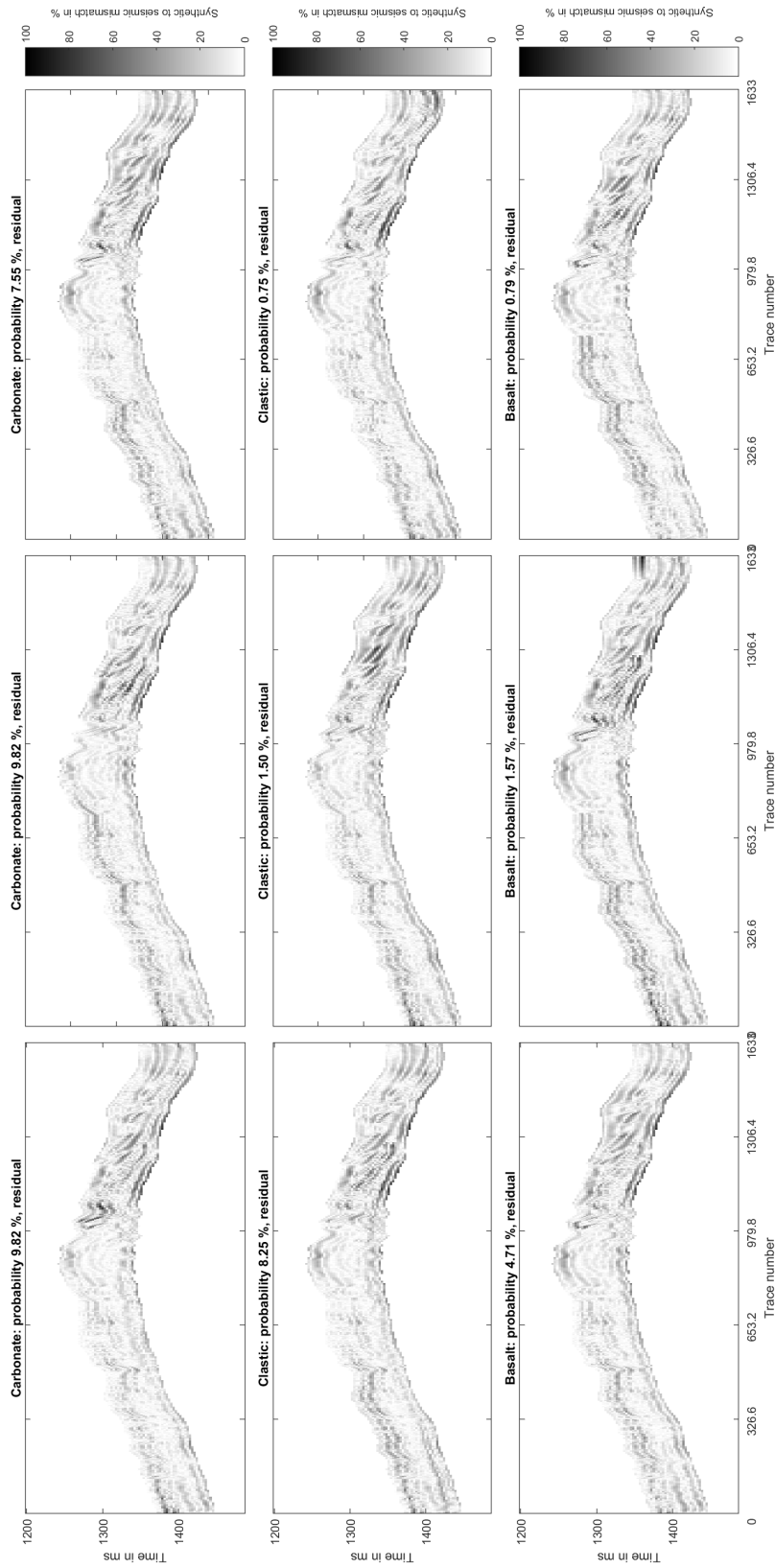


Figure A-3: Residuals of porosity scenarios for the Shuaiba Formation when comparing synthetic to seismic using ORCS ($P_a = 0.45$ and $t_{or} = 0.10$). Mismatch is the absolute deviation between the seismic section and the synthetics and is shown relative to the strongest amplitude in the seismic section.

A-2 ORCS-simulation with $P_a = 0.75$ and one rank update ratio = 0.10

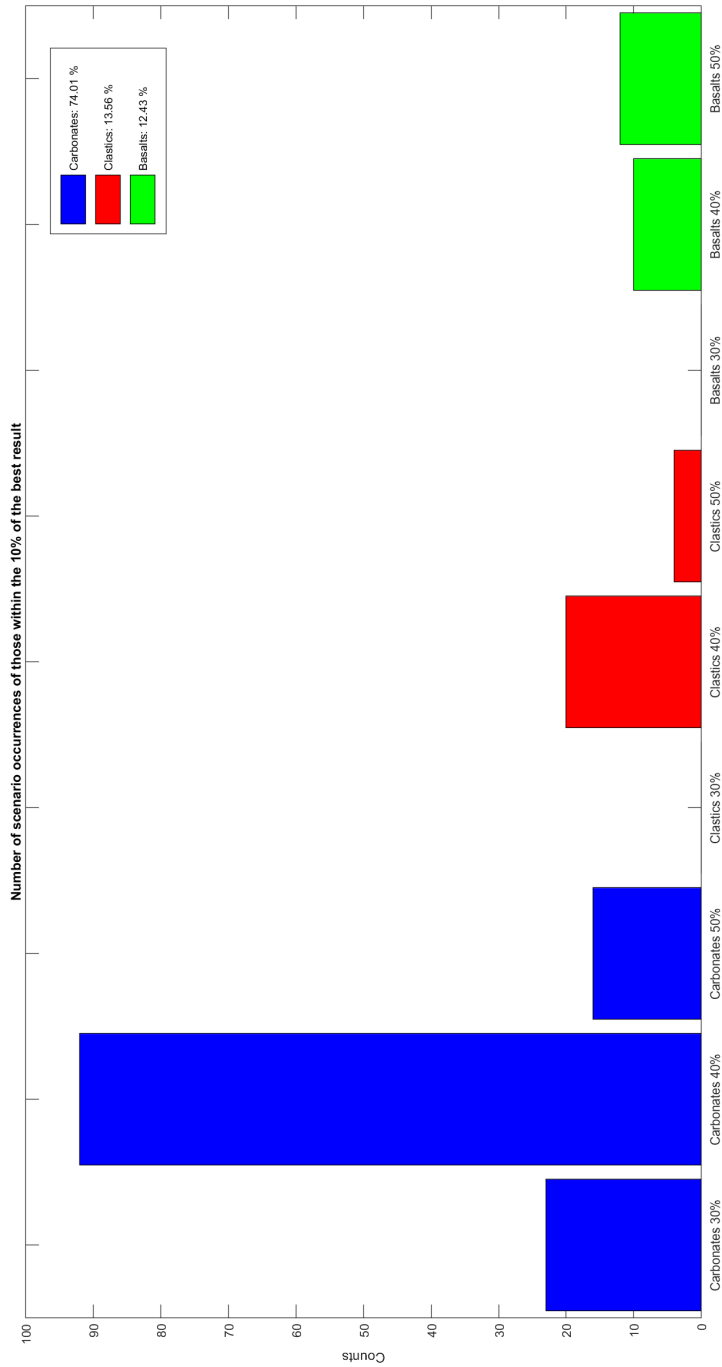


Figure A-4: Probable mineralogy scenarios for the Shuaiba Formation using One Rank Cuckoo Search. Parameters for ORCS: $P_a = 0.75$, $t_{or} = 0.10$. Scenarios are obtained after counting outcomes within 10% of the best results after the entire simulation has finished (HH-value range: 1.12-1.23).

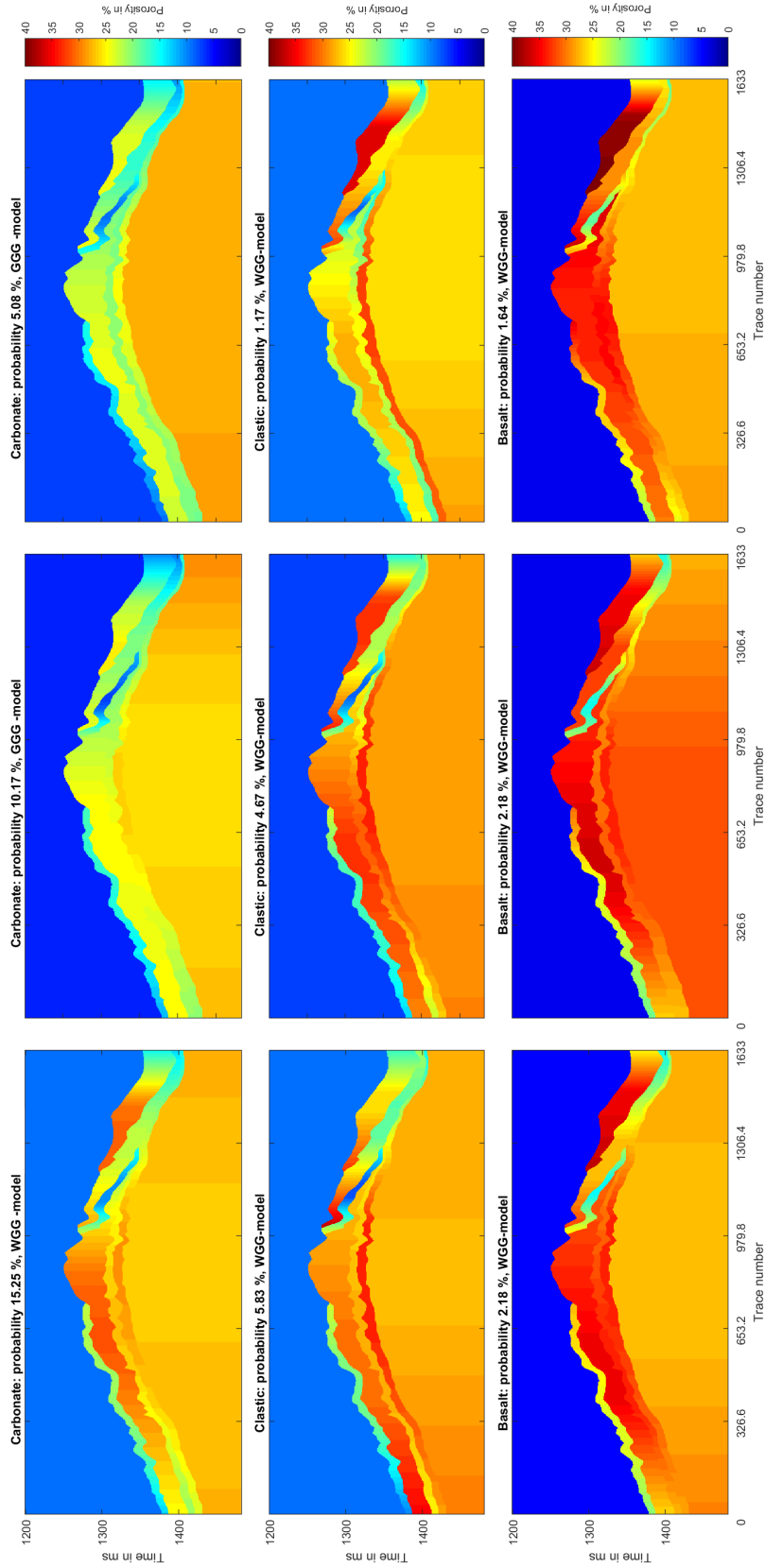


Figure A-5: Probable porosity scenarios for the Shuaiba Formation using One Rank Cuckoo Search. Parameters for ORCS: $P_a = 0.75$, $t_{or} = 0.10$. The scenarios show probability (based on their occurrences) and the most used velocity model to create the scenario.

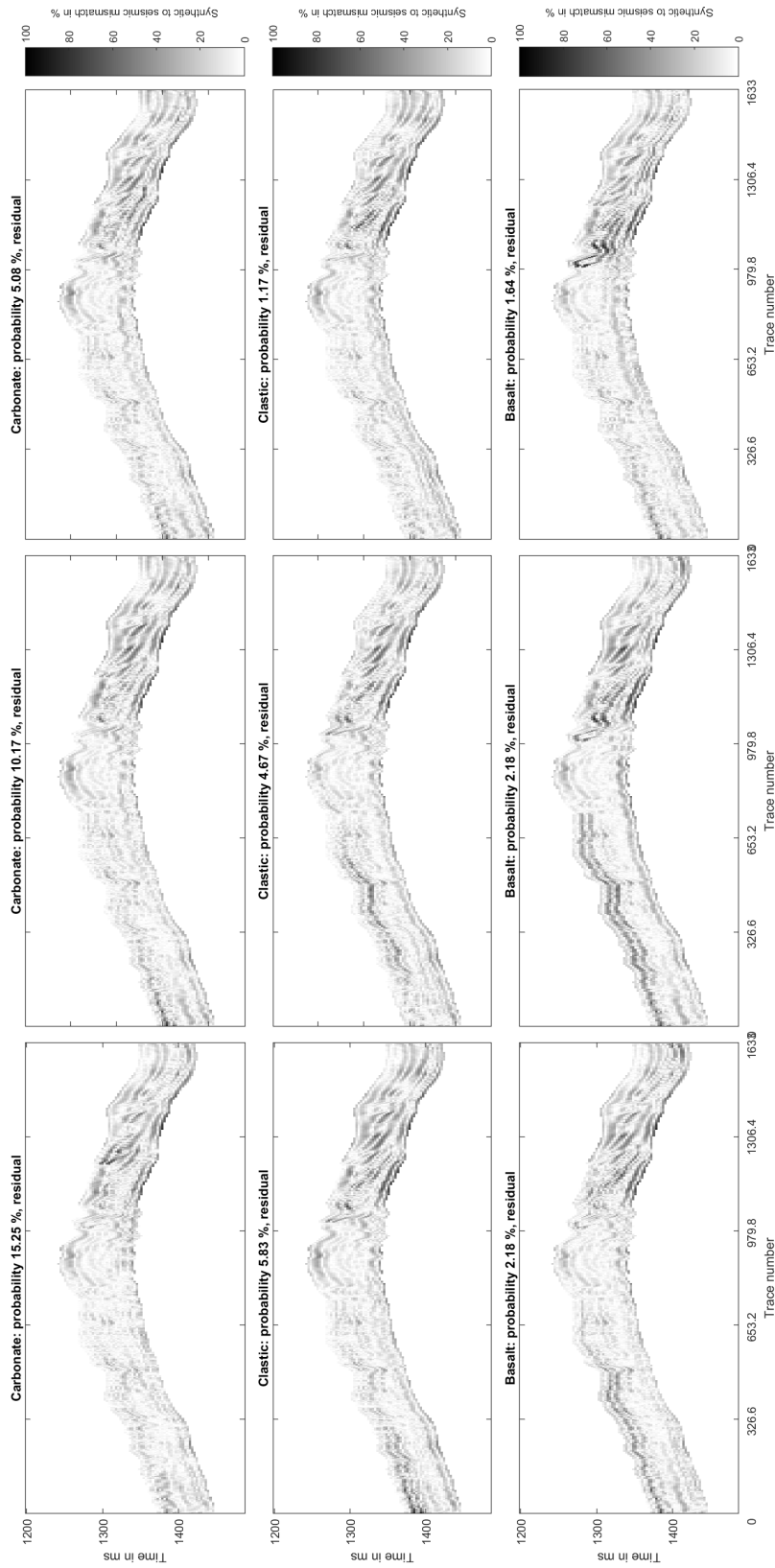


Figure A-6: Residuals of porosity scenarios for the Shuaiba Formation when comparing synthetic to seismic using ORCS ($P_a = 0.75$ and $t_{or} = 0.10$). Mismatch is the absolute deviation between the seismic section and the synthetics and is shown relative to the strongest amplitude in the seismic section.

A-3 ORCS-simulation with $P_a = 0.25$ and one rank update ratio = 0.03

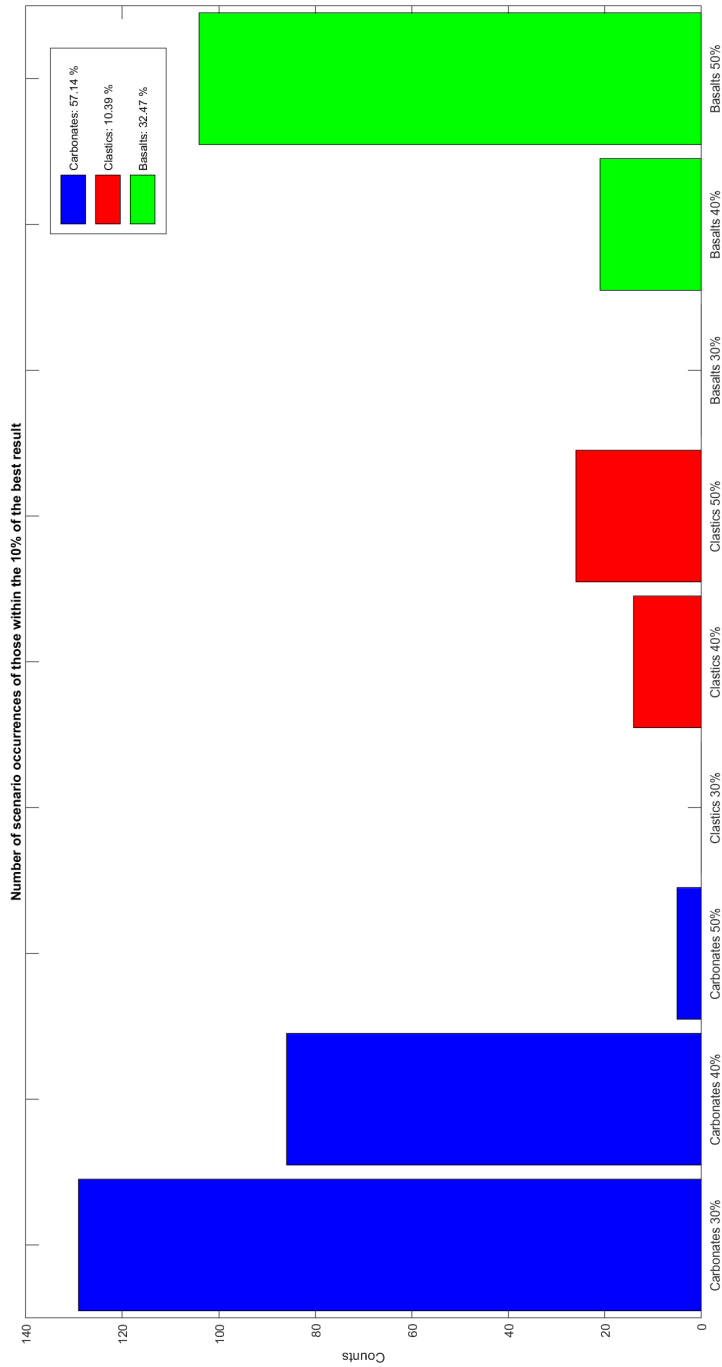


Figure A-7: Probable mineralogy scenarios for the Shuaiba Formation using One Rank Cuckoo Search. Parameters for ORCS: $P_a = 0.25$, $t_{or} = 0.03$. Scenarios are obtained after counting outcomes within 10% of the best results after the entire simulation has finished (HH-value range: 1.06-1.17).

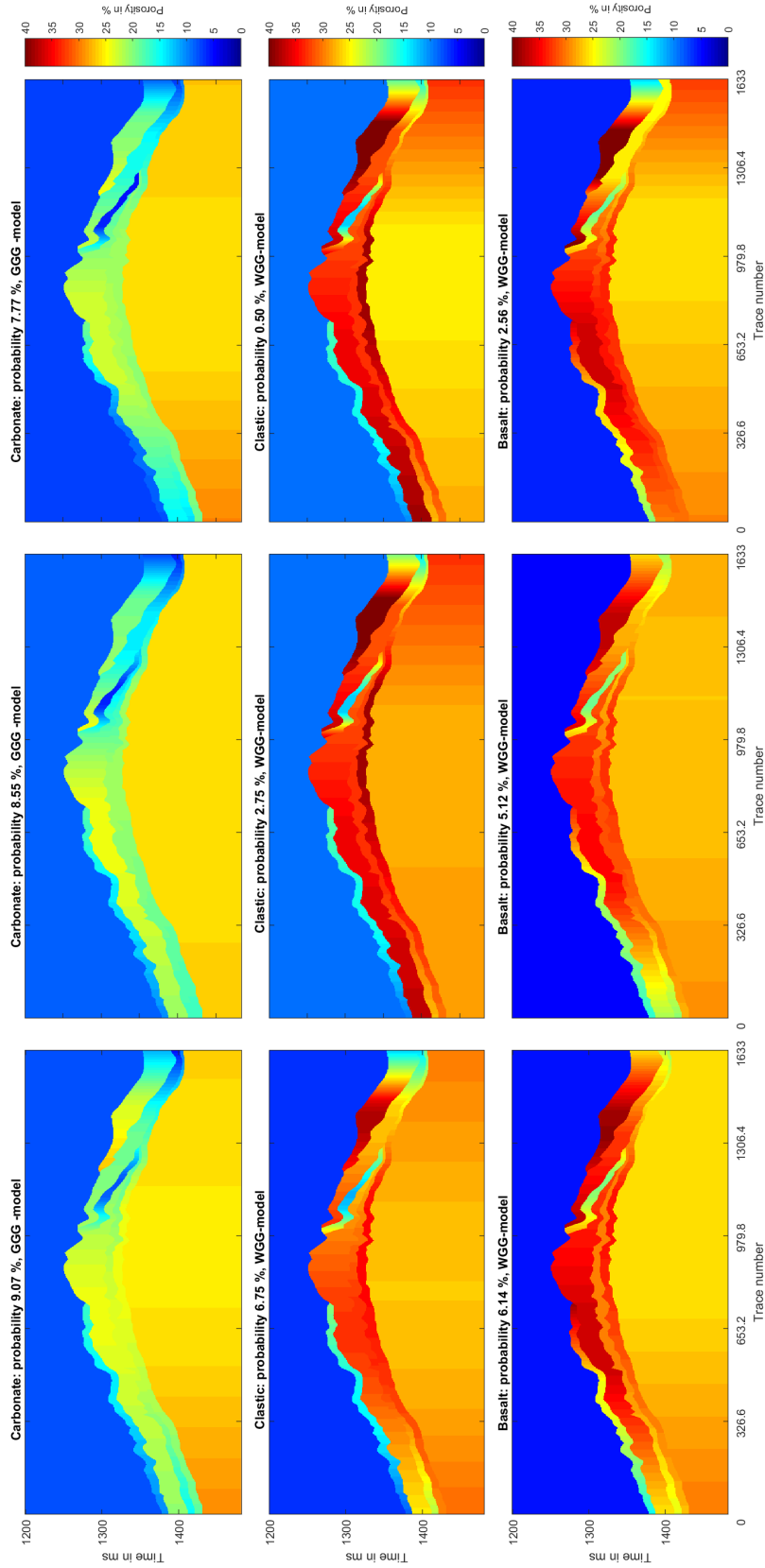


Figure A-8: Probable porosity scenarios for the Shuaiba Formation using One Rank Cuckoo Search. Parameters for ORCS: $P_a = 0.25$, $t_{or} = 0.03$. The scenarios show probability (based on their occurrences) and the most used velocity model to create the scenario.

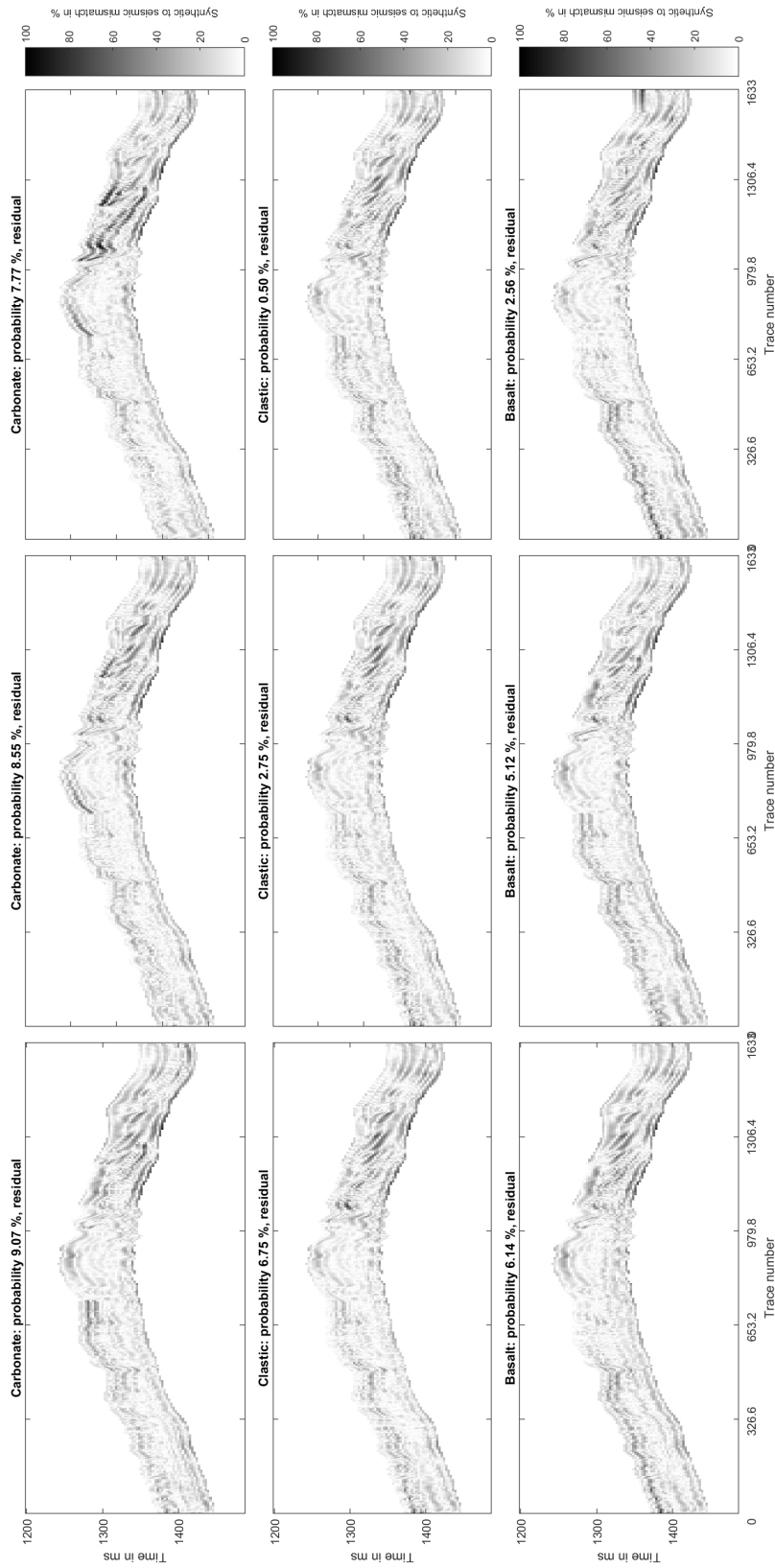


Figure A-9: Residuals of porosity scenarios for the Shuaiba Formation when comparing synthetic to seismic using ORCS ($P_a = 0.25$ and $t_{or} = 0.03$). Mismatch is the absolute deviation between the seismic section and the synthetics and is shown relative to the strongest amplitude in the seismic section.

Appendix B

PSO-simulation outcomes

B-1 PSO-simulation with cooling timestep 1.15

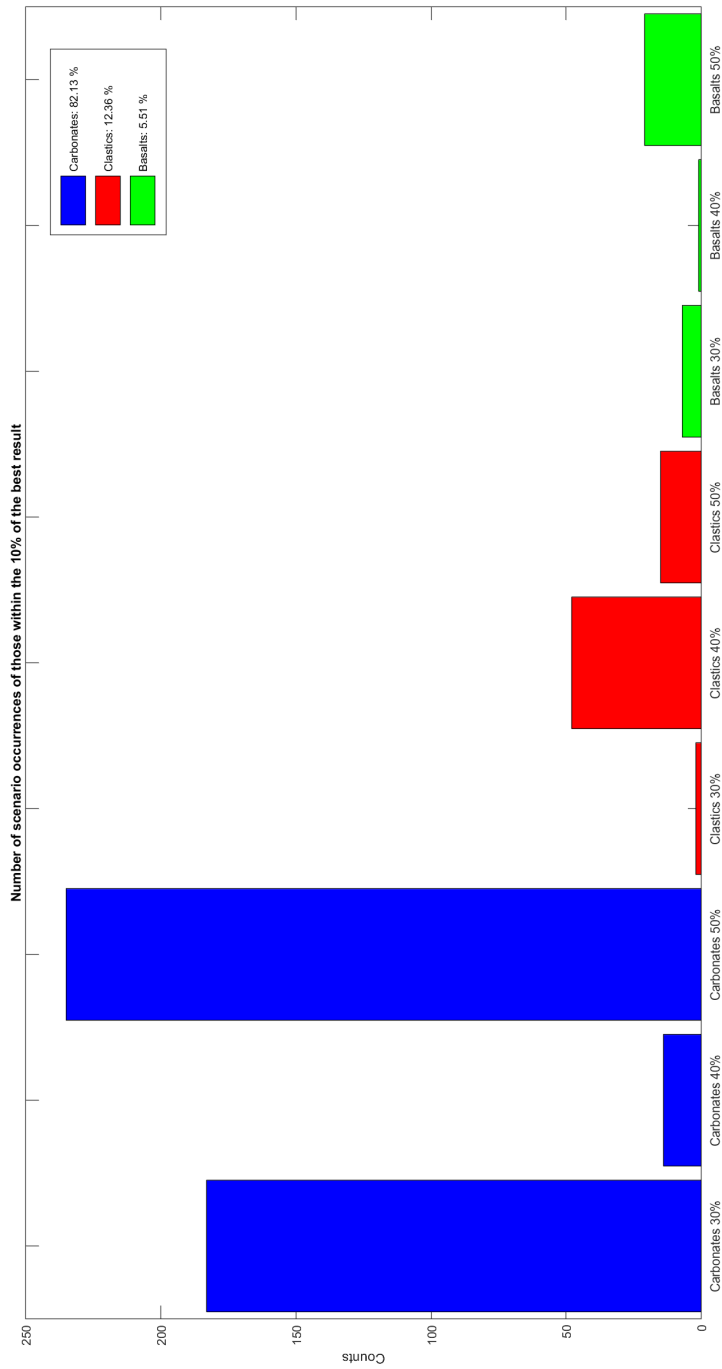


Figure B-1: Probable mineralogy scenarios for the Shuaiba Formation using Centered-Progressive Particle Swarm Optimization. Parameters for PSO: $\Delta t = 1.15$. Scenarios are obtained after counting outcomes within 10% of the best results after the entire simulation has finished (HH-value range: 1.08-1.19).

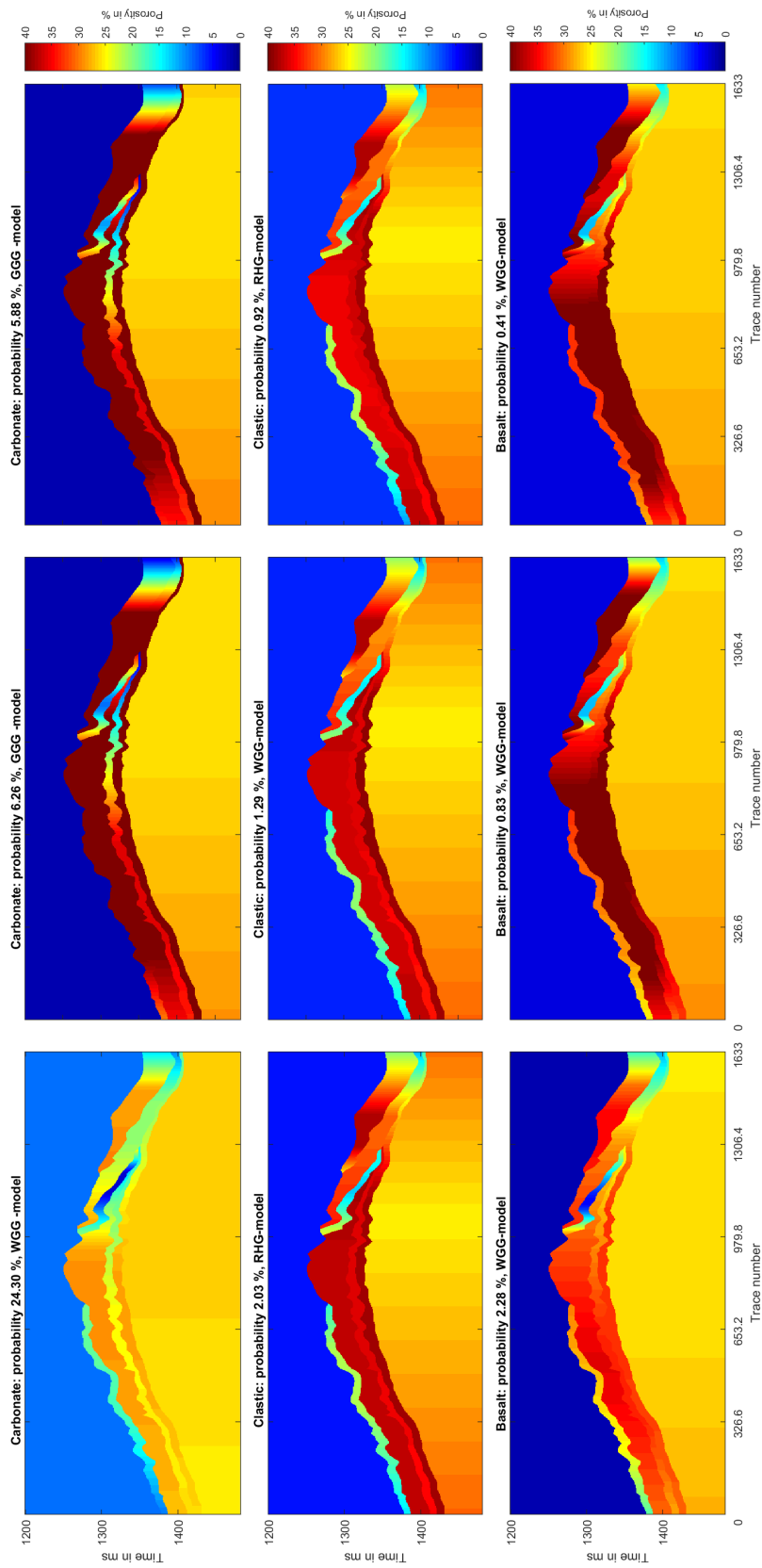


Figure B-2: Probable porosity scenarios for the Shuaiba Formation using Centered-Progressive Particle Swarm Optimization. Parameters for PSO: $\Delta t = 1.15$. The scenarios show probability (based on their occurrences) and the most used velocity model to create the scenario.

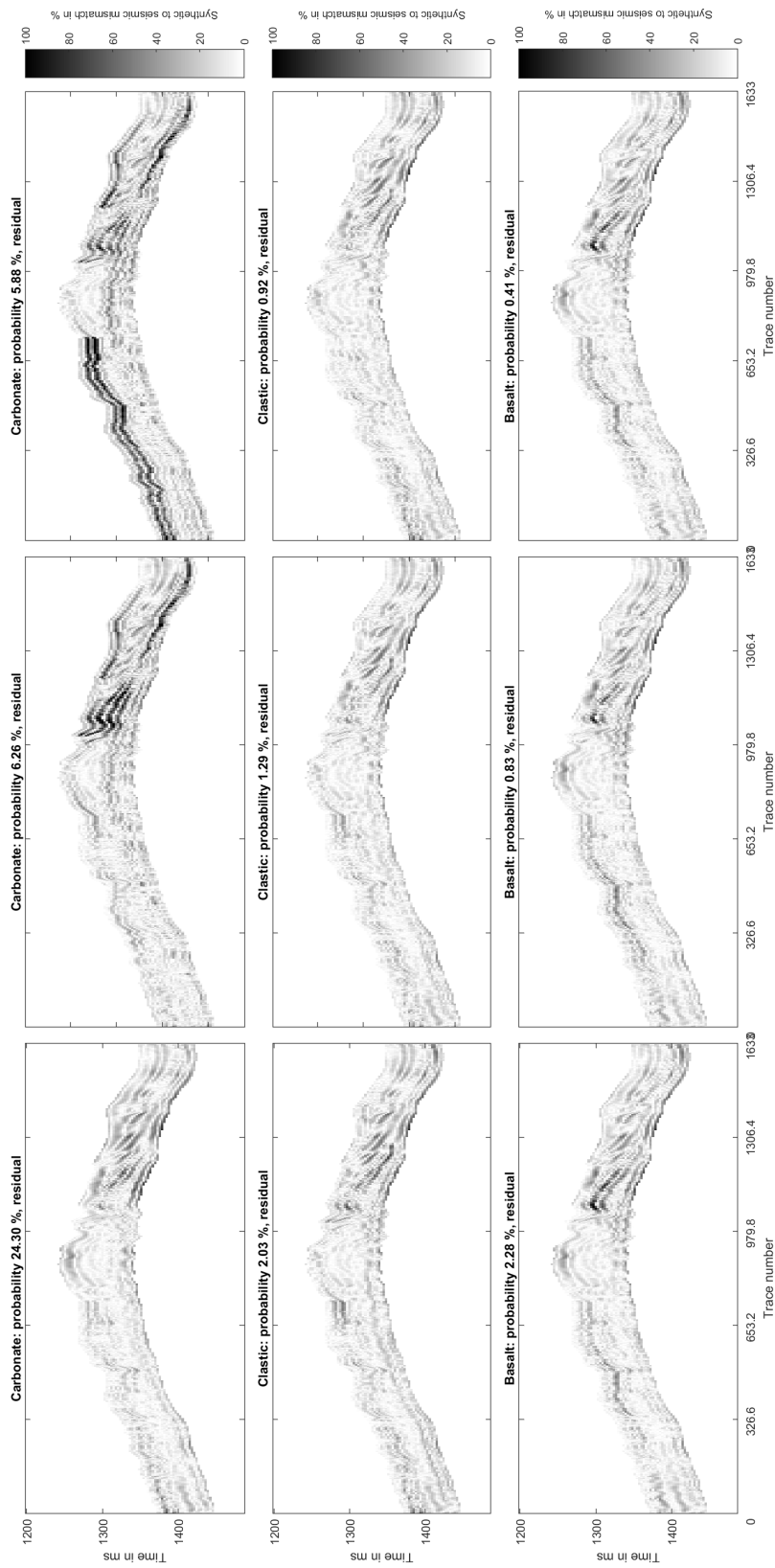


Figure B-3: Residuals of porosity scenarios for the Shuaiba Formation when comparing synthetic to seismic using PSO. Mismatch is the absolute deviation between the seismic section and the synthetics and is shown relative to the strongest amplitude in the seismic section.

Sun model simulation outcomes

C-1 ORCS-simulation including the Sun-model ($P_a = 0.25$ and one rank update ratio = 0.10)

The figures below show the results if the Sun velocity relation is included in the simulation (for carbonates only). The HH-RMSE value range is better for the Sun-relation (0.94-1.04), which is probably due to the large porosity variation causing only a relatively small velocity change. Therefore, porosity values found across the entire range of 1% to 50% are found and the 50% upper bound porosity model is nearly always the best solution. In general, the Sun-model thus overestimates the porosity in this model setting, as suggested in chapter 5. Please note there are no clastic or basalt scenarios visible anymore, because these fall out of the 10% best model results, because no Sun velocity relation is available for those types of rocks in this model (therefore, it in fact is an unequal comparison).

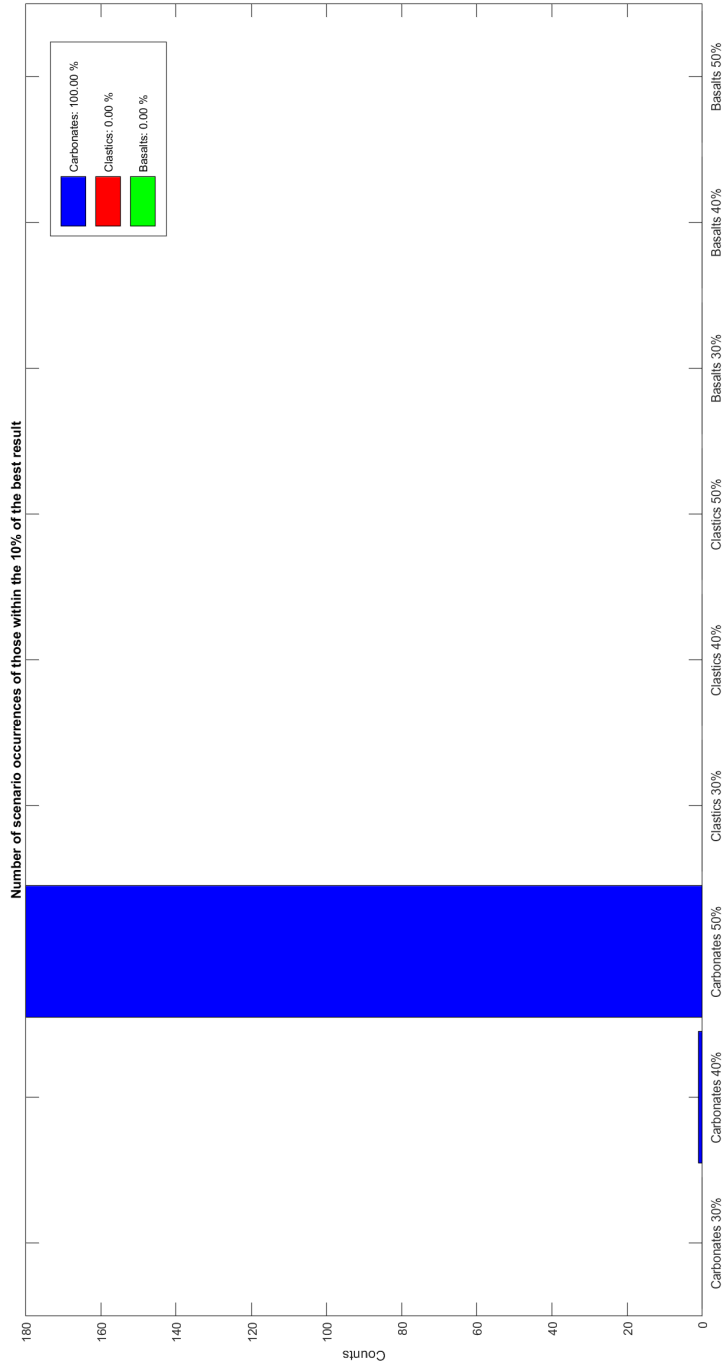


Figure C-1: Probable mineralogy scenarios according to the Sun-relation for the Shuaiba Formation using One Rank Cuckoo Search. Parameters for ORCS: $P_a = 0.25$, $t_{or} = 0.10$. Scenarios are obtained after counting outcomes within 10% of the best results after the entire simulation has finished (HH-value range: 0.94-1.04).

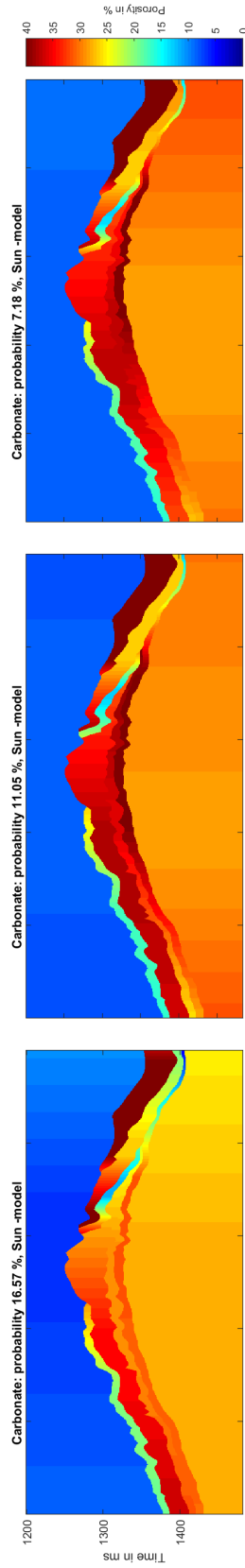


Figure C-2: Probable porosity scenarios according to the Sun-relation for the Shuaiba Formation using One Rank Cuckoo Search. Parameters for ORCS: $P_a = 0.25$, $t_{or} = 0.10$. The scenarios show probability (based on their occurrences) and the most used velocity model to create the scenario.

